

AD613545

RESPONSE OF DEEP REINFORCED CONCRETE SLABS

R. K. Gregory

R. C. DeHart

W. J. Austin

Southwest Research Institute
San Antonio, Texas
Contract AF 29(601)-5385

TECHNICAL DOCUMENTARY REPORT NO. WL-TDR-64-54



Research and Technology Division
AIR FORCE WEAPONS LABORATORY
Air Force Systems Command
Kirtland Air Force Base
New Mexico

COPY	2	OF	3	153
PER COPY		\$.	—	
MICROFORME		\$.	—	

February 1965

DDC
APR 13 1965
DDC-IRA E

ARCHIVE COPY

Research and Technology Division
AIR FORCE WEAPONS LABORATORY
Air Force Systems Command
Kirtland Air Force Base
New Mexico

When U. S. Government drawings, specifications, or other data are used for any purpose other than a definitely related Government procurement operation, the Government thereby incurs no responsibility nor any obligation whatsoever, and the fact that the Government may have formulated, furnished, or in any way supplied the said drawings, specifications, or other data, is not to be regarded by implication or otherwise, as in any manner licensing the holder or any other person or corporation, or conveying any rights or permission to manufacture, use, or sell any patented invention that may in any way be related thereto.

This report is made available for study with the understanding that proprietary interests in and relating thereto will not be impaired. In case of apparent conflict or any other questions between the Government's rights and those of others, notify the Judge Advocate, Air Force Systems Command, Andrews Air Force Base, Washington, D. C. 20331.

DDC release to OTS is authorized.

RESPONSE OF DEEP REINFORCED CONCRETE SLABS

R. K. Gregory

R. C. DeHart

W. J. Austin

Southwest Research Institute
San Antonio, Texas

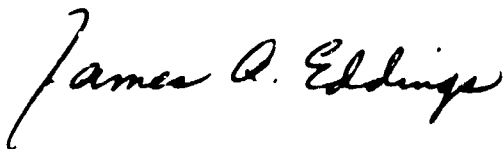
TECHNICAL DOCUMENTARY REPORT NO. WL-TDR-64-54

February 1965

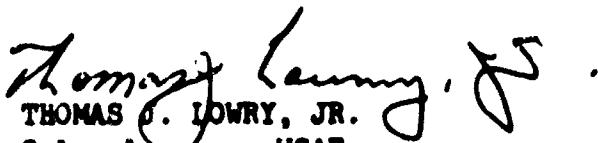
FOREWORD

This report was prepared by Southwest Research Institute under USAF Contract AF 29(601)-5385, Project 5710, DASA subtask No. 13.157, Program Element 7.60.06.01.5. Inclusive dates of research were July 1962 to April 1964. The work was initiated under the direction of the Air Force Special Weapons Center, Dr. Walter E. Fisher, project engineer. The report was submitted 10 February 1965, by the project officer, 1/Lt James A. Eddings, Air Force Weapons Laboratory (WLDC).

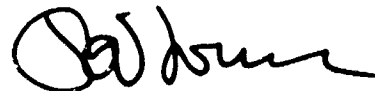
This report has been reviewed and is approved.



JAMES A. EDDINGS
1/Lt USAF
Project Officer



THOMAS J. LOWRY, JR.
Colonel USAF
Chief, Civil Engineering Branch



R. A. HOUSE
Colonel USAF
Chief, Development Division

ABSTRACT

The response of deep reinforced concrete slabs to uniformly distributed dynamic loads as high as 700 psi was measured and compared with the static behavior of companion slabs. Comparisons between theoretical and experimental results were made.

Experience has shown that one of the major difficulties in predicting the static behavior of reinforced concrete slabs results from the varying friction between the slab and bearing plate. The pressure seals and seal devices presented the primary experimental difficulty and made it impossible to yield the strongest slabs.

WL-TDR-64-54

This page is purposely left blank

TABLE OF CONTENTS

	<u>P. ge</u>
1. INTRODUCTION	
2. PURPOSE AND SCOPE OF THE INVESTIGATION	
3. EXPERIMENTAL DETAILS	
4. DISCUSSION OF THE RESULTS OF STATIC TESTS	
5. RESULTS OF DYNAMIC TESTS	
6. COMPARISON OF DYNAMIC TEST RESULTS WITH STATIC TEST RESULTS	
7. SUMMARY AND CONCLUSIONS	
APPENDIX A - DESCRIPTION OF TEST FACILITY	
APPENDIX B - PREDICTION OF STATIC BEHAVIOR	
LIST OF REFERENCES	1
DISTRIBUTION	1

LIST OF ILLUSTRATIONS

<u>Figure</u>		<u>Page</u>
1	Details of Specimens 1 through 5 and 9	8
2	Details of Specimens 6 and 8	9
3	Details of Specimens 7 and 10	10
4	Three-Way Reinforcement Layout for Circular Specimen 11	14
5	Location of Dial Indicators	15
6	Location of Strain Gages	17
7	Pressure versus Midspan Deflection for Slab 7	29
8	Pressure versus Strain for Slab 7	30
9	Profile of Tensile Surface for Slab 7	31
10	Pressure versus Midspan Deflection for Slab 4	32
11	Pressure versus Strain for Slab 4	33
12	Profile of Tensile Surface for Slab 4	34
13	Pressure versus Midspan Deflection for Slab 5	35
14	Pressure versus Strain for Slab 5	36
15	Profile of Tensile Surface for Slab 5	37
16	Pressure versus Midspan Deflection for Slab 2	38
17	Pressure versus Strain for Slab 2	39
18	Profile of Tensile Surface for Slab 2	40
19	Pressure versus Midspan Deflection for Slab 1	41

LIST OF ILLUSTRATIONS (Cont'd)

<u>Figure</u>		<u>Page</u>
20	Pressure versus Strain for Slab 1	42
21	Profile of Tensile Surface for Slab 1	43
22	Pressure versus Midspan Deflection for Slab 3	44
23	Pressure versus Strain for Slab 3	45
24	Profile of Tensile Surface for Slab 3	46
25	Pressure versus Midspan Deflection for Slab 9	47
26	Pressure versus Strain for Slab 9	48
27	Profile of Tensile Surface for Slab 9	49
28	Pressure versus Midspan Deflection for Slab 10	50
29	Pressure versus Strain for Slab 10	51
30	Profile of Tensile Surface for Slab 10	52
31	Pressure versus Midspan Deflection for Slab 11	53
32	Pressure versus Strain for Slab 11	54
33	Profile of Tensile Surface for Slab 11	55
34	Pressure versus Midspan Deflection for Slab 6	56
35	Pressure versus Strain for Slab 6	57
36	Profile of Tensile Surface for Slab 6	58
37	Observed Cracking Pattern for Slab 7	60
38	Post-Test Photograph of Tensile Side for Slabs 7 and 2	61
39	Cracks at 865 psi and after Test for Slab 5	62

LIST OF ILLUSTRATIONS (Cont'd)

<u>Figure</u>		<u>Page</u>
40	Compressive Surface after Test for Slabs 5 and 10	63
41	Dynamic Test, Slab 15, Showing Time History Data . . .	68
42	Post-Test Photograph of Slab 15	69
43	Dynamic Test, Slab 17, Showing Time History Data . . .	71
44	Pressure Decay through a 1-1/4-Inch Diameter Valve . .	72
45	Lower Cavity Pressure Release Blow-Off Disc	72
46	Pressure Decay through a 2-Inch Diameter Blow-Off Disc	73
47	Dynamic Test, Slab 18, Showing Time History Strain Data	73
48	Pressure Decay through 2-Inch Blow-Out Disc with Water-Filled Reservoir	75
49	Dynamic Test, Slab 20, Showing Time History Data . . .	76
50	Oscillograms from Slab 20	77
51	Post-Test Photographs of Slab 20	78
52	Comparison of Dynamic Strain Response of Slab 18 with the Static Behavior of Slab 4	81
A1	Square Slab Test Fixture	85
A2	Rectangular Slab Test Fixture	86
A3	Round Slab Test Fixture	87
A4	Schematic of Specimen Loading and Supporting Arrangement	88
B1	Typical Pressure-Deflection Diagram	91

LIST OF ILLUSTRATIONS (Cont'd)

<u>Figure</u>		<u>Page</u>
B2	Expected Cracking Pattern for Square Slabs	91
B3	Internal Forces on the Slab	93
B4	Assumed Stress-Strain Curve for Concrete	93
B5	Typical Stress-Strain Curve for the Reinforcing Steel	95
B6	Strain and Stress Relationships at Yielding of Tensile Reinforcement Concrete Not Yielded	97
B7	Strain and Stress Relationships at Yielding of Tensile Reinforcement Concrete Yielded	97
B8	Stress and Strain Relationships at Ultimate	99
B9	Assumed Edge Forces at Midedge for Deflected Position	99
B10	Slab Subjected to Edge Moments	105
B11	Slab Subjected to Horizontal Edge Compressive Forces	105
B12	Predicted Pressure-Deflection Diagrams for Slabs with Span-Depth Ratios of 4.22	111
B13	Effect of Span-Depth Ratio on Pressure-Deflection Diagrams	112
B14	Effect of Span-Depth Ratio on Pressure at Yield and Ultimate	113
B15	Assumed Edge Forces at Midedge for Slab Subjected to Edge Pressures	117
B16	Pressure-Deflection Diagram for Specimens 1, 6 and 7 with and without Edge Pressure	120
B17	Expected Cracking Pattern for Rectangular Slabs	121
B18	Distribution of Load on Reactions	125

LIST OF ILLUSTRATIONS (Cont'd)

<u>Figure</u>		<u>Page</u>
B19	Predicted Pressure-Deflection Diagrams Comparing Rectangular, Square, and Circular Specimens	129
B20	Yield-Line Analysis for Circular Slabs	131

LIST OF TABLES

<u>Table</u>		<u>Page</u>
I	Schedule of Specimen Parameters	7
II	Dimensions of Specimens	12
III	Concrete Strengths and Ages	20
IV	Summary of Predicted and Observed Results	109
V	Theoretical Solutions	110

This page is purposely left blank

1. INTRODUCTION

Reinforced concrete structures provide unique capabilities for hardening protective shelters to withstand nuclear attack. This is particularly true in superhardened shelters for strategic facilities. Such concrete structures have favorable strength characteristics, inherent economy, and supply good radiation shielding.

To be serviceable as protective shelters, reinforced concrete structures sometimes must be "thick," that is, the thickness must be an appreciable fraction of the linear dimensions. Our knowledge of the strength of such "thick" structures is less than that for similar "thin" structures where the structure may be considered as a membrane or a "thin plate." Beams and slabs of such "thick" proportions are called "deep" beams and slabs.

Knowledge of deep structural member behavior was so limited prior to 1957 that the Air Force undertook an investigation of deep beams. Literature surveys, experiments on deep concrete and steel beams, and theories have been published.¹⁻⁷ The results of the research on deep beams revealed a distinct departure from normal reinforced concrete beam behavior. The most distinctive characteristic of the deep beam was its behavior as a tied arch. The dynamic tests revealed that triangular load pulses with a peak intensity of at least twice the static yield load did not reduce the static strength.² The rise time of the pulses was about 1.5 times the natural period of the beam.

Deep beam behavior suggests that deep slab behavior may be significantly different from normal slab behavior. This and the absence of previous work on deep slabs prompted the initiation of an experimental program to determine the strength characteristics of deep slabs.

Manuscript released by authors March 1964 for publication as an Air Force Weapon Laboratory Technical Documentary Report.

2. PURPOSE AND SCOPE OF THE INVESTIGATION

The purpose of this investigation was to determine the structural response of simply supported reinforced concrete deep slabs to nuclear blast generated shock wave loading.

The scope of the investigation consisted of:

- (1) A review of the state-of-the-art of deep beam and slab design.
- (2) An analytical formulation of design theories and techniques for predicting and interpreting the experimental results.
- (3) Design, fabrication, and instrumentation of deep slab specimens for testing.
- (4) Design of loading and supporting fixtures to accommodate the slab specimens in the test facility in a manner that best simulates simple support edge conditions and laterally applied uniform loads.
- (5) Tests of the deep slab specimens with uniformly distributed static and dynamic loads applied laterally on the slab specimens.
- (6) Evaluation of the effects on the overall behavior of the slab of the following variables: reinforcement content, compressive reinforcement, depth, planform shape of the slab (square, rectangular and circular planforms), and edge supporting conditions.

3. EXPERIMENTAL DETAILS

A. Static Test Conditions

The static tests of companion specimens were conducted to establish the static strength properties of deep slabs of given proportions. The scope of the experiments had been restricted to simply supported edges and uniform lateral loads.

Simply supported edges were of primary interest because of the unique flexure purity they impart to the slab--the entire slab being subjected to positive moments only. While such purity is neither practical nor economical in the field, it is desirable in a research program.

Even pseudo-simple support was undesirable. Negative edge moment due to the load being applied to the edge overhang was not permitted. The edge overhang was required to provide sufficient bearing surface on the concrete. Frictional reactive forces in the plane of this bearing surface induced negative edge moments because the friction force was eccentric with respect to the slab. Such frictional moments were undesirable but unavoidable. Since the movement of the slab varies along the edge, friction reducing devices were too complex to be included within the scope of this investigation. Lubricated plastic sheets between the slab and bearing plate were reasonable provisions to minimize friction for this investigation. Analytical evaluation of the effect of the frictional moments on overall slab behavior was also a reasonable provision for this investigation.

To avoid the effects of applied axial load--that is, applied load in the plane of the slab--and the "beam-column" effects, the uniform load was required to act on the slab only within the planform dimensions of the clear span. This load configuration thus avoided load acting on the edge overhang. The effect of such axial load on the overall slab behavior had been found analytically to be quite severe, as shown in Appendix B, so the test conditions had been established accordingly.

The test facility that provided these test conditions, as well as the dynamic test conditions described later, is described in detail in Appendix A. The problems encountered in the development and use of the facility are described in some detail in the following paragraphs.

Fluid pressure produced the uniform load desired in a satisfactory manner but introduced severe pressure seal problems. Holding the pressure off the edge overhang and the vertical edge face was a severe requirement since (1) sealing directly to the concrete was complicated by large surface irregularities inherent in the concrete and by the porosity of the concrete, (2) the hold-down structure could not be made rigid enough to prevent some relative upward translation of the slab, and (3) a floating

seal mechanism bearing on the slab disturbed the uniform pressure condition.

By sealing the pressure beneath a flexible membrane, as described in Appendix A, Figure A4, the fluid pressure was contained so that the required uniform load was provided and the three complicating factors above were eliminated. This, however, introduced the following requirements for the membrane: (1) flexibility so that all the pressure was transferred to the specimen, (2) ductility so that the membrane could stretch as the slab flexed and translated with the deformations of the supporting structure, and (3) strength so the membrane could span the gap along the edges that were produced as the slab translated.

In order to seal the membrane to the pressure reservoir, a bolting frame was provided that held the membrane edge and gripped the O-ring. The planform dimensions of this frame corresponded to those of the clear span so as to confine the load to the span dimensions.

The space between the specimen and the membrane inside the bolting frame was filled with flexible spacers or fillers to reduce the amount of membrane stretch required. A plywood spacer was used in contact with the slab and 1/2-inch thick neoprene material was used between the membrane and the plywood, Figure A4. Recesses were provided in the plywood to prevent contact pressures on the strain gages mounted on the concrete surface. In addition, the plywood filled the gap that opened (under load) above the bolting frame as the specimen translated upward with the deformation of the supporting structure. As the slab deflected, the rotation of the edge of the plywood opened a small gap between it and the bolting frame. Since the neoprene material could flow horizontally under the load rather than rotate at the edge, the gap that opened at the edge of the plywood was filled.

The bolting frame carried the portion of the applied pressure that acted on the edge of the membrane. This edge width was the distance between the O-ring seal and where the membrane made contact with the spacers. For a flexible membrane this loaded edge width was about 1/4 inch, but for the stiffer, stronger aluminum membranes this width was found to be as much as one inch.

B. Dynamic Test Conditions

The dynamic load was to have the same characteristics as the shock wave generated by the detonation of a nuclear weapon. Such a dynamic load is characterized by a shock front followed by an exponential decay. The time required for the pressure to rise to its peak magnitude is almost instantaneous. The decay time or duration of the shock wave is 1 to 2 seconds, depending on the weapon yield and the distance from the detonation.

The test facility (Appendix A) was designed and developed to dynamically load slab specimens with a load pulse similar to the shock wave described above. The peak pressure capability was to approach 2000 psi. The time for the pressure to rise to peak magnitude was to be as short as possible, and the duration was to be about one second. All the edge conditions and load conditions discussed previously were to be maintained during the pressure rise and decay.

With two pressure reservoirs to seal, the pressure sealing requirements for each dynamic test became more complex. The lower reservoir was sealed exactly as for a static test. The upper reservoir seal requirements were similar to those for the lower reservoir. The membranes and flexible spacers were required as for the lower seals. Relative movement of the slab with respect to its sealing surfaces was again encountered. This relative movement occurred because the loaded slab area on the upper side was larger than the loaded area on the lower side. If equal pressures were applied, the net downward thrust would hold the slab down while the vessel supporting structure deflected with the upward thrust. To insure a net upward thrust on the specimen to prevent opening of the sealing surfaces, a pressure in the lower reservoir 20 to 30 percent higher than in the upper reservoir was required.

The key to the success of a dynamic loader of this nature is the rapid decay of the upper pressure; therefore, the procedure was to use the upper pressure reservoir with restraining diaphragm that was thin enough to be easily and rapidly removed. Ductile mild steel diaphragms were loaded extensively into the plastic behavior region to obtain high pressure capacities on relatively thin diaphragm materials. Having thin diaphragms minimized the size of the explosive charge required to cut the diaphragm and also minimized the inertia of the diaphragm so the pressure could be more rapidly released. When the 1/4-inch diaphragm was strained so extensively, the corners would rise causing a space to develop over the O-ring. Furthermore, the membrane tension forces were very large. The bolts required to hold the pressure seal could not carry these membrane forces. The horizontal component of the membrane forces had to be carried with a system of lugs and machined bars that fit the pivot in such a manner that after detonation the edge of the slab would be free to rotate and slip with respect to the pivot. Before detonation a net upward thrust from the pressure was required to insure the secure seating of this mechanism; otherwise, the cylindrical seat would not carry the horizontal forces but would wedge between the pivot and the bearing plate, causing bolt failure and thus loss of pressure.

C. Test Specimens

The structural element to be investigated was a flat, prismatic slab, conventional in all respects except the span/depth ratio. Span/dep

ratios were to vary from the very deeply proportioned to the more moderately proportioned, e.g., ratios from 3 to 6. Square, rectangular and round configurations were of interest. The effect of amount of steel reinforcement was to be evaluated so steel percentages of 1/2 percent, 1 percent, and 1-1/2 percent were to be included. Compressive steel of 1/2 percent was provided in most specimens to evaluate its effect. Of course, conventional design, fabrication, cure and testing procedures were to be maintained. The specimen schedule for the above parameters is shown in Table I.

All the slabs were cast with a commercially available concrete mix proportioned to have a strength of 5000 psi. An aggregate size of 3/8 inch was used because of the minimum cover of 1/2 inch on the reinforcement. Intermediate grade steel bars with standard hooks for anchorage were used.

Standard procedures of the ACI code were followed for taking test cylinder samples and for casting the specimens. Since these slabs weighed up to 3200 pounds, they were cured outdoors under a sprinkler system. Care was exercised to cure the test cylinders in the same fashion the slabs were cured. Specimen geometry is summarized in Table II.

1. Square Specimens

The square slabs had outside dimensions of 45 by 45 inches. The bearing plates were 6 inches wide. The pivot supports were centered on the bearing plates so the clear span was 39 by 39 inches.

Slab thicknesses of 8, 11, and 15-1/4 inches were chosen to give the desired range of span/depth ratio. Three specimens, Slabs 1, 6 and 7, see Figures 1, 2 and 3, were designed to study the effect of span/depth in that all had the same reinforcement content.

Specimens 1, 2 and 3 (Fig. 1) were identical except for the amount of tensile reinforcement which varied from 0.5 to 1.5 percent. Results of tests of these specimens were to give information on the effect of the amount of tensile reinforcement on the strength and other properties.

Specimens 4 and 5 were the same as Specimens 1 and 2 except that no compressive reinforcement was used. These tests were designed to investigate the effects of compressive reinforcement. Specimens 4 and 5 are illustrated in Figure 1.

Both the tensile and compressive reinforcements were composed of two layers of bars which formed a square mesh with the bars running parallel to the edges of the slabs. The bars were equally spaced

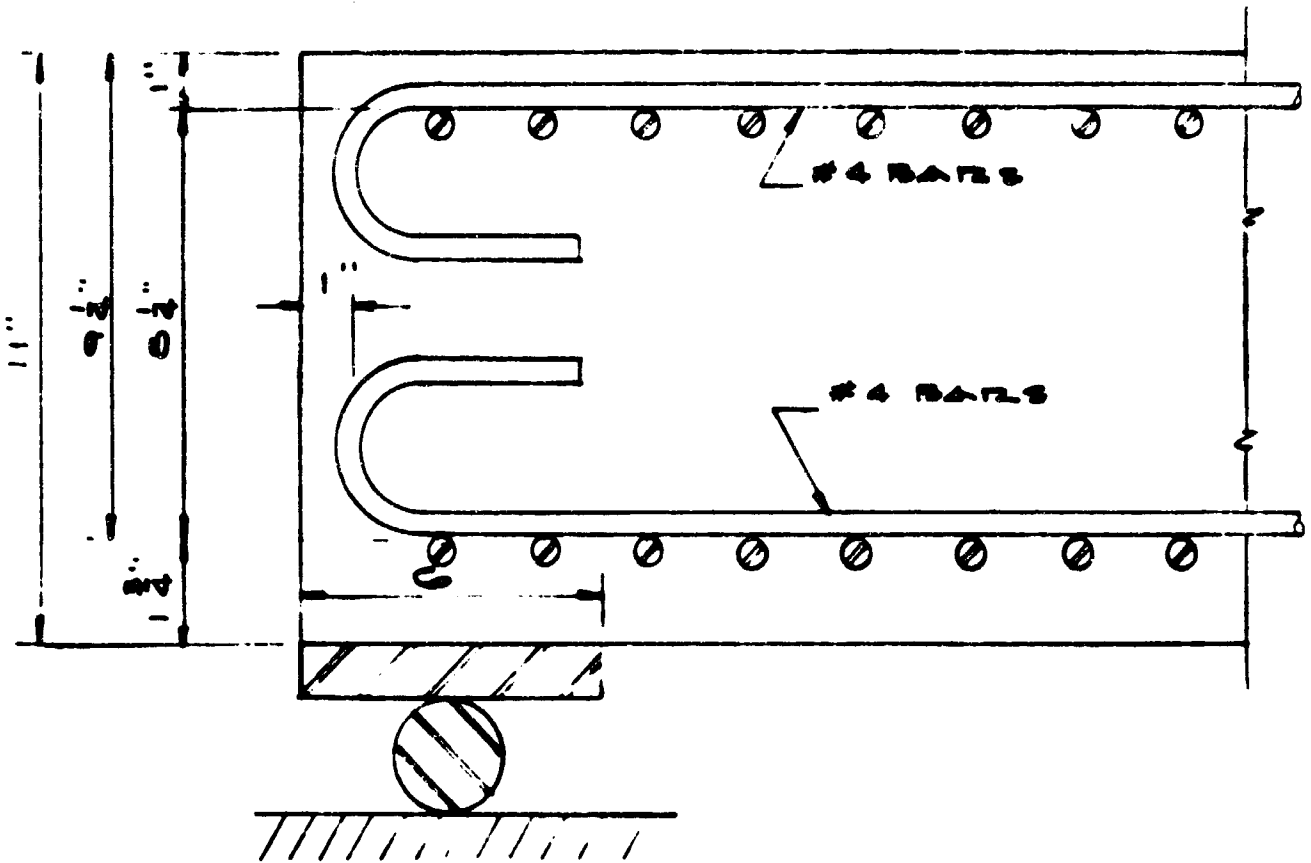


FIGURE 1. DETAILS OF SPECIMENS 1 THROUGH 5 AND 9

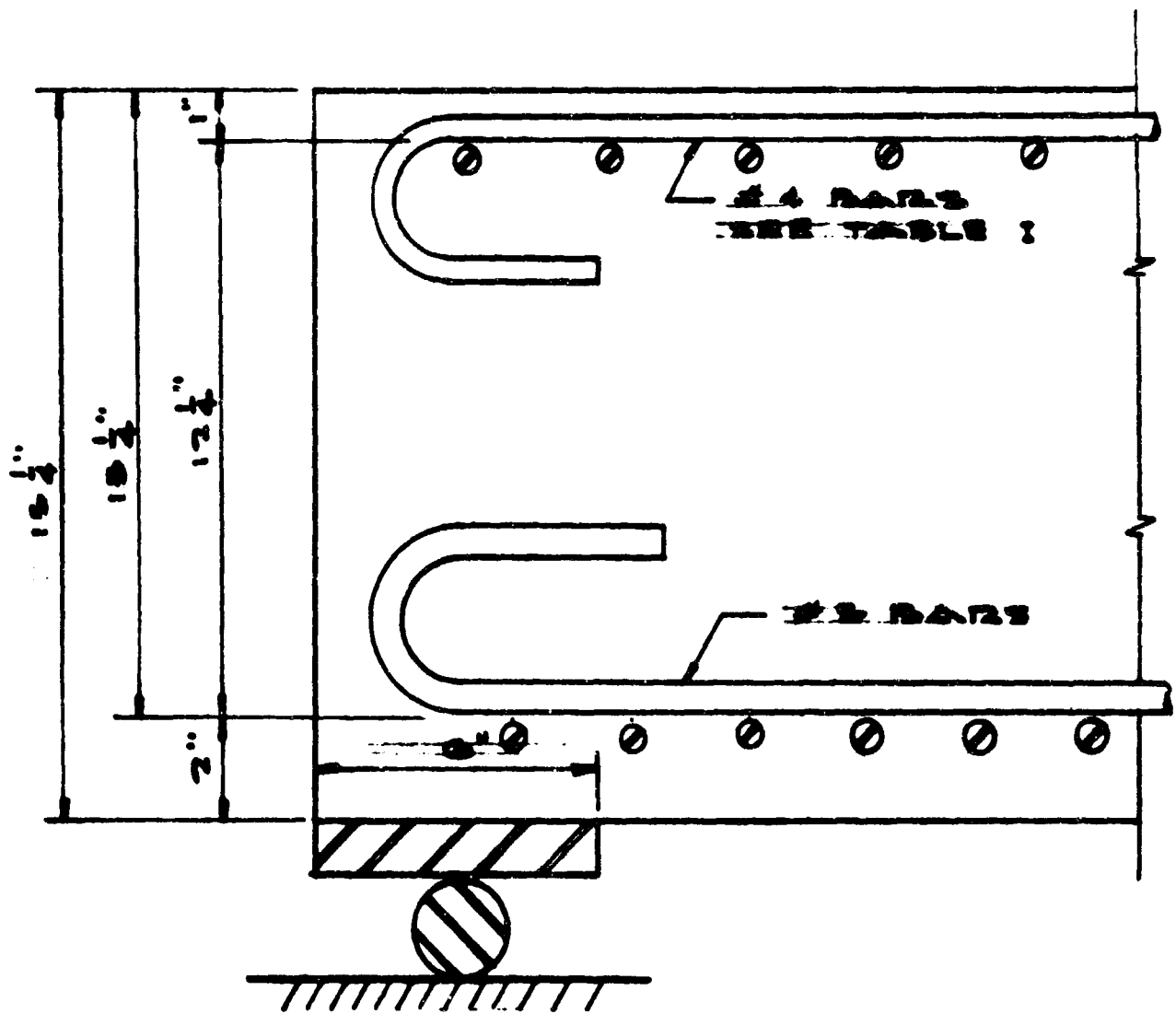


FIGURE 2. DETAILS OF SPECIMENS 6 AND 8

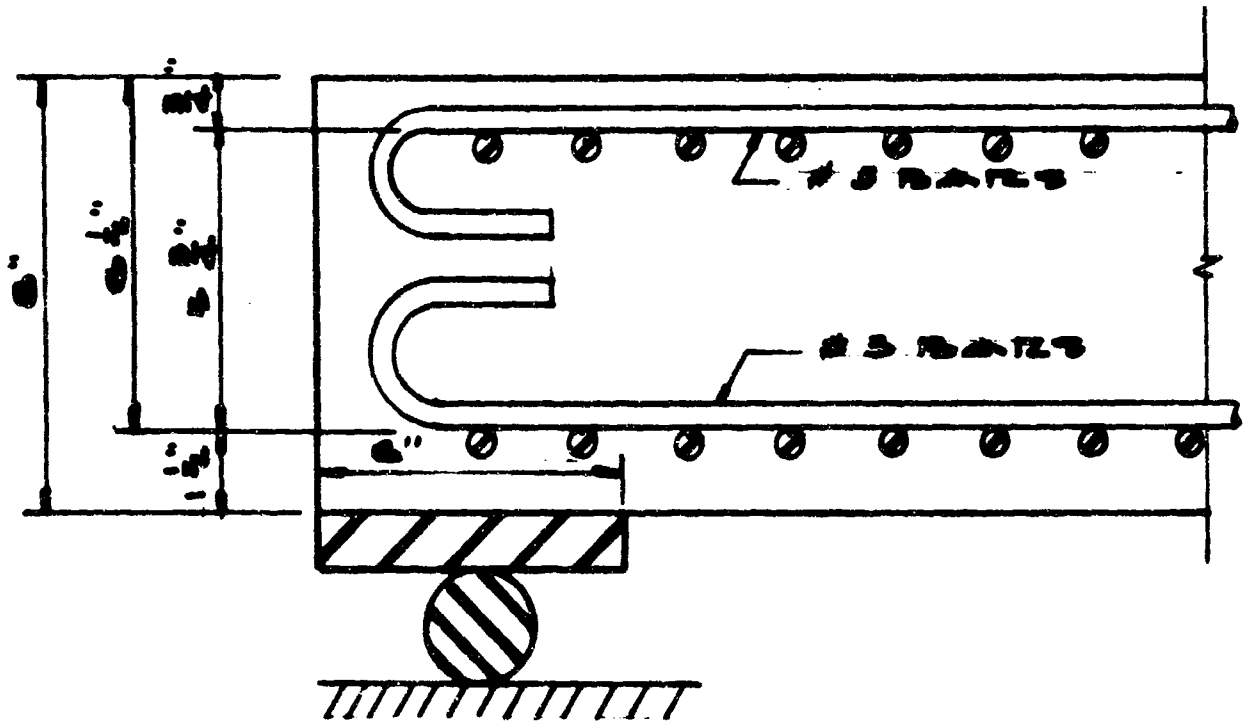


FIGURE 3. DETAILS OF SPECIMENS 7 AND 10

in both directions over the entire slab. For each set of bars, the central bar was placed on the midspan line. Parallel bars of the tensile and compressive reinforcement were either both on the top layers of their meshes or both on the bottom layers so that the distance between the tensile and compressive reinforcement was the same for each set of parallel bars. In the analysis (Appendix B) the properties of the beam strips in each direction are assumed to be the same, i.e., equal to an average beam strip with reinforcement at the centroidal plane of the actual orthogonal systems. The centroidal plane was the plane of contact of the two orthogonal systems of bars.

To give a secure anchorage, standard hooks were specified for both ends of each bar of the reinforcement. From the experience with deep beams, it seemed advisable to provide enough bond strength in the anchorage to develop the full strength of the bars. This has been done without exceeding a bond stress of $0.19 f'_c$, which is considered to be safe. Edge details are shown in Figures 1, 2, and 3.

For the dynamic tests, companion specimens were cast. Slabs 17, 18, 20, 19 and 15 were dynamic companions, respectively, to static specimens numbered 1, 4, 5, 6 and 7, as shown in Table I. The results of these tests are discussed later.

2. Rectangular Specimens

To fit the square structure and the square hole in the lid of the test facility, rectangular dimensions of 35 in. by 48 in. for the span were required. Overall dimensions of 45 in. by 54 in. were used for fabrication convenience. Obviously, the slab edge overhangs the 6-inch wide bearing plates. The aspect ratio, width/length, was taken as 35/48 or 0.729. Test facility dimensions dictated the use of slab thicknesses of 8, 11, and 15-1/2 inches.

All the rectangular specimens, Numbers 8, 9 and 10 as illustrated in Figures 1, 2 and 3, had the same percentage of reinforcement as square Specimens 1, 6 and 7.

Following the practice of the ACI Code and the US Army Corps of Engineers, the reinforcement in the long direction was proportioned according to the moment requirement. For an aspect ratio of 0.729, the moment in the long direction was 0.53 of the moment in the short direction. The reinforcement percentage in the long direction was, therefore, reduced to half that in the short direction, as can be seen in Table II.

In all other respects, the rectangular specimens were designed like the square specimen, i.e., standard hooks, intermediate grade steel, 5000-psi ready mix, 3/8-inch aggregate, etc. Specimens

TABLE II. DIMENSIONS OF SPECIMENS

Specimen No.	Total Depth h, inches	Effective Depth d, inches	Span, inches	Span/Depth, L/d	Tensile Reinforcement		Compressive Reinforcement	
					Bar Size and Spacing	Percent	Bar Size and Spacing	Percent
1 & 17	11.00	9.25	39	4.22	#4 at 2.16 inches	1.00	#4 at 4.32 inches	0.50
2	11.00	9.25	39	4.22	#4 at 4.32 inches	0.50	#4 at 4.32 inches	0.50
3	11.00	9.25	39	4.22	#5 at 2.23 inches	1.50	#4 at 4.32 inches	0.50
4 & 18	11.00	9.25	39	4.22	#4 at 2.16 inches	1.00	None	0
5 & 20	11.00	9.25	39	4.22	#4 at 4.32 inches	0.50	None	0
6 & 19	15.25	13.25	39	2.94	#5 at 2.34 inches	1.00	#4 at 3.02 inches	0.50
7 & 15	8.00	6.50	39	6.00	#3 at 1.69 inches	1.00	#3 at 3.38 inches	0.50
8 & 23	15.25	13.25	35 X 48	2.64	Short Span p = 1%	Long Span p = 1/2%	Short Span p' = 1/2%	Long Span p' = 1/4%
9 & 22	11.00	9.25	35 X 48	3.79	Bar and Spcg, inches	Bar and inches	Bar and Spcg, inches	Bar and Spcg, inches
10 & 21	8.00	6.50	35 X 48	5.38	#5 at 2.34	#4 at 3.02	#4 at 3.02	#3 at 3.31
11 & 24	14.00	12.25	48 φ	3.91	#4 at 2.16	#4 at 3.32	#4 at 3.32	#3 at 4.75
					#3 at 1.69	#3 at 3.38	#3 at 3.38	#2 at 3.06
					#4 at 2.50 at 60° = 1%		#3 at 2.75 at 60° = 1/2%	

numbered 23, 22 and 21 were the dynamic companions to static specimens numbered 8, 9 and 10, respectively, as shown in Table I. The results of these tests are discussed later.

3. Round Specimens

A round slab having a clear span of 48 inches was selected since this was optimum for the test facility. A 56-inch outside diameter slab provided a one-inch overhang on the 6-inch-wide bearing plate. A slab thickness of 14 inches and effective depth of 12.25 inches was selected to give a span to depth ratio of 3.91.

The orthogonal reinforcement layout for the square slabs would not be isotropic in the round slabs so the "three-way" reinforcement layout shown in Figure 4 was used. Such a reinforcement layout requires in each of the three directions $2/3$ of the reinforcement required in a two-way or orthogonal system. Therefore, the steel bar sizes and spacings were selected to provide two-thirds of the percentages used in the computations as shown in Tables I and II.

In all other respects, the round specimens were like the square and rectangular specimens.

D. Instrumentation

Measurements of load, strain and deflection were to be taken. The instrumentation for these measurements was distinctly different for the static and dynamic tests.

1. Static Instrumentation

The load was measured by reading the static pressure on the reservoir with a standard helicoid gage. The accuracy was at least 1 percent.

Deflections were measured with five standard dial indicators. The accuracy of the dials is 0.001 inch. The location of dials for all the tests is shown in Figure 5.

Strain measurements were generally taken (1) on the tensile and compressive reinforcement, (2) on the compressive surface of the concrete, and (3) within the concrete with embedment gages. Conventional SR-4 type gages with 1/2-inch gage length were used for the steel and concrete surface strains, and a valore brass envelope type embedment gage was used for the concrete strains beneath the surface. These gages are generally accurate to 20 microinches/inch.

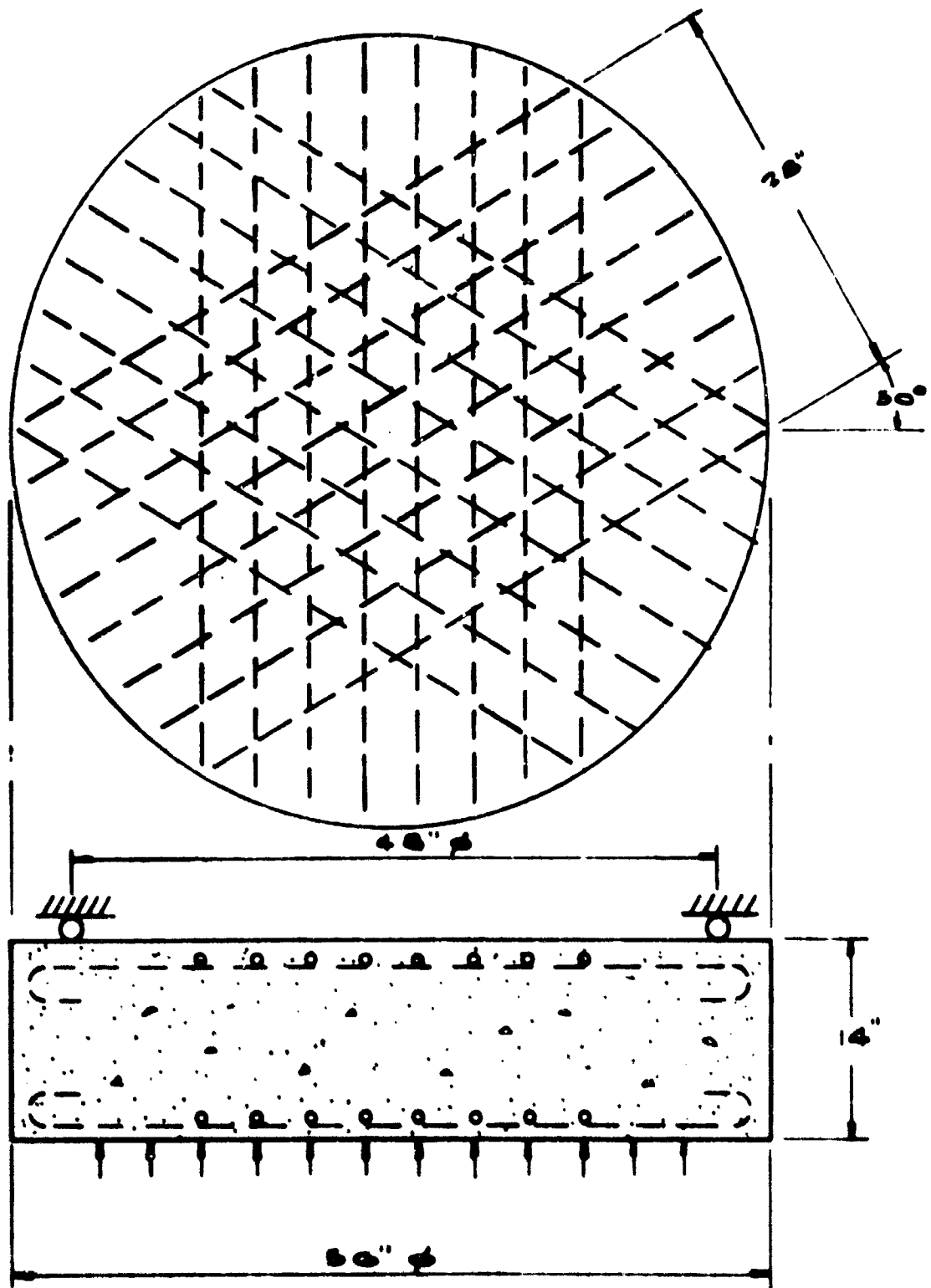


FIGURE 4. THREE-WAY REINFORCEMENT LAYOUT FOR CIRCULAR SPECIMEN II

Gage locations on the reinforcement generally followed the pattern shown in Figure 6. In a few cases, additional gages were used as indicated on the figures.

The surface gage and the embedment gage were generally located only at midspan with the depth of the embedment gage 1/4 inch from the compressive steel. Additional off-center gages were used occasionally as indicated.

2. Dynamic Instrumentation

Oscilloscope recording of the time histories of the pressure, strain and deflection was the basic instrumentation.

Since midspan deflection and tensile steel strain were of prime importance, measurements of these quantities were made. The deflection transducer was a Linear Variable Differential Transformer mounted within the lower pressure reservoir. The accuracy of this deflectionometer was 0.01 inch and the full range was 2-1/4 inches.

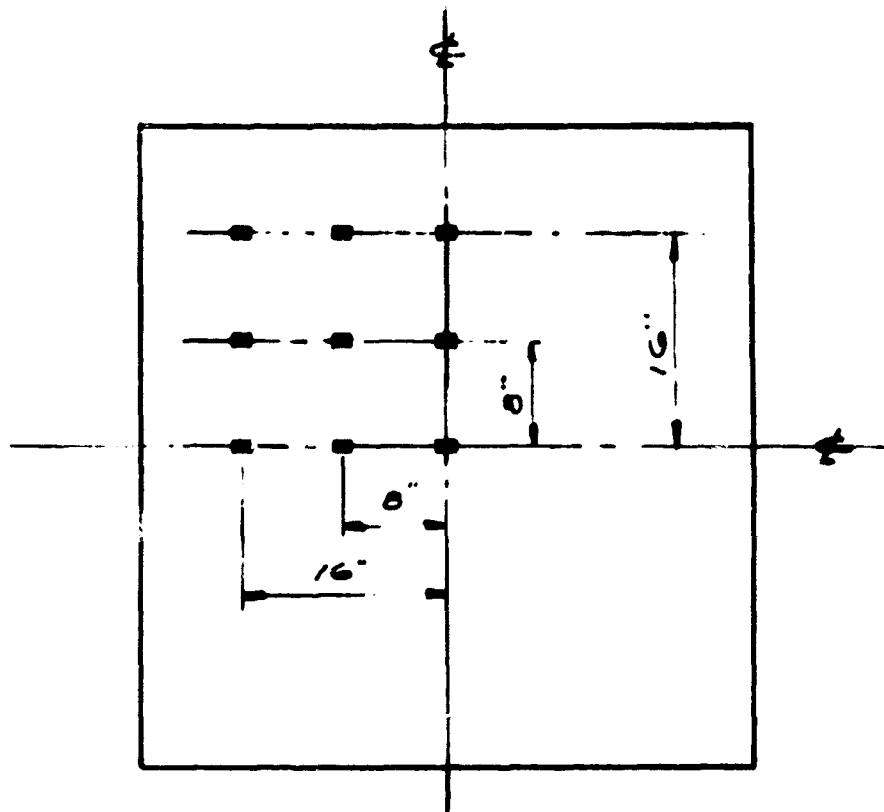
The specimen load was determined by the net pressure between the two opposing pressure reservoirs (Appendix A). The pressure-time histories of both reservoirs were separately measured so the net pressure could be determined.

A Photocon transducer and amplifier system was used to display the calibrated pressure signal on the oscilloscope. This system has a response time of 0.007 millisecond and is accurate to better than 1 percent.

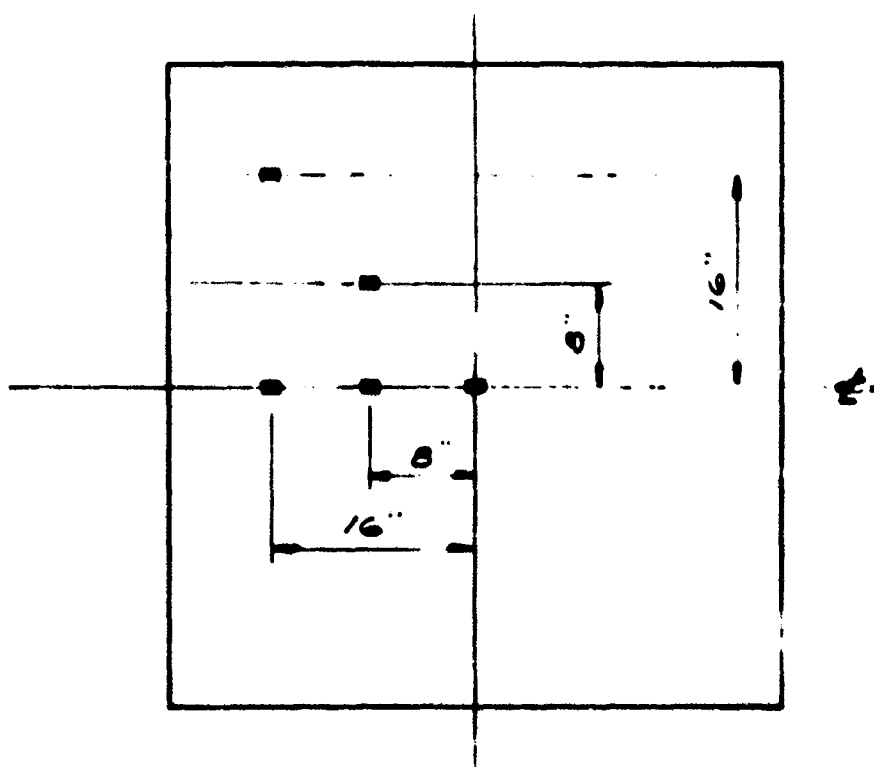
The transducer locations in each reservoir were such as to minimize inaccuracies and time lags.

The pressure transducer signals were displayed on Tektronix 502 dual beam oscilloscopes. The measurements were recorded with DuMont Type 302 Polaroid cameras. The optical distortion of the lens and time response of scope were adequate for these measurements.

Time synchronization between the scope trigger and detonation of the explosive was accomplished with a cam timer device equipped with relays, safety switches, etc. At first the scope was triggered at the same time the explosive was detonated. However, on the slower sweep rates, this procedure was not adequate so the timer was set to pre-trigger the scopes.



GAGES ON TENSILE STEEL



GAGES ON COMPRESSIVE STEEL

FIGURE 6. LOCATION OF STRAIN GAGES

E. Test Procedure

For the static tests, the reservoir beneath the slab was pressurized in steps and the pressure held while the strain gages were read and the dial readings were recorded.

For the dynamic tests, the strains, deflections, and pressures were continuously recorded on Tektronix 502 oscilloscopes. The procedure was to pressurize both reservoirs above and below the specimen while monitoring the scopes. At a predetermined pressure level, the pressure was held constant, while the oscilloscopes, cameras, and safety devices were readied. The cam timer was then activated. The timer executed the preset program of triggering the scope, detonating the prepositioned linear-shaped charge explosive and opening the solenoid valves. The test records were contained entirely on the oscilloscope camera films.

It later developed (Section 5) that valves excessively restricted the draining of the lower reservoir; therefore, a 2-inch diameter blow-off disc was substituted for the valves. The disc was blown with sheet explosives detonated at the same time that the linear-shaped charge was detonated.

4. DISCUSSION OF THE RESULTS OF STATIC TESTS

The results of each static test are presented in the form of (1) observed pressure-midspan deflection diagrams superimposed on predicted diagrams, (2) pressure-strain plots of observed strains, and (3) observed deflections plotted to show profiles of the tensile surface of the slab at several pressures. These graphs are shown in Figures 7 through 36.

All the tests were conducted to the highest pressure that could be carried by the membrane seals as previously discussed. As the membranes and seals were improved, greater pressures and deflections were achieved. When the seal failed during the seal development stage, retests of the specimens involved were later conducted. Results of these retests can be seen on Figures 10, 13 and 16.

A. Slab 7

The First Test was a static loading of Specimen No. 7 (Slab 7) which was an 8-inch deep square slab (span-depth ratio of 6.00) that contained one percent tensile and one-half percent compressive reinforcement. This specimen was mounted and partially loaded several times while the seals, membranes, and spacers were perfected. The loading data are shown in Figures 7, 8, and 9; however, the test was conducted without the use of friction reducing material or lubrication at the supports.

The concrete cylinder strength f'_c of 5200 psi (Table III) was higher than the 4000 psi that had been assumed in the preliminary computations. The use of the correct concrete strength of 5200 psi in the equations (Appendix B) did not change the predicted "yield" pressure (that pressure required to cause yielding of the midspan tensile reinforcement). The increase in concrete strength did increase the predicted "ultimate" pressure since that is the pressure required to crush the concrete at midspan of the slab. Furthermore, the increase in concrete strength increased the predicted "ultimate" midspan deflection since such deflection is a function of ultimate concrete strain. The increase in predicted ultimate pressure and deflection was essentially linear, i. e., a linear extension of the "plastic" portion of the pressure-deflection diagram. The predicted response using both concrete strengths and a friction coefficient μ of 0.05 are shown in Figure 7.

At this point in the investigation a review of the analysis was made because the experimental response showed considerably greater strength than had been predicted. This reanalysis revealed that the clear span area of the slab was not completely loaded, i. e., the load area was

TABLE III. CONCRETE STRENGTHS AND AGES

Slab No.	Depth d, inches	Shape	Cylinder Tests		Slab Tests		
			f' _c , psi	Age, days	Age, days	q Max., psi	δ Max., inches
1	9.25	Square	4000	55	49	1000	0.8
2	9.25	Square	5400	53	44	850	1.2
3	9.25	Square	5400	35	30	1200	0.23
4	9.25	Square	4700	59	40	920	1.08
5	9.25	Square	4700	59	48	875	2.25
6	13.25	Square	4700	168	107	1400	0.17
7	6.50	Square	5200	14	34	670	0.86
8	13.25	Rectangular					
9	9.25	Rectangular	3000	11	20	775	1.0
10	9.25	Rectangular	6400	79	57	575	2.2
11	12.00	Round	5000	126	126	700	0.19
15	6.50	Square	5900	93	114	575	1.5
16	6.50	Square	5400	84	97		
17	9.25	Square	6400	126	129	690	0.2
18	9.25	Square	6400	126	140	660	0.4
19	13.25	Square					
20	9.25	Square	5400	35	46	600	-

36 inches by 36 inches, whereas the clear span dimensions were 39 inches by 39 inches. In addition, the reinforcement extended beyond the clear span, i. e., the reinforcement bars were spaced over a width 42 inches by 42 inches. Both of these factors caused an increase in the predicted yield and ultimate pressures, as shown in Appendix B, Section C7. This increase has been included in all the predicted slab responses.

To evaluate experimentally the effects of friction, a simple test was conducted. The horizontal force required to slide a 50-pound steel weight on the concrete surface of the specimens was measured with a dynamometer. The horizontal force varied from 0.4 to 0.5 of the normal force. With lubricated plastic sheets under the weight, the horizontal force was about 0.3 of the normal force. The friction coefficient should be independent of the normal force but only insofar as the contact surface is independent of the normal force. The bearing stress under the weight was less than one psi, whereas bearing stresses of $0.19 f'_c$ or about 1000 psi were allowable. There were no means available for measuring friction coefficients under such high normal loads. One fact was clear, the actual coefficient was greater than the 0.05 that had been assumed in the preliminary computations.

An analytical evaluation of the effects of friction on overall slab behavior was made by computing the yield and ultimate pressures and deflections for several values of the coefficient of friction. These predicted responses for Slab 7 are shown in Figure 7. It can be seen that the coefficient of 0.3 gives close correlation between the theoretical and the experimental results. Since the plastic sheets had been omitted, a relatively large coefficient of friction is reasonable. It is clear that such close correlation does not fully corroborate the theory. The data do, however, illustrate the significant effect on slab behavior of forces in the plane of the slab, such as friction forces.

The onset of yielding near midspan at a pressure of 480 psi and at midspan at 500 psi is shown in the observed strain data (Figure 8). The progression of the yield front toward the edges was also measured. At the corner the strain gage indicated tensile yielding at 460 psi, prior to midspan yielding. Strains at the quarter point of the diagonal, gage T₅, were higher than the corner strains up to 420 psi, but not thereafter. The cause of the early yielding at the corner was not immediately apparent. The midspan deflection diagram showed an increasing rate of deflection beyond 350 psi, indicating yielding somewhere in the slab. For concrete, non-uniformity of moments, bond, bar placement, etc., could easily have caused higher stresses in the reinforcement at locations other than where the strain gages were positioned. Of the two orthogonal grids of tensile bars the deepest grid contained the strain gages, therefore the depth of the grid cannot be the cause of this anomaly of apparent slab yielding prior to measured yield strains.

The embedment strains were compressive until the slab yielded and the neutral axis moved up to the gage, then the gage did not show additional strains. The deflections on the diagonal were measured (Figure 9) along with the deflections along the centerline. The sharp change in slope at midspan is apparent. In the later tests it was much more pronounced.

B. Slab 4

The Second Test was a static loading of Slab 4 which was an 11-inch deep slab (span-depth ratio of 4.22). Slab 4, like Slab 7, had one percent tensile reinforcement but had no compressive reinforcement. The test data are shown in Figures 10, 11 and 12. The observed pressure-deflection diagram (Figure 10) shows some initial nonlinearity which is attributed to mechanical slack and mismatch in the bearing surfaces. At higher loads Slab 4 behaved linearly, but the deflections were twice the predicted deflections. Yield in the slab occurred and a 0.3-inch deflection at midspan was noted when the pressure seal failed at 900 psi.

When this slab was retested after Slabs 5 and 2 were tested and retested, new bearing plates free to rotate at the corners were installed in place of the bearing plate "frame" that had been welded at the corners. The torsional strength of the frame had imparted additional negative edge moments on the slab, causing higher pressures to be required to yield Slab 4 on the first loading. These torsional edge moments have been quantitatively analyzed in Appendix B, Section C8. The effect of the torsional restraint on the overall slab behavior is shown in Figure 10.

The reload diagram shows a flat slope after yielding, which is not pure flexural behavior of the slab. A supporting fixture was yielding, thus allowing upward translation of the slab with increasing load. Actually, a total midspan movement of 1.81 inches was recorded but was not plotted because that portion of the diagram would have been horizontal and would have been misleading.

The observed strains are shown in Figure 11. The onset of yielding was measured both in the tensile reinforcement and in the concrete as measured by the embedment gage. The low compressive strains on the concrete surface do not correlate with the data from the embedment gage and are believed to be incorrect. The yielding at the quarter point prior to midspan is attributed to nonuniform slab properties.

The deflected profile (Figure 12) of the tensile surface is for the first load case only because the reload deflection measurements contained translation components of unknown magnitude. This profile shows the sharp change in slope at midspan at the higher pressures. For the load range shown on this profile, it is observed that the deflections along the

diagonal were about the same as the deflections along the centerline. The expected deflection behavior as described in the yield line analysis in Appendix B was due primarily to rotation about diagonal bend lines. Theoretically, deflections due to rotation of the triangular quarter-pieces would be the same along lines parallel to the edges. Thus, the deflections along the diagonal would be exactly the same as the corresponding deflections along the centerline. The elasticity of the slab prior to formation of the diagonal bend lines generally gives some deflections along the centerline that are larger than the corresponding deflections along the diagonal, such as observed in the Slab 7 profile.

C. Slab 5

The Third Test was a static loading of Slab 5 using the bearing plate frame described above. Slab 5 was also 11 inches deep but contained only a half percent of tensile reinforcement and no compressive reinforcement. The test data are shown in Figures 13, 14 and 15. The initial non-linear deflection diagram is attributed to mechanical slack. The linear behavior up to onset of yielding of the tensile reinforcement was the expected typical behavior except that the magnitude of the deflection was more than twice the predicted deflection, as for Slab 4. Typical strains have been superimposed on the deflection diagram (Figure 13) to illustrate the onset of yielding and the progression of the yield front toward the edge. At 500 psi and 0.23 inch of midspan deflection the seal was lost.

The slab was later retested and the reload deflections have been superimposed on the first load permanent set to illustrate the reload deflection behavior. The reload strain behavior is also shown in Figure 14.

The observed pressure-deflection diagram compares fairly well with theoretical predictions. The steep slope of the observed diagram between yield and ultimate is probably caused by the torsional resistance of the bearing plate frame. However, there may be tensile membrane action contributing to the behavior⁸, as discussed later.

The magnitude of the compressive strains at the concrete surface and beneath the surface where the embedment gage was located have been plotted versus slab depth (Figure 14 insert). This plot shows the distribution of concrete strains and illustrates the movement of the neutral axis from the computed depth (2.38 inches) to a depth less than one inch. Reload strains show that the depth of neutral axis continued to decrease with increase in pressure beyond 500 psi. At 540 psi the embedment strains became tensile, indicating that the neutral axis had moved across the embedment gage to a more shallow depth.

The deflected profile of the tensile surface (Figure 15) is the reload profile. As in the previous profiles, the rotation at midspan is

evidenced by the sharp change in slope at midspan shown in the profile. The deflections along the diagonal were generally 80 percent of the deflections along the centerline which indicated that the diagonal bend lines mode of deflection did not predominate in the deflection behavior of Slab 5.

D. Slab 2

The Fourth Test was a static loading of Slab 2 which was 11 inches deep (span-depth ratio of 4.22) and contained a half percent of tensile and compressive reinforcement. The observed data are shown in Figures 16, 17 and 18. This loading and the later reloading were conducted with the bearing plate frame as previously described.

The load-deflection diagram (Figure 16) shows the initial mechanical slack as in the previous tests and also shows deflections at least twice as large as predicted. The reload diagram is linear, but the slope of the elastic portion is significantly less steep than the slope of predicted deflection diagram. This indicates that the predicted yield deflection is too low.

The reload behavior was different from the first load behavior. The pressure required to yield the slab was 20 percent higher when reloaded than when first loaded. This apparent increase in strength can be attributed to an increase in friction coefficient.

The slope of the "plastic" portion of the observed diagram is very similar to that of Slab 5. The torsional resistance of the bearing plate frame probably caused such a steep slope.

The strain behavior (Figure 17) of Slab 2 was typical. This behavior indicated yielding of the tensile reinforcement at or near midspan followed by progression of the yield front to the edges and corners. Inelastic behavior of the concrete also contributed to this typical slab behavior.

The deflected profile of the tensile surface (Figure 18) is the reload profile and is similar to those previously obtained. At the highest pressure the deflections on the diagonal were 90 percent of the deflections on the centerline. This indicates that the piece-wise mode of deflection was becoming predominate.

E. Slab 1

The Fifth Test was a static loading of Slab 1 which was an 11-inch deep square slab (span-depth ratio of 4.22) containing one percent tensile and half percent compressive reinforcement. This test and all subsequent tests were conducted with bearing plates free to rotate at the

corners to avoid the edge moments induced by the torsional resistance of the bearing plate frame. The nuts were tightened more than previously to remove all the mechanical slack.

The observed load-deflection behavior (Figure 19) was quite linear up to 500 psi. The inelastic behavior from 500 psi to 850 psi was typical of transition behavior from fully elastic to fully plastic behavior.

For correlation purposes, the midspan tensile and compressive strains have been superimposed on the deflection diagram. The inelastic concrete strain behavior coincided with the inelastic slab deflection behavior which occurred prior to observed yielding of the tensile reinforcement. This inelastic behavior also occurred in Slabs 7 and 4.

The predicted deflections, as in previous tests, were about half the magnitude of the observed deflections. The effect of friction on the predicted deflections has been determined using different coefficients of friction in the equations. This same procedure was used on Slab 7 which was an 8-inch deep slab containing the same reinforcement as Slab 1. It can be seen that with an increase in friction coefficient from 0.05 to 0.2 the increase in predicted yield pressure would be 26 percent for Slab 7 but would be 37 percent for Slab 1. The increased effect of friction on the behavior of the deeper slabs results from the increased eccentricity of the friction forces acting on the plane of the bearing surface which were more eccentric on the deeper slabs.

The variation of the concrete strains with depth of the concrete is illustrated in the insert on Figure 19. The observed concrete strains appeared reasonable and consistent; however, the relative magnitudes do not corroborate the computed depth of neutral axis in this case. This might be attributed to a slab concrete strength f'_c higher than that observed in the sample cylinder strength tests.

The observed strain data (Figure 20) show the onset of yielding around midspan and at the corner at 750 psi. Yielding progressed as the pressure was increased to 900 psi. The gages that do not show yielding probably yielded too rapidly to be recorded with the strain indicator or the gage may have failed prematurely.

The deflection profile (Figure 21) is similar to the previous profiles except that the sharp change of slope at midspan is more pronounced at such large deflections.

F. Slab 3

The Sixth Test was a static loading of Slab 3 which was an 11-inch deep square slab (span-depth ratio of 4.22) that contained one and

a half percent tensile and a half percent compressive reinforcement. Slab 3 was considerably stronger than the previous slabs as evidenced by the predicted yield pressure of 1500 psi.

The observed pressure-deflection diagram (Figure 22) is linear up to 1000 psi. The inelastic behavior from 1000 to 1200 psi coincided with the inelastic strain behavior exhibited by the gage on the concrete compressive surface. At 1200 psi the tensile reinforcement strains were at yield magnitude but did not exhibit any yield behavior (Figure 23). At 1200 psi and midspan deflection of 0.23 inch the pressure seal failed. Therefore, Slab 3 was not loaded until yielding occurred.

The predicted deflection diagram (Figure 22) was not fully corroborated by this test. The observed elastic deflections were again over twice the predicted deflections.

The deflected profile (Figure 24) is different from the previous tests. Since there was no yielding, the change of slope at midspan is not sharp. Also, deflections at the corner were observed to be relatively large. This was caused by a slab that was not initially planar. The clamping force of the bolts was insufficient to force the slab into the plane of the bearing surface. As the pressure was applied, the low corner exhibited some movement.

G. Slab 9

After the Sixth Test, the dynamic test facility was assembled to proceed with the development of the pressure seals, diaphragms, and related hardware. While machining operations were in progress, a static loading of Slab 9 was conducted as the Seventh Test. Slab 9 was an 11-inch deep (span-depth ratio of 3.79) rectangular slab that had a width-length ratio of 0.73. The reinforcement was the same as the reinforcement for Slab 1, one percent tensile and half percent compressive.

The deflection diagram (Figure 25) is linear up to 450 psi. The inelastic behavior up to yielding of the tensile reinforcement at 625 psi was caused by the pronounced inelastic behavior of the concrete gage (Figure 26). The increasingly large deflections and absence of any slope in the plastic portion of the deflection diagram were unusual. Such behavior was caused by an off-center pivot (Figure 25). The off-center pivot caused the bearing plate to rotate and locally crush the 3000-psi concrete under the edge of the plate.

Yielding of the tensile reinforcement at midspan and along the diagonal occurred at the same pressure, 625 psi (Figure 26). Extensive straining of the concrete compressive surface was measured. Compressive strains of such a magnitude were not observed on any of the other tests.

The deflected profile (Figure 27) shows the relatively large deflections near the edges that were caused by the off-center pivot and consequent local concrete crushing.

The locations of the "diagonal" dial indicators on the rectangular slabs were slightly off the true rectangular diagonal. This was unavoidable because the hole in the lid of the test facility provided access only to a square 31-1/2 inches by 31-1/2 inches. This affects the profile primarily at the corner deflections. Nevertheless, the profile typically illustrates the midspan yield line by the sharp change in slope. Furthermore, the deflections along the "diagonal" were very nearly the same as the deflections along the centerline, thus demonstrating the piecewise mode of plastic deflection.

Comparison with Slab 1 shows that the square slab was about 30 percent stronger than a rectangular slab of the same depth and reinforcement content. The fact that the spans were slightly different (39 inches by 39 inches square span versus 35 inches by 48 inches rectangular span) would lead to the conjecture that a square slab tested on a span of 35 inches square would be about 50 percent stronger than Slab 9. This comparison is theoretically evaluated in Appendix B.

H. Slab 10

The Eighth Test was a static loading of Slab 10 which was an 8-inch deep (span-depth ratio of 5.38) rectangular slab that contained one percent tensile and half percent compressive reinforcement. Slab 7 was the square 8-inch deep companion specimen containing the same reinforcement as Slab 10.

The deflection diagram is quite linear in the plastic portion as well as the elastic portion. The agreement with the predicted response is good. However, the observed maximum pressure was 35 percent greater than the predicted "ultimate" pressure. In addition, the maximum observed midspan deflection was almost twice the predicted "ultimate" deflection. This slab behavior suggests that there exists greater load carrying capability and considerably greater overall ductility than the theory takes into consideration.

The strain behavior was normal and similar to Slab 7. The onset of yielding in the midspan tensile reinforcement at 275 psi and the progression of the yield front to the corner at 330 psi and to the edge at 380 psi were as expected and as previously experienced. The movement of the neutral axis was measured as shown in the concrete strain distribution plot (Figure 29). The "compressive" reinforcement strains became tensile after the neutral axis moved, much like the Slab 7 behavior.

The plastic analysis in Appendix B does not take into account the compressive reinforcement going into tension as observed. The computed depths of the neutral axis (Table V) did not indicate Slabs 7 and 10 would behave in such a manner.

The deflection profiles (Figure 30) were also similar to Slab 7. The deflections along the centerline were considerably greater than those along the diagonal. This indicates a predominance of a "spherical" bending mode of deflection of the slab, as opposed to the piecewise mode of deflection.

I. Slab 11

The Ninth Test was a static loading of Slab 11 which was the circular slab. Slab 11 was 14 inches deep and contained three-way reinforcement of one percent tensile and half percent compressive. The circular span of 48 inches in diameter gave a span-depth ratio (L/d) of 3.92. The reinforcement content and span-depth ratio of square Slab 1 and rectangular Slab 9 were similar to provide an evaluation of the effect of shape on slab behavior.

The pressure-deflection diagram (Figure 31) shows some initial mechanical slack but after 80 psi is quite linear. If the mechanical slack were subtracted out of the deflections, the observed deflections would be about 50 percent greater than the predicted deflections.

At 700 psi the pressure seal failed. A retest of this slab was not accomplished. Consequently, the predicted deflection diagram was not corroborated. Any comparison with square and rectangular slab behavior must be based on the predicted deflection diagram which assumes the theory is valid. A cross plot of the predicted diagrams of Slabs 1, 9 and 11 is shown in Appendix B. In general, the circular slab showed about the same yield pressure as the square slab but about 40 percent greater ultimate deflection and 20 percent greater ultimate pressure. The rectangular slab has been shown to be about 75 percent as strong as the square slab.

The magnitudes of the strains (Figure 32) and the strain rates indicated that yielding probably would have occurred around 1100 psi.

The mechanical slack apparent in the pressure-deflection diagram is also apparent in the deflected profiles (Figure 33). The slack was in the vicinity of the corner dial indicator. The profiles are so distorted that no trends can be observed or conclusions drawn as to slab behavior.

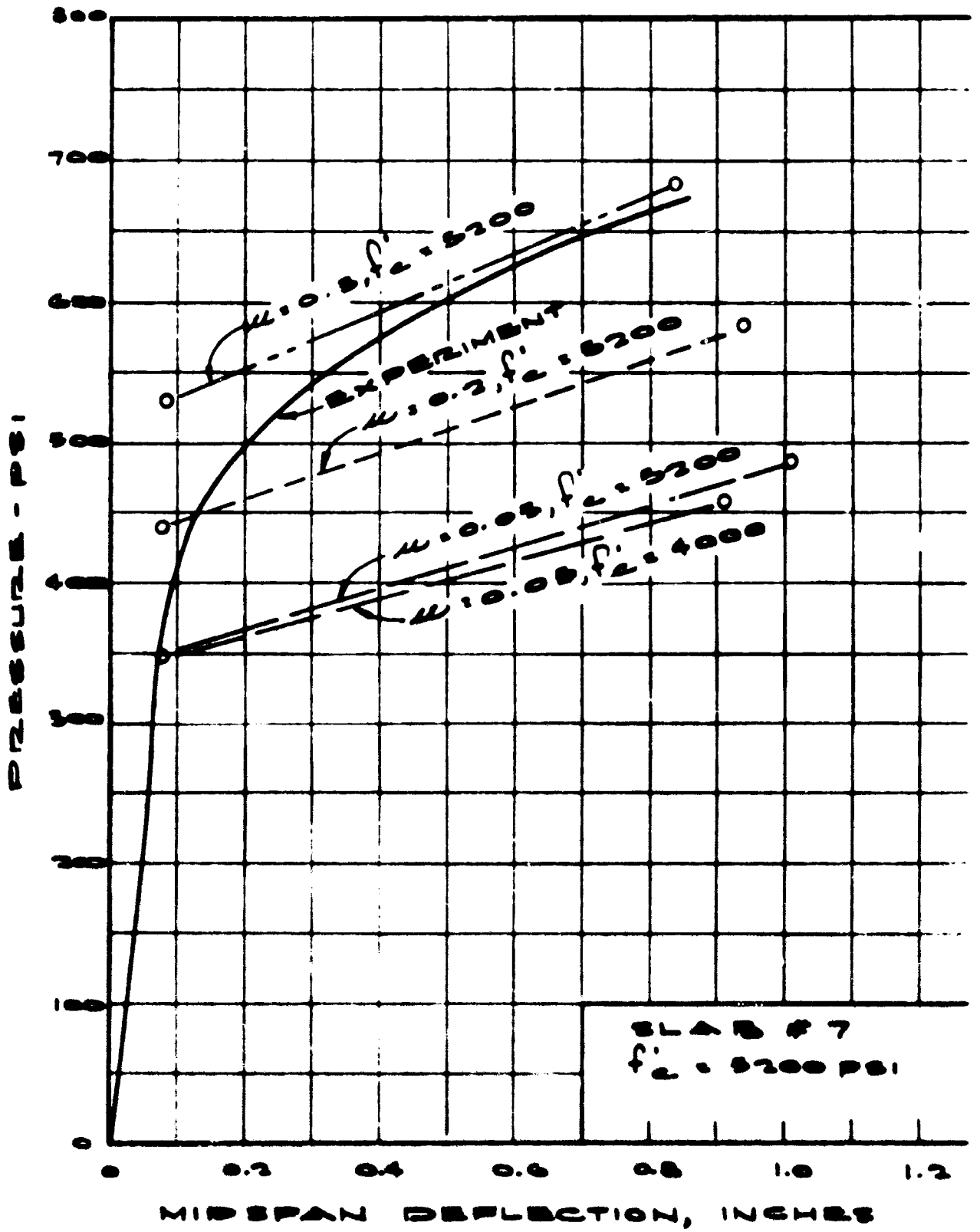


FIGURE 7. PRESSURE VERSUS MIDSPAN DEFLECTION FOR SL.

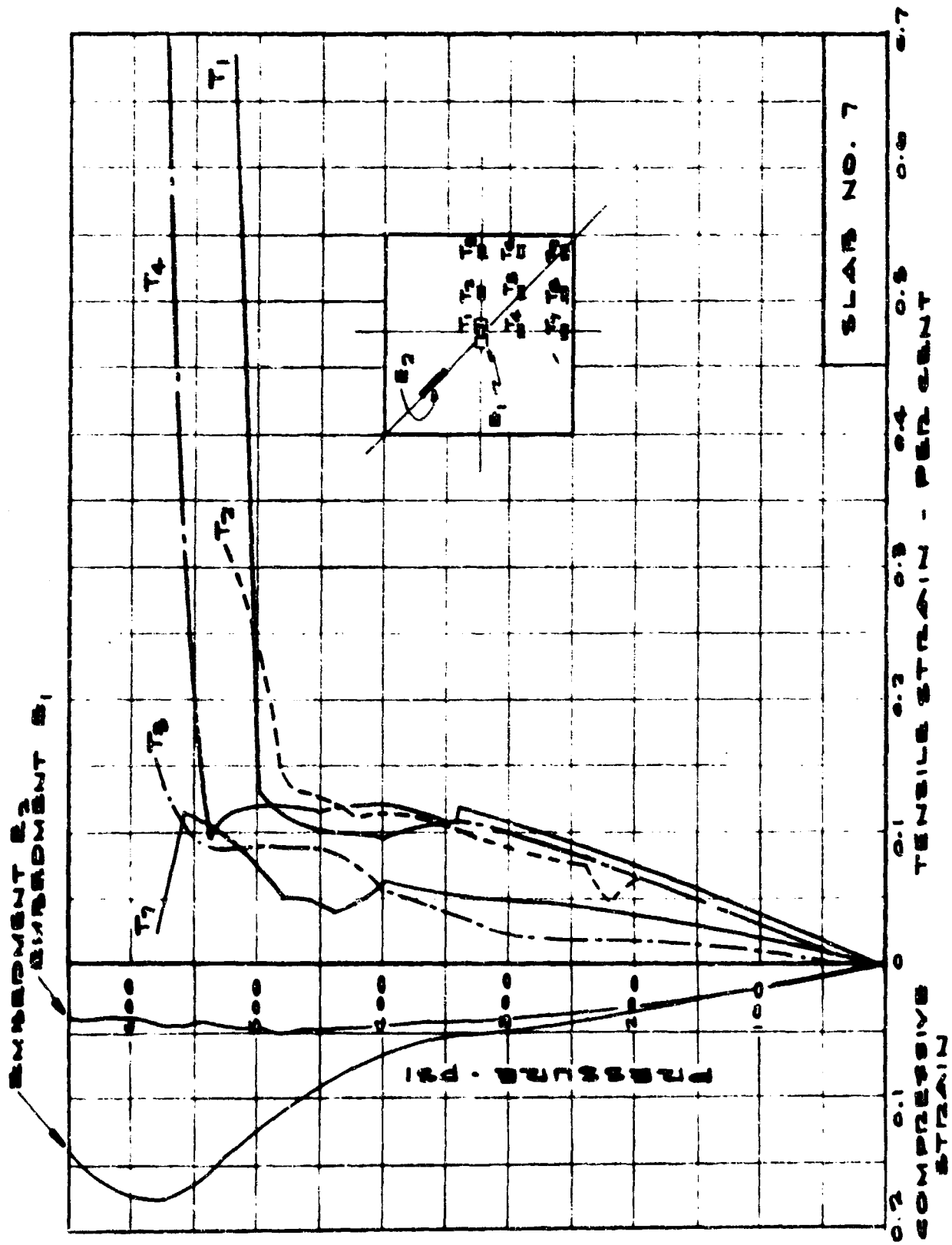


FIGURE 8. PRESSURE VERSUS STRAIN FOR SLAB 7

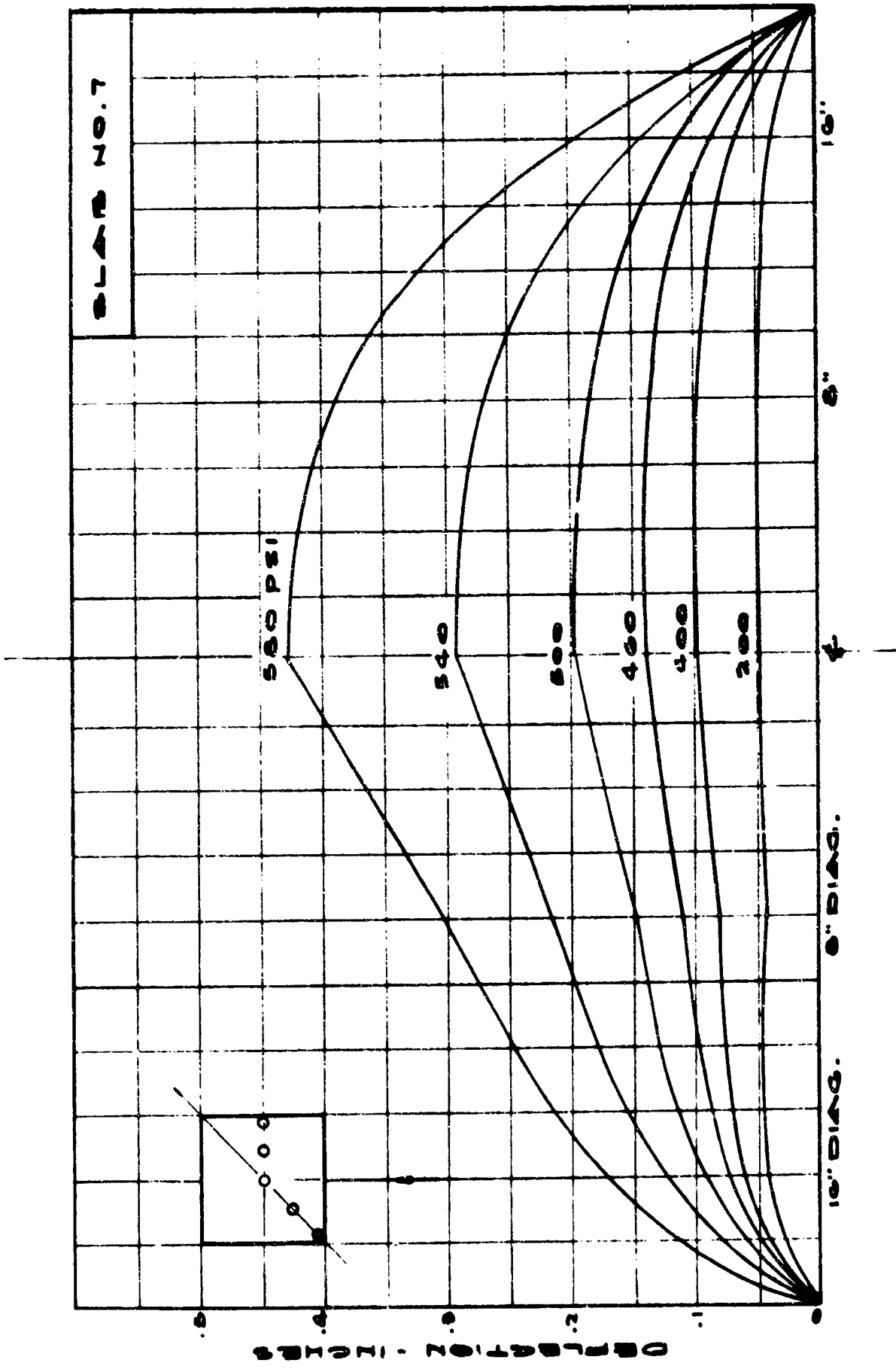


FIGURE 9 PROFILE OF TENSILE SURFACE FOR SLAB 7

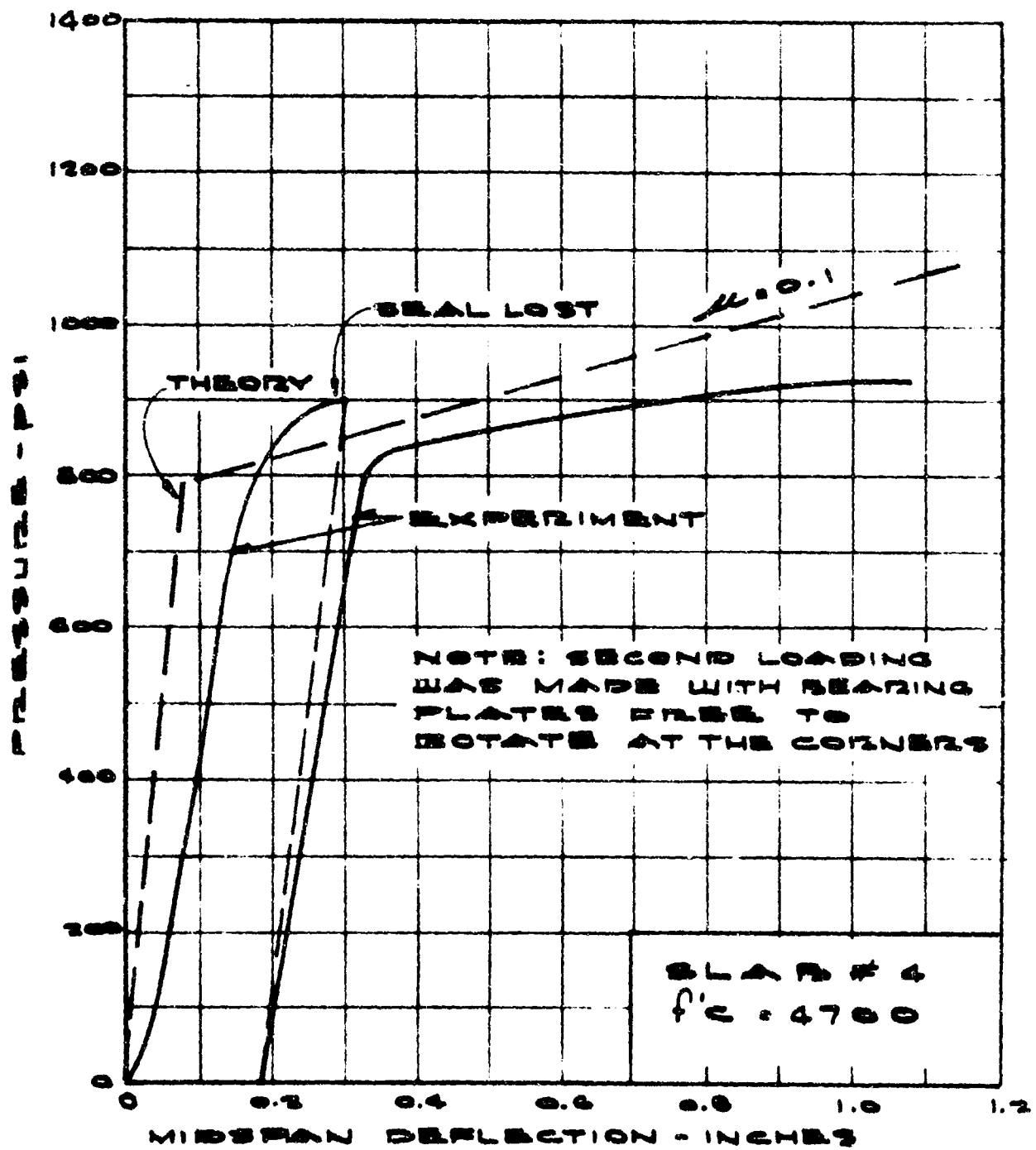


FIGURE 10. PRESSURE VERSUS MIDSPAN DEFLECTION FOR SLAB 4

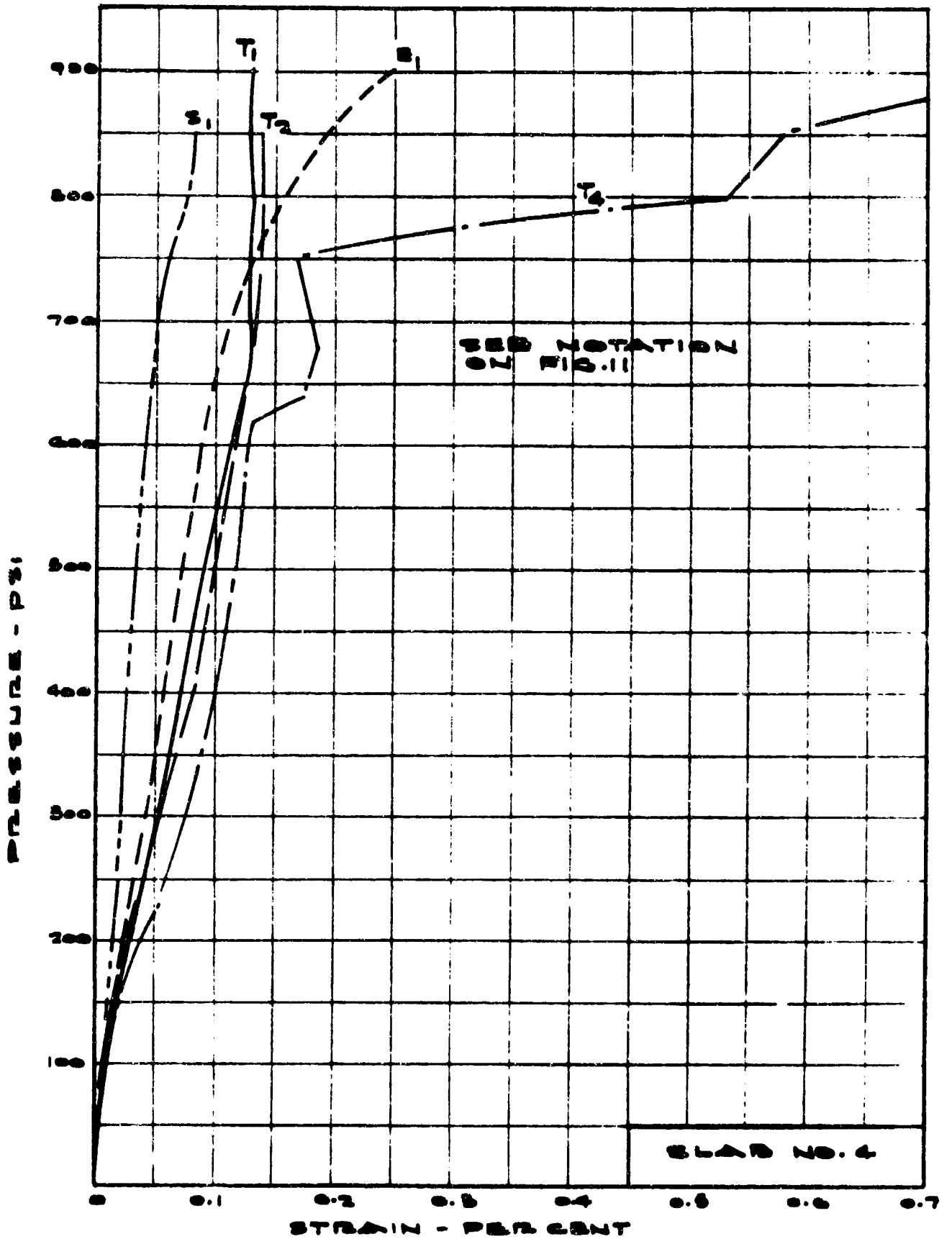


FIGURE 11. PRESSURE VERSUS STRAIN FOR SLAB 4

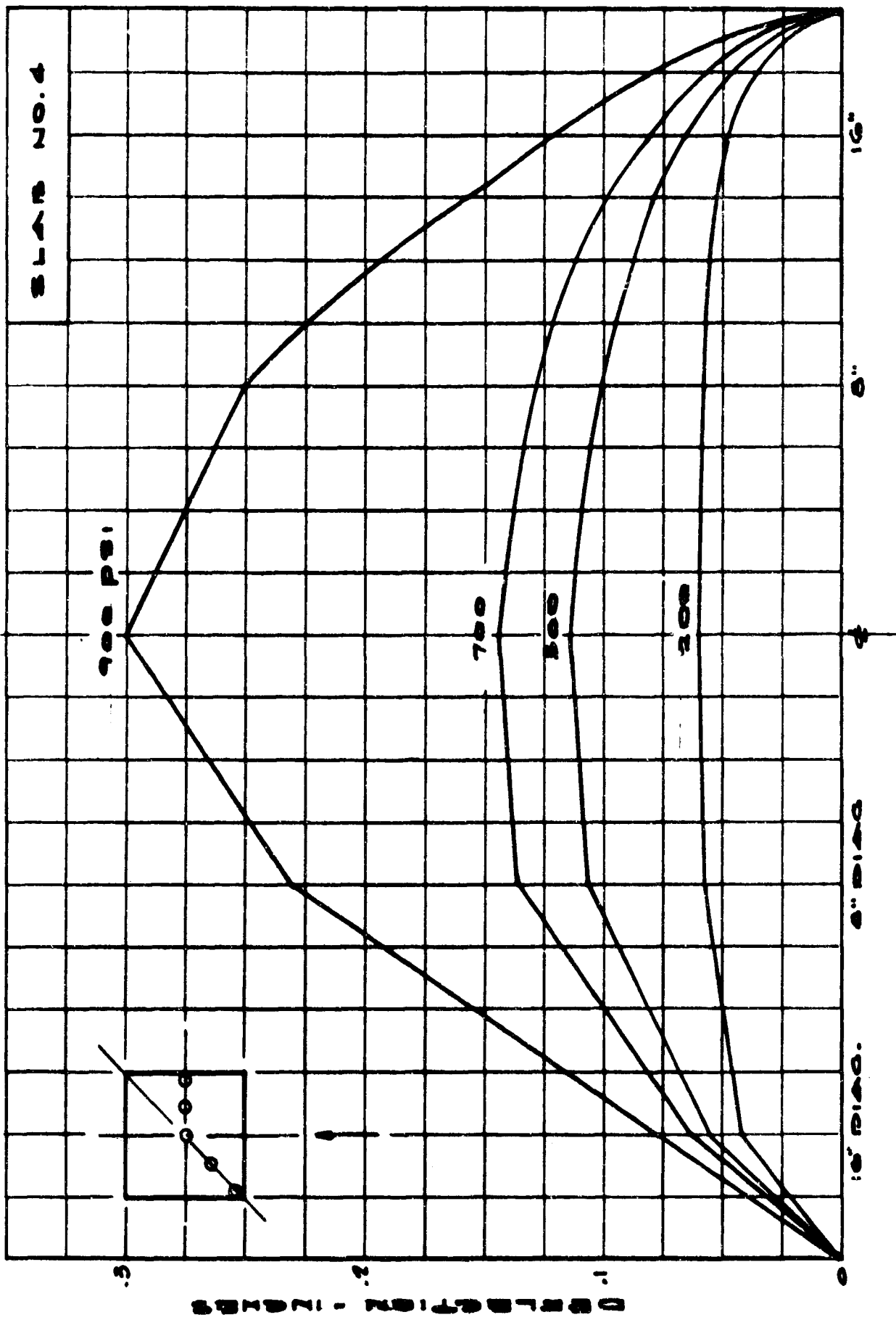


FIGURE 12. PROFILE OF TENSILE SURFACE FOR SLAB 4

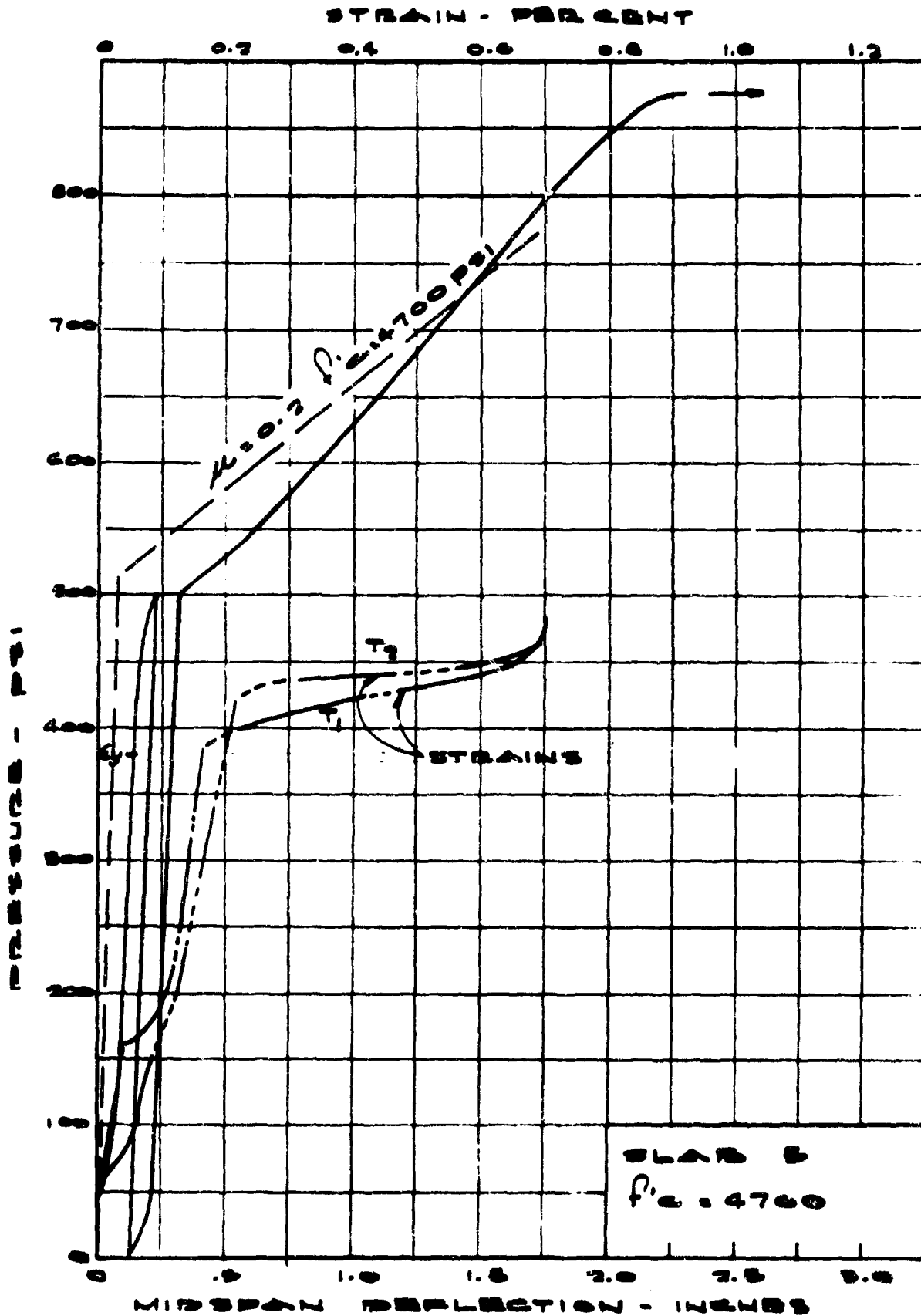


FIGURE 13. PRESSURE VERSUS MIDSPAN DEFLECTION FOR SLAB 5

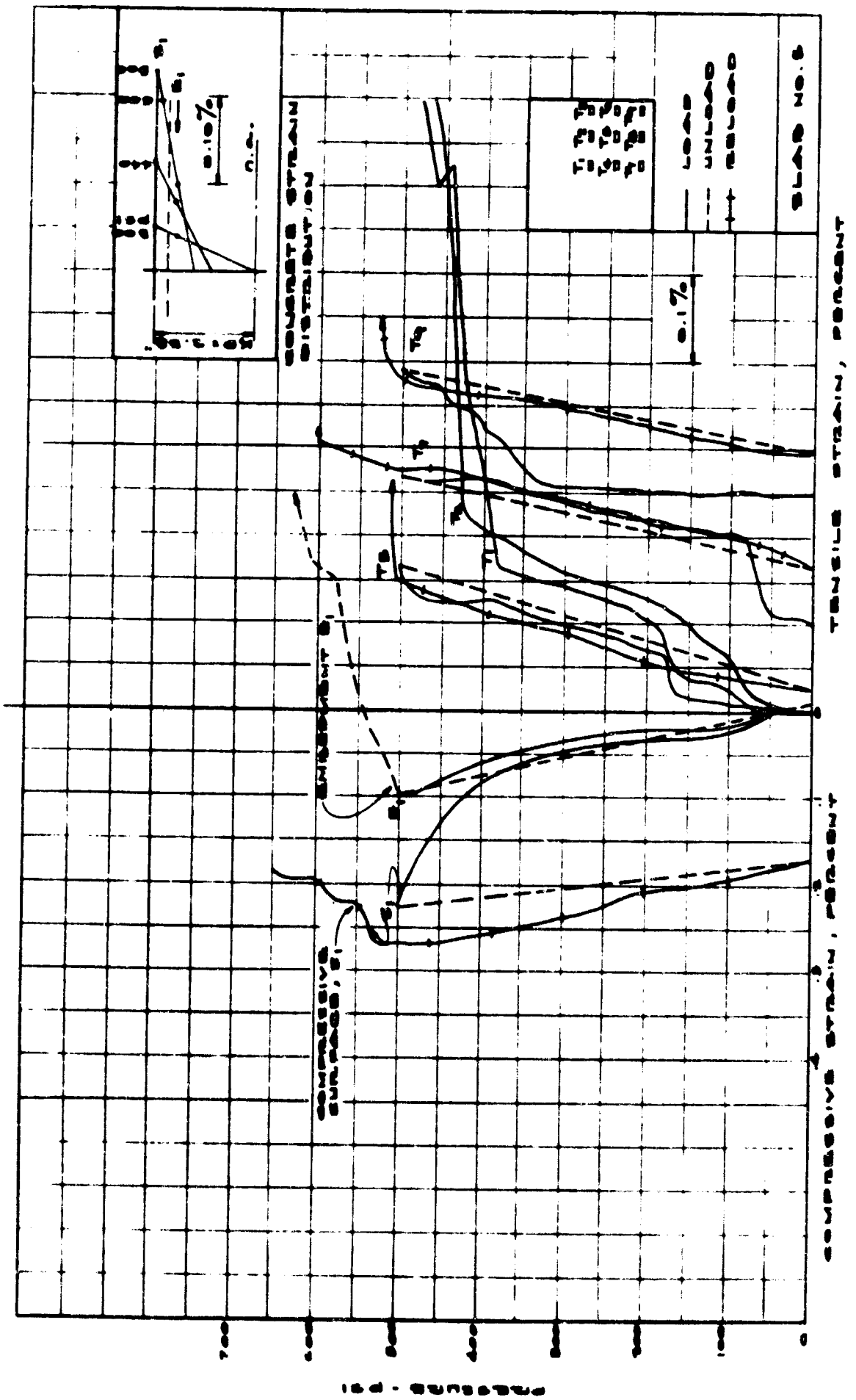


FIGURE 14. PRESSURE VERSUS STRAIN FOR SLAB 5

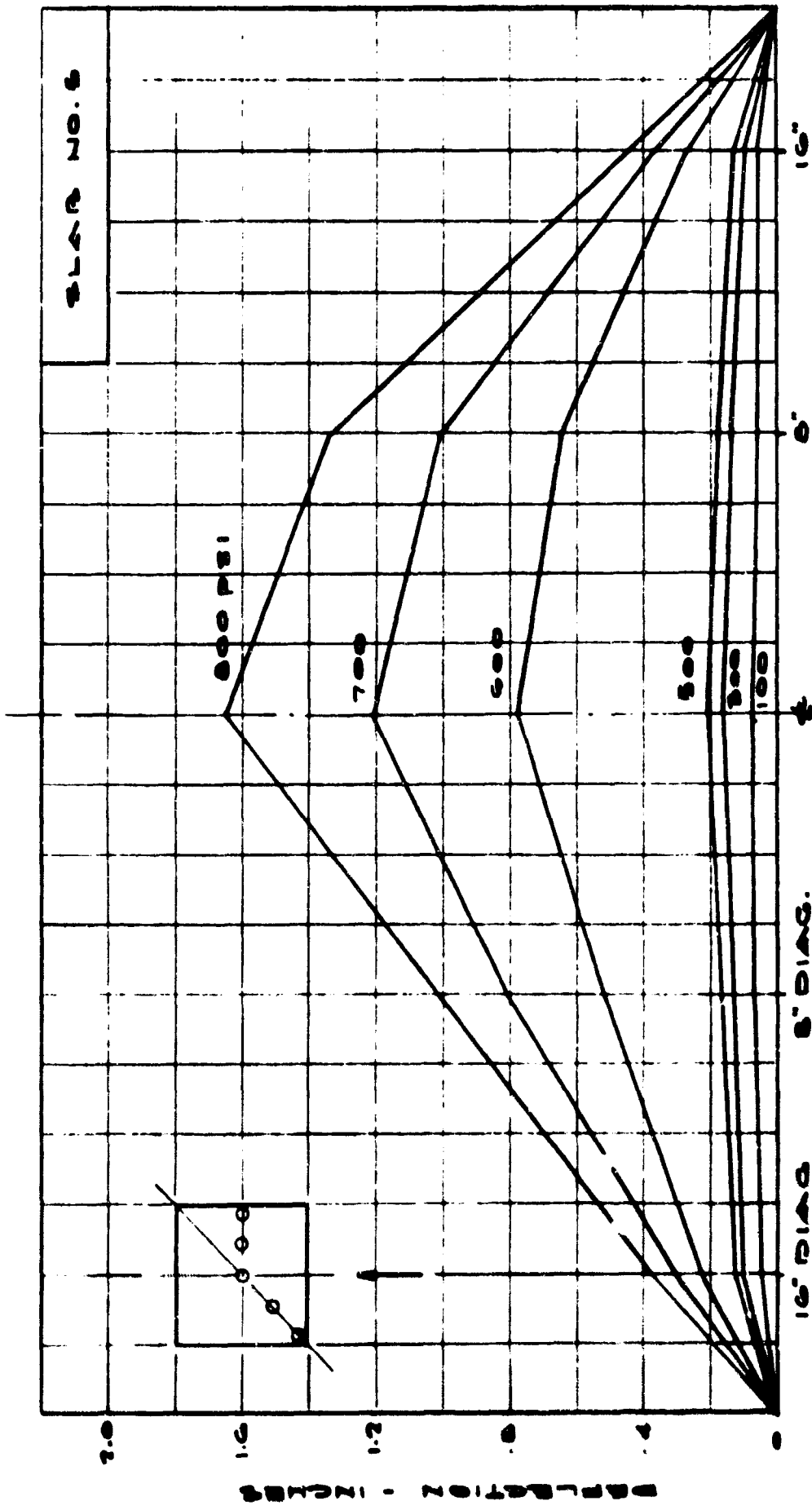


FIGURE 15. PROFILE OF TENSILE SURFACE FOR SLAB 5

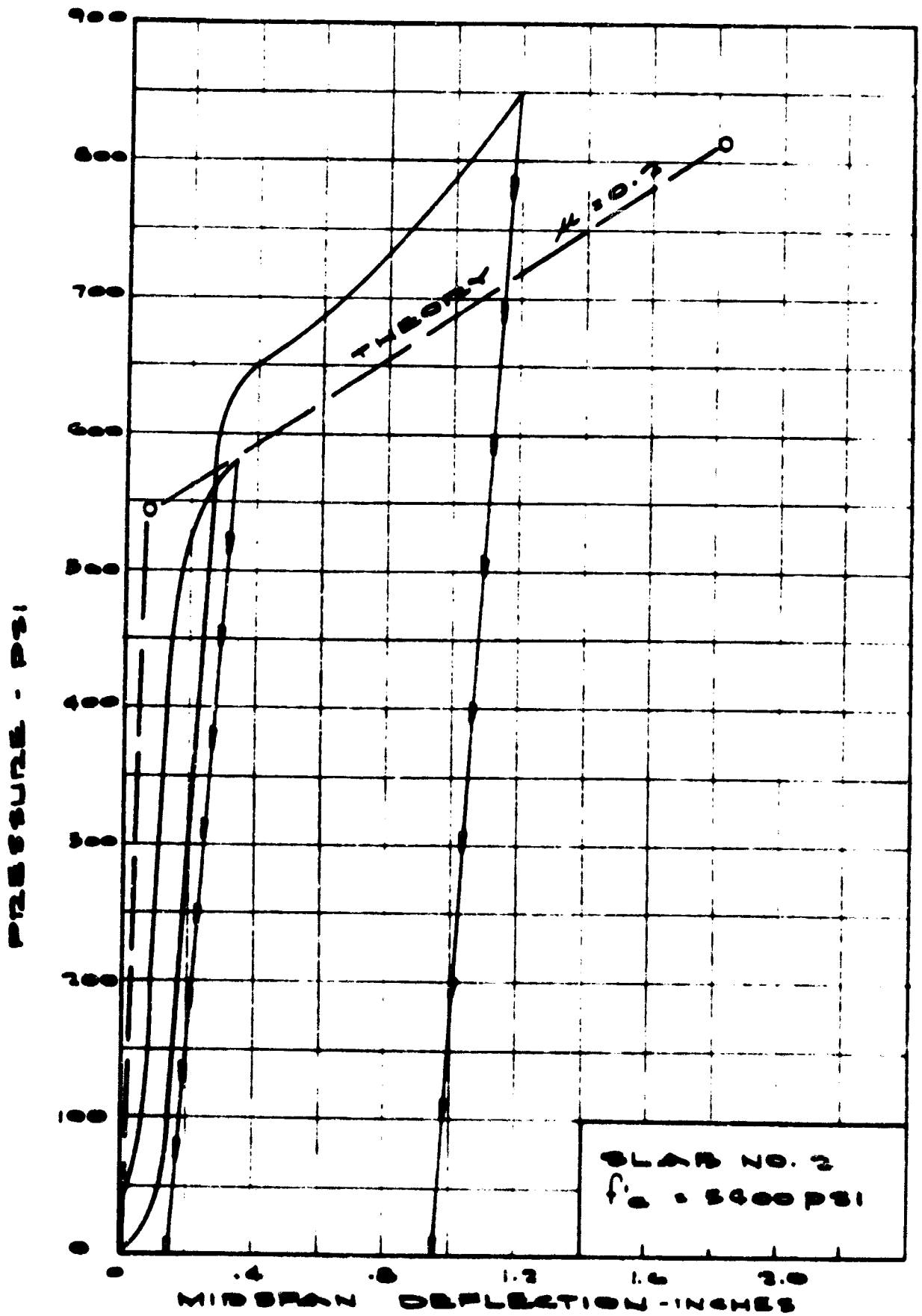


FIGURE 16. PRESSURE VERSUS MIDSPAN DEFLECTION FOR SLAB 2

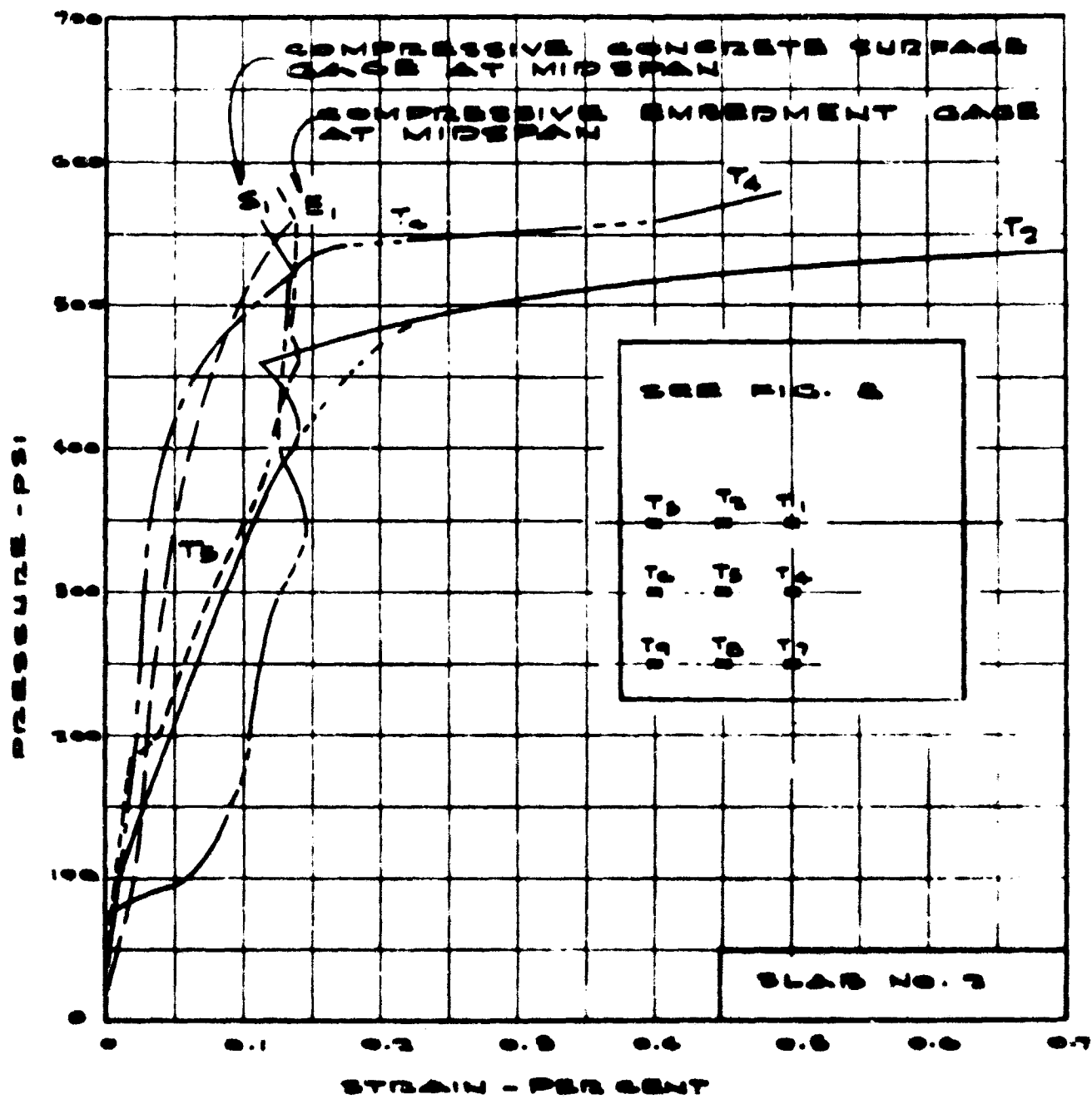


FIGURE 17 PRESSURE VERSUS STRAIN FOR SLAB 2

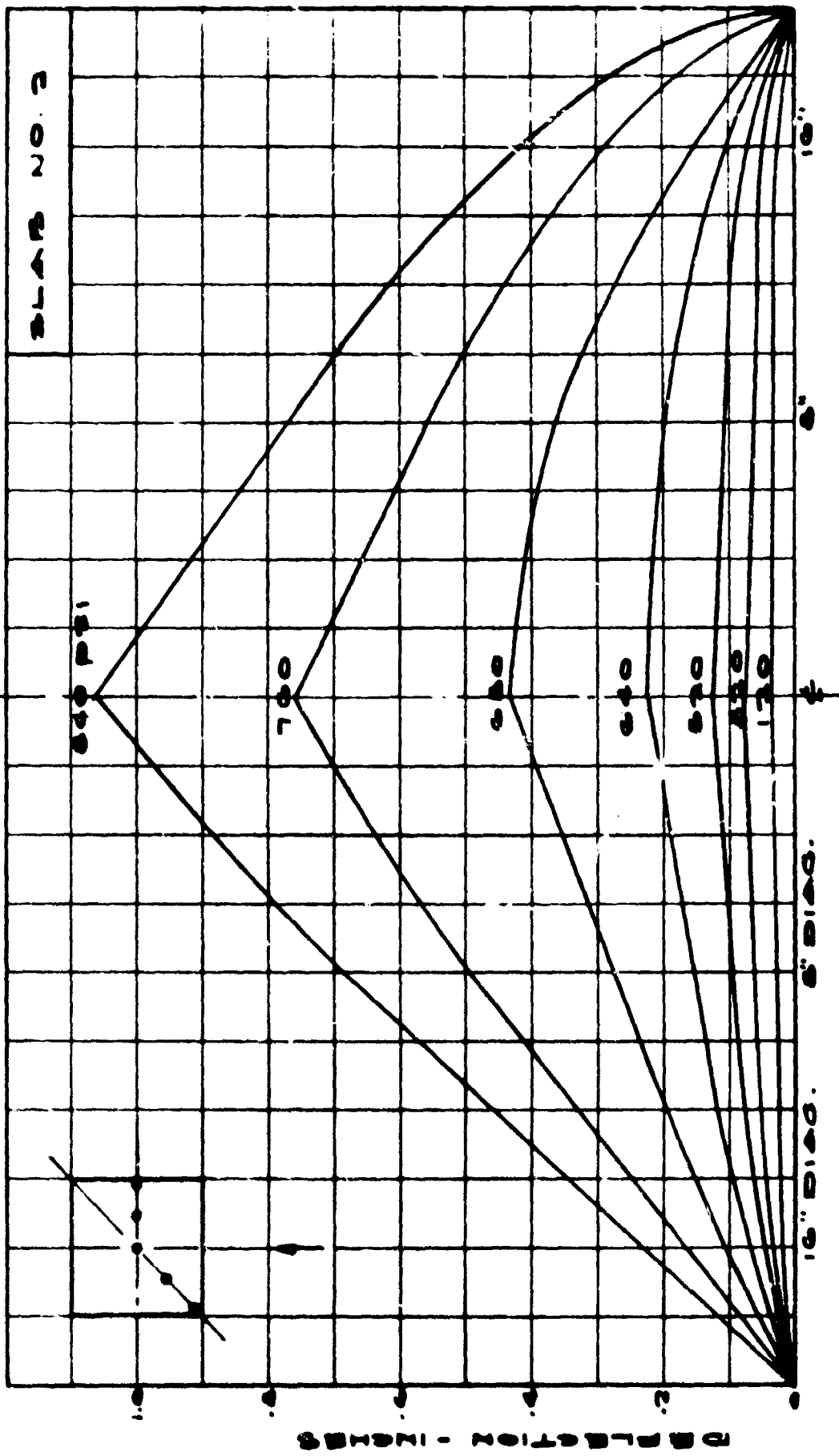


FIGURE 18. PROFILE OF TENSILE SURFACE FOR SLAB 2

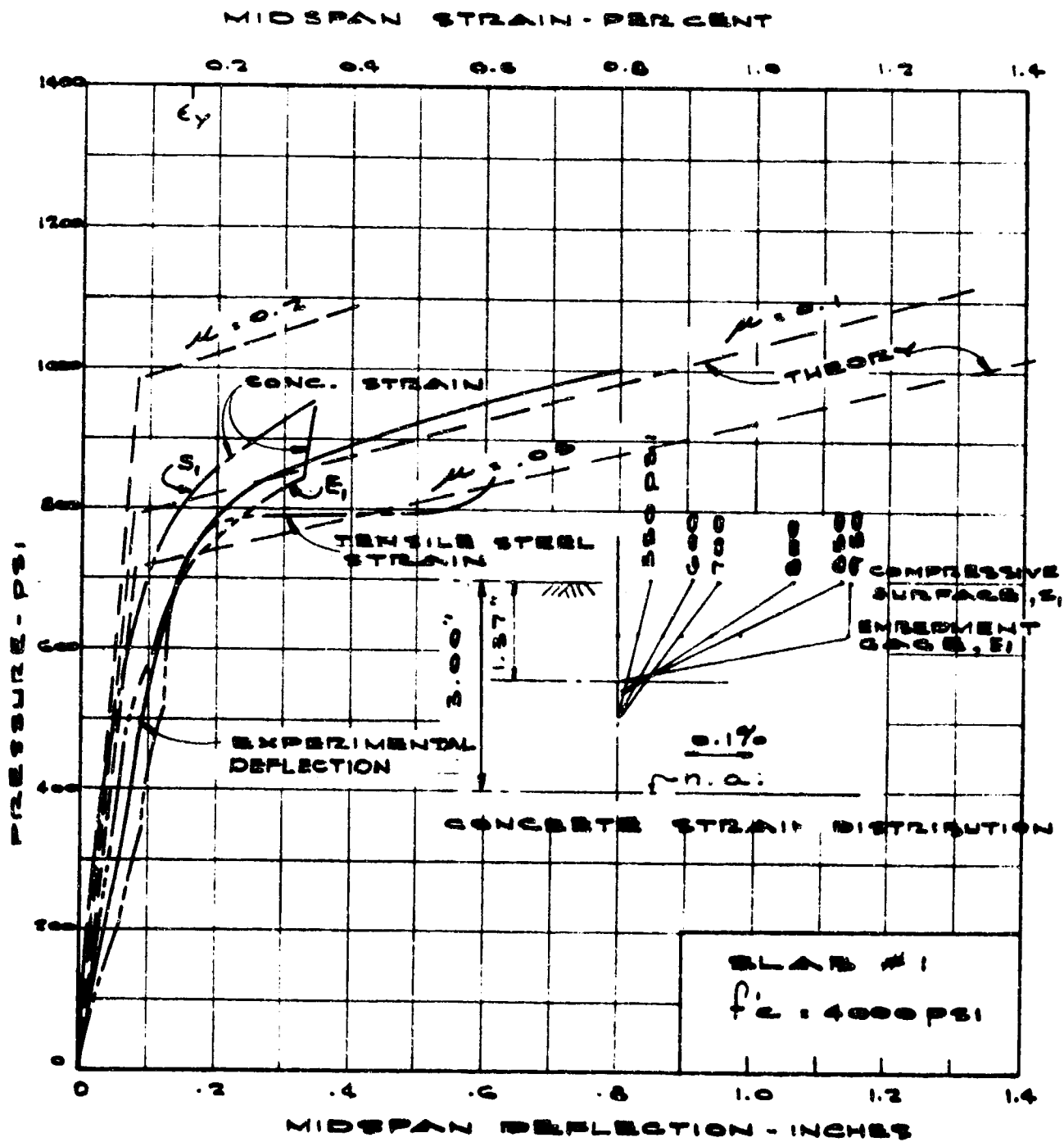


FIGURE 19. PRESSURE VERSUS MIDSPAN DEFLECTION FOR SLAB 1

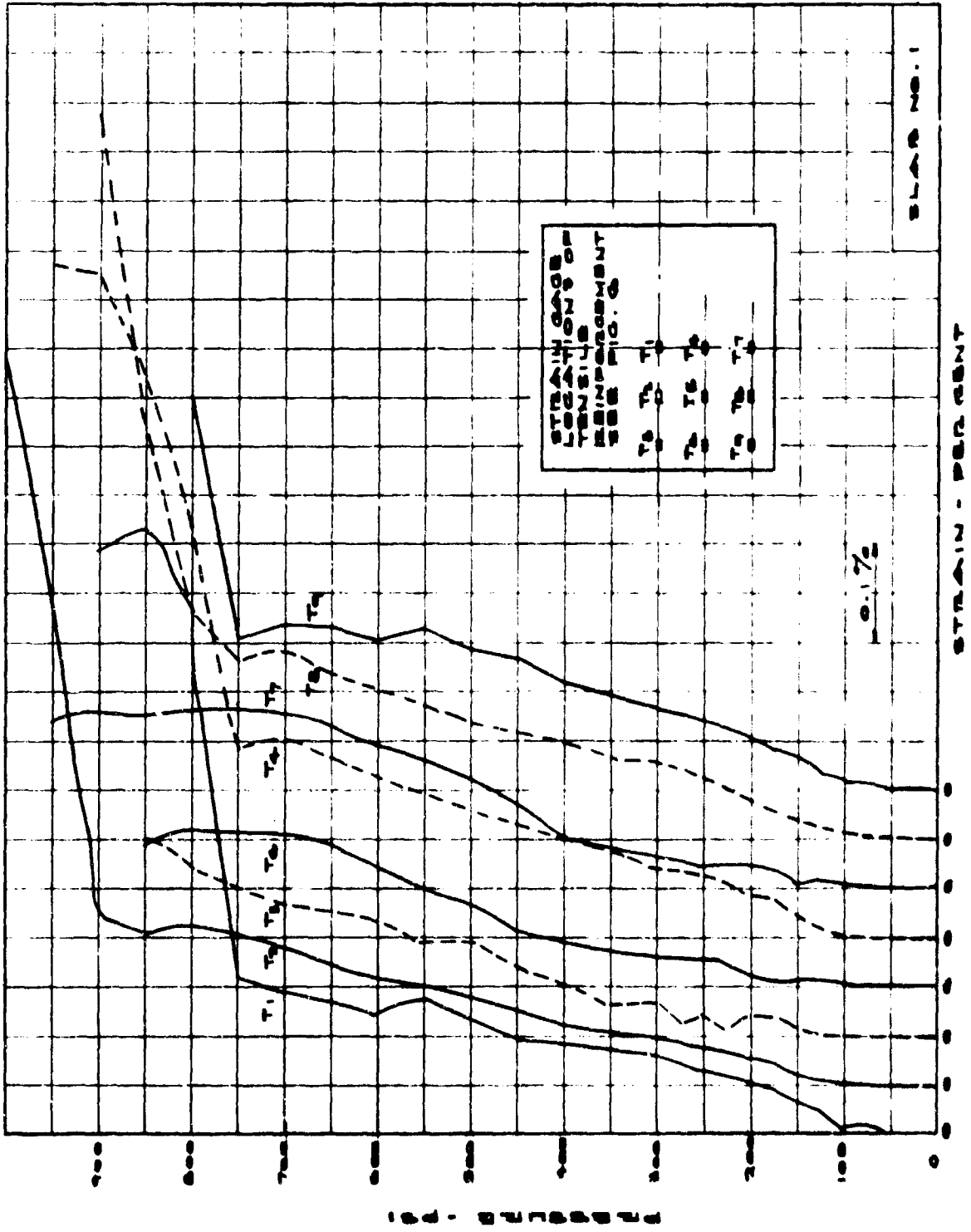


FIGURE 20. PRESSURE VERSUS STRAIN FOR SLAB 1

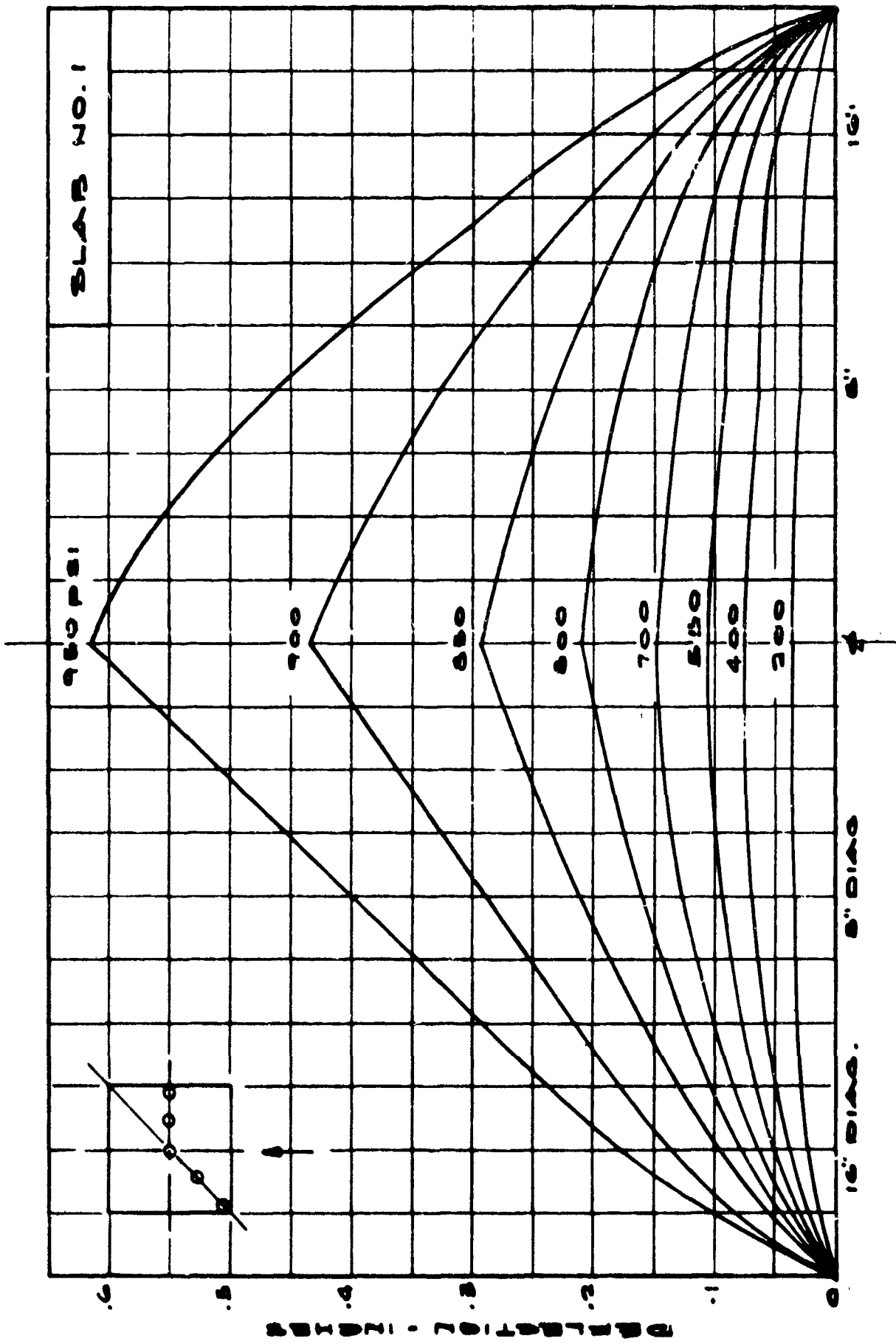


FIGURE 21. PROFILE OF TENSILE SURFACE FOR SLAB 1

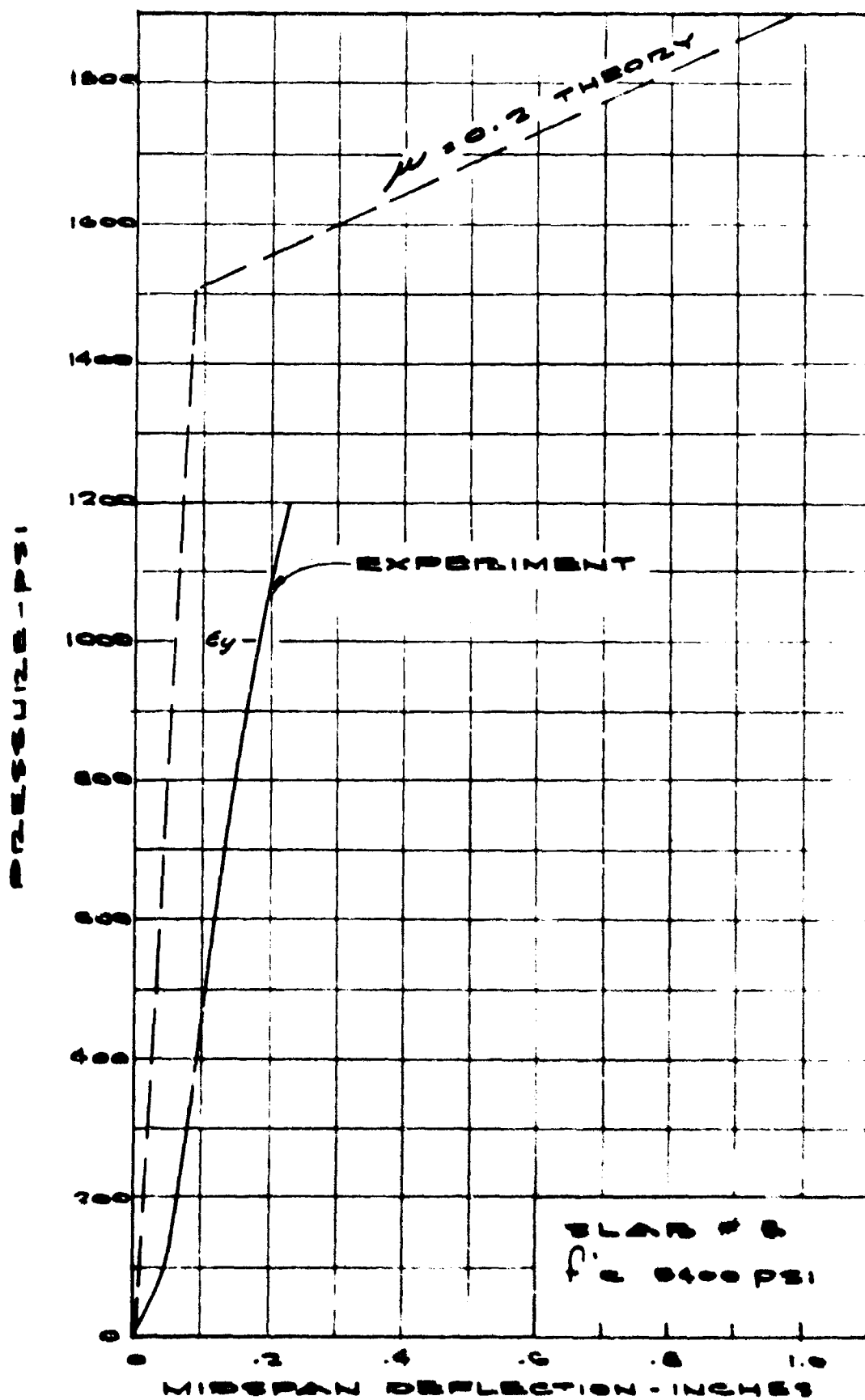


FIGURE 22. PRESSURE VERSUS MIDSPAN DEFLECTION FOR SLAB 3

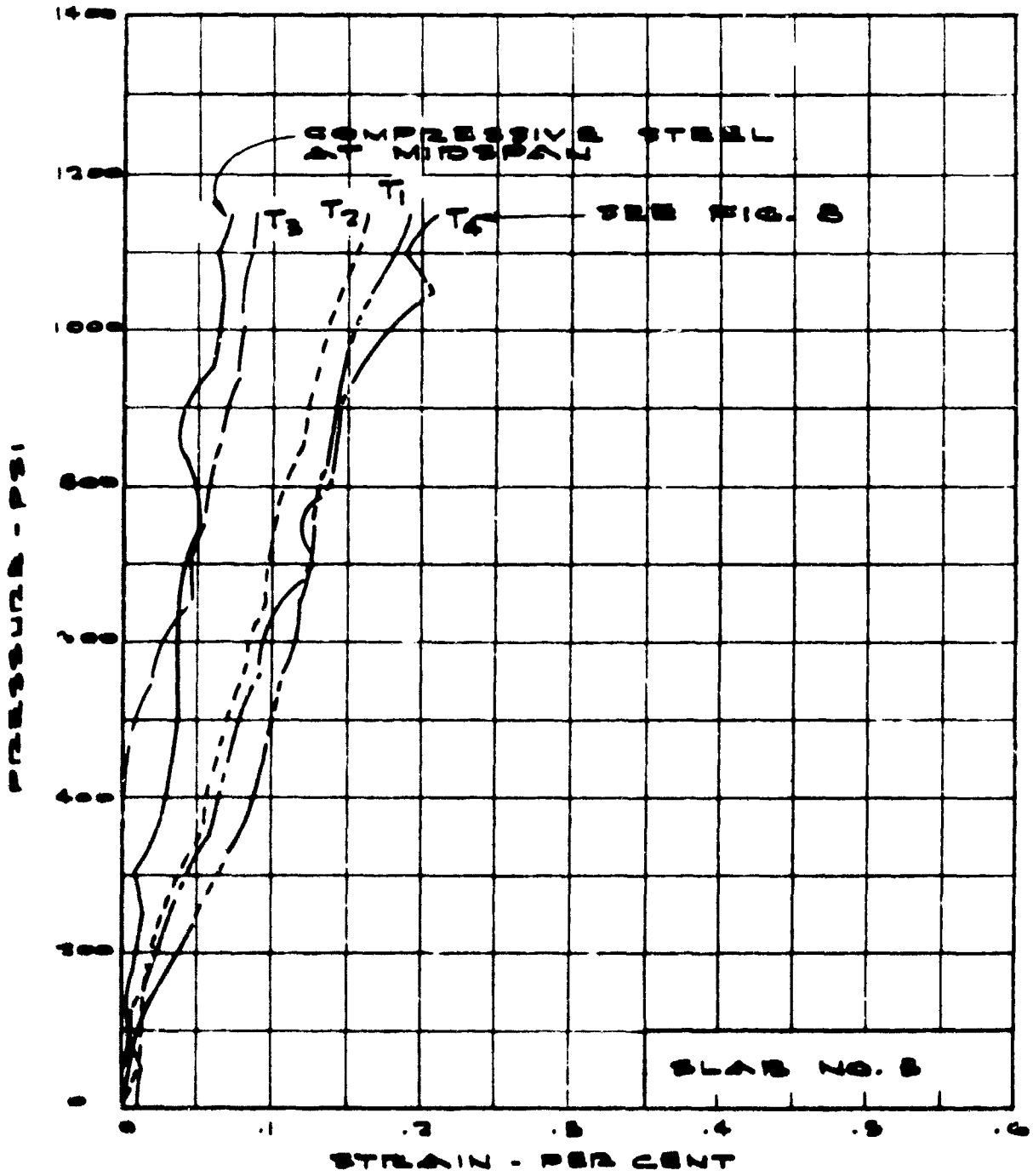


FIGURE 23. PRESSURE VERSUS STRAIN FOR SLAB 3

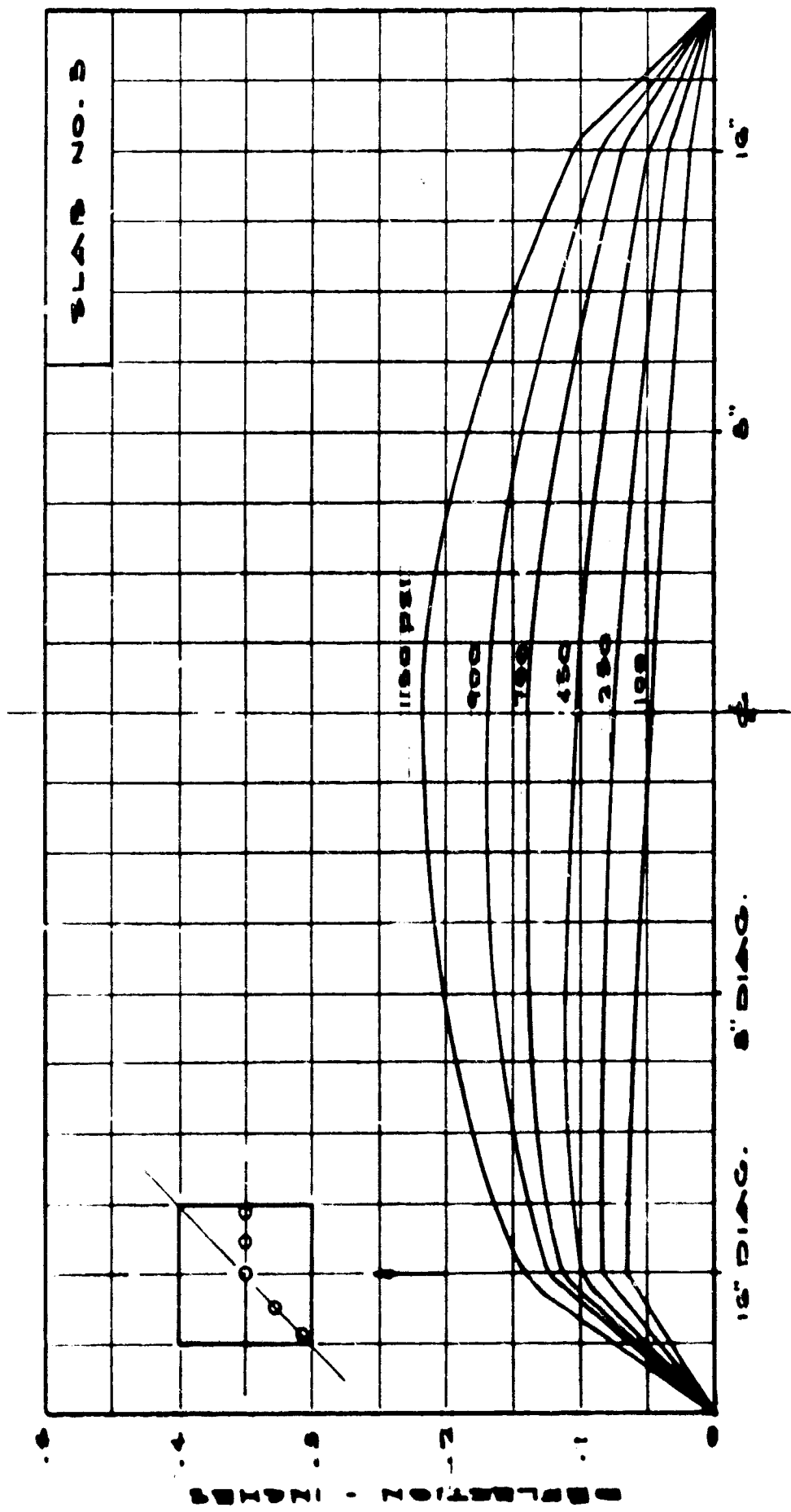


FIGURE 24. PROFILE OF TENSILE SURFACE FOR SLAB 3

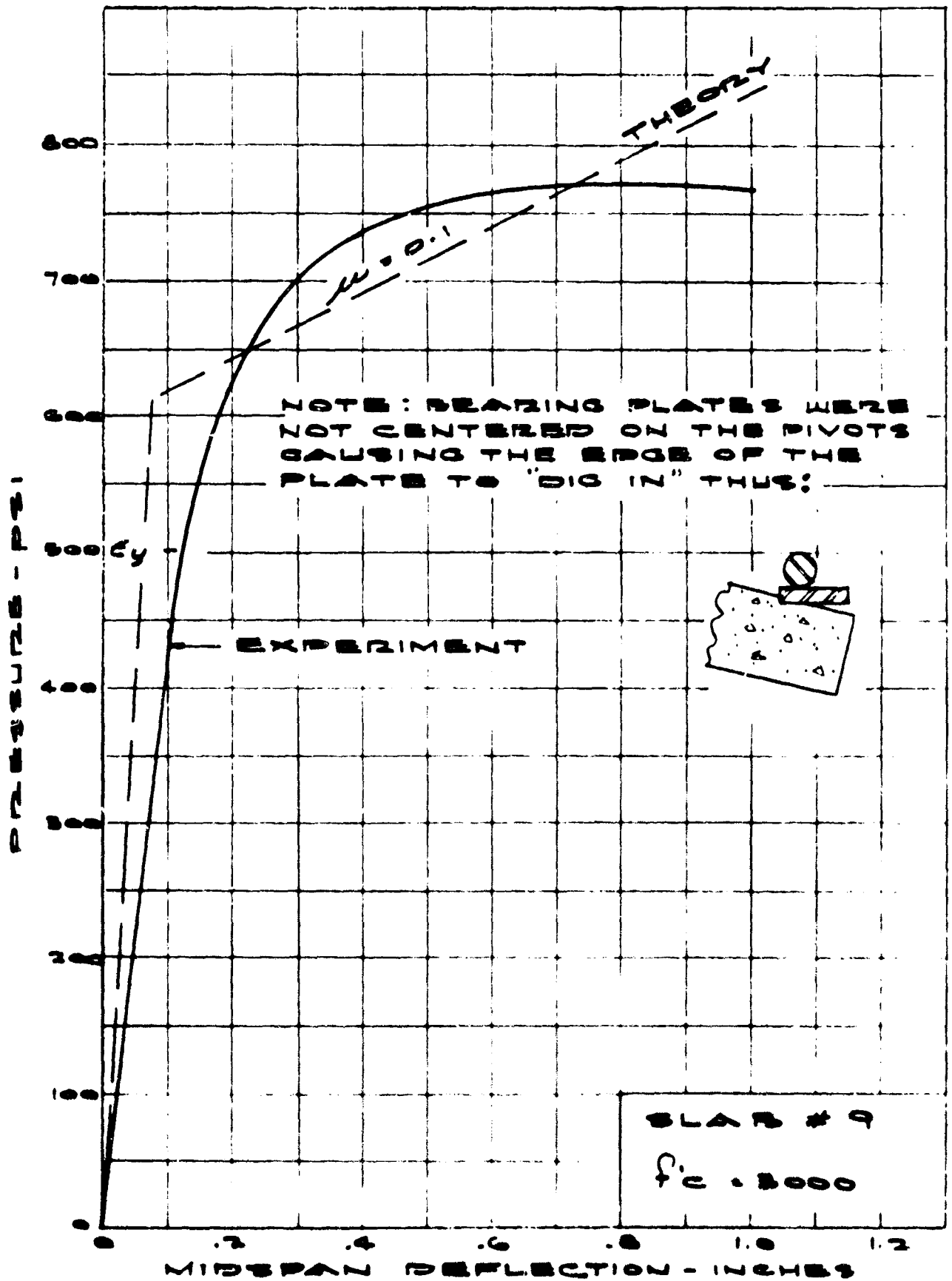


FIGURE 25. PRESSURE VERSUS MIDSPAN DEFLECTION FOR SLAB 9

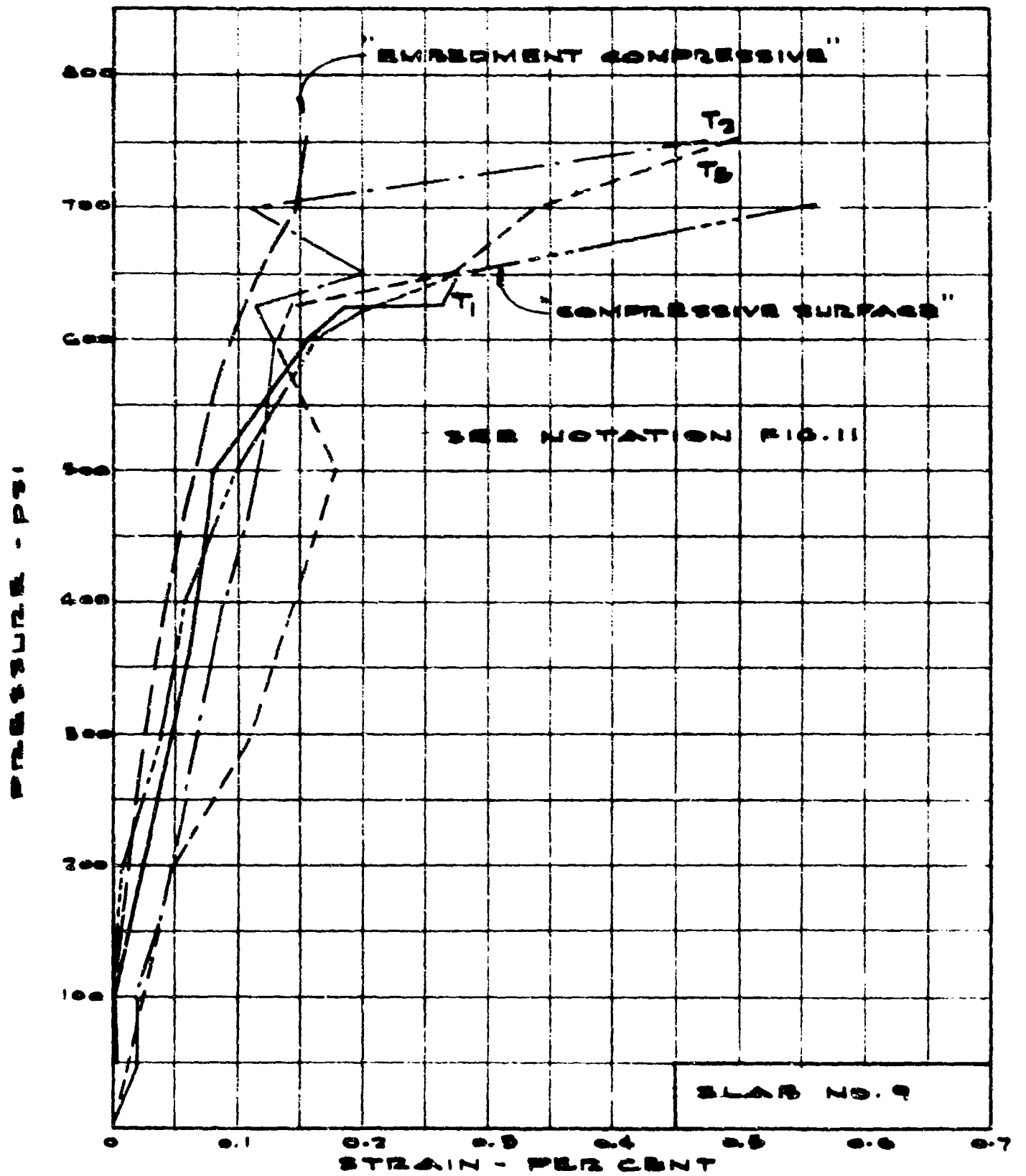


FIGURE 26. PRESSURE VERSUS STRAIN FOR SLAB 9

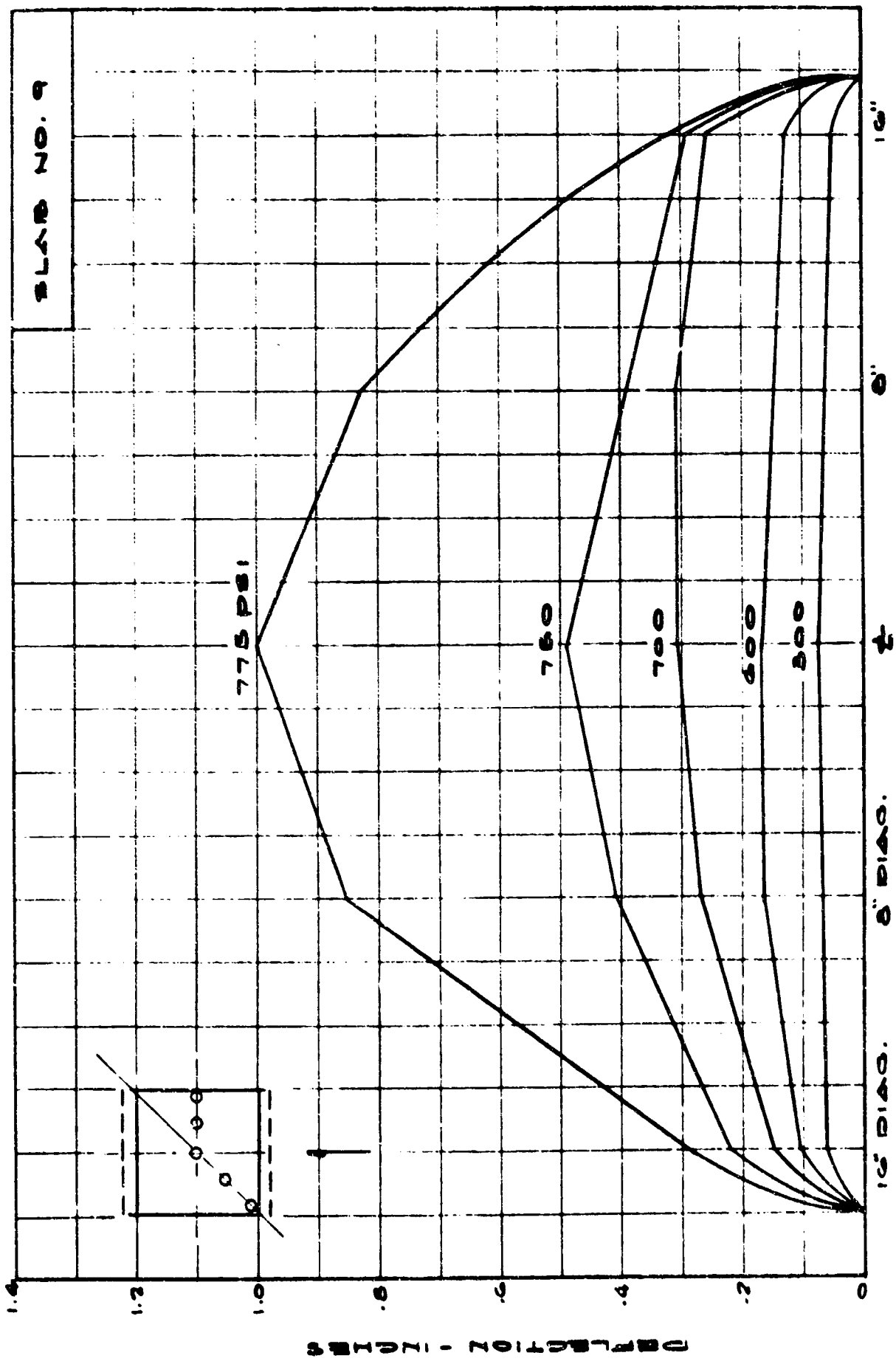


FIGURE 27 PROFILE OF TENSILE SURFACE FOR SLAB 9

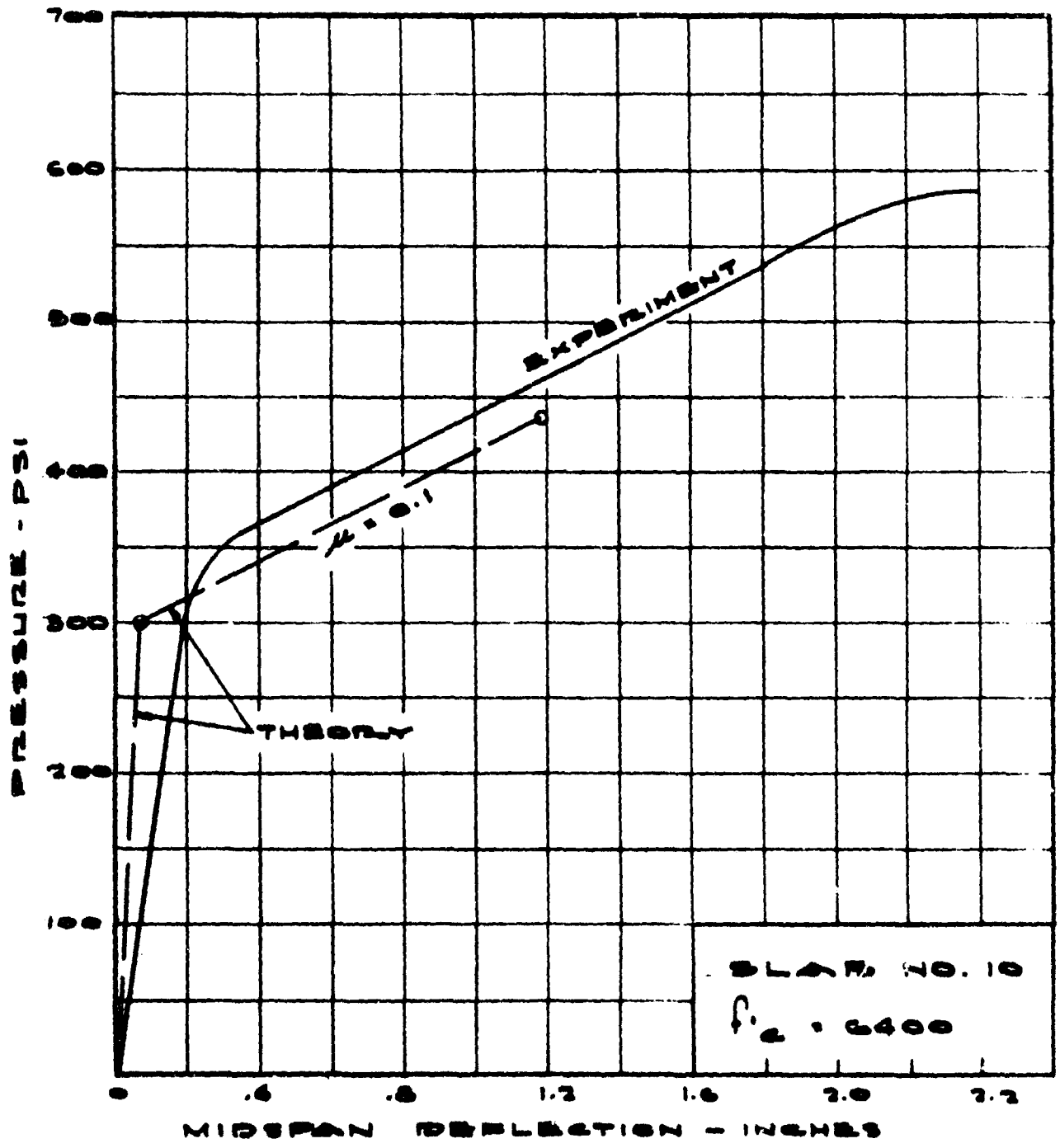


FIGURE 28. PRESSURE VERSUS MIDSPAN DEFLECTION FOR SLAB 10

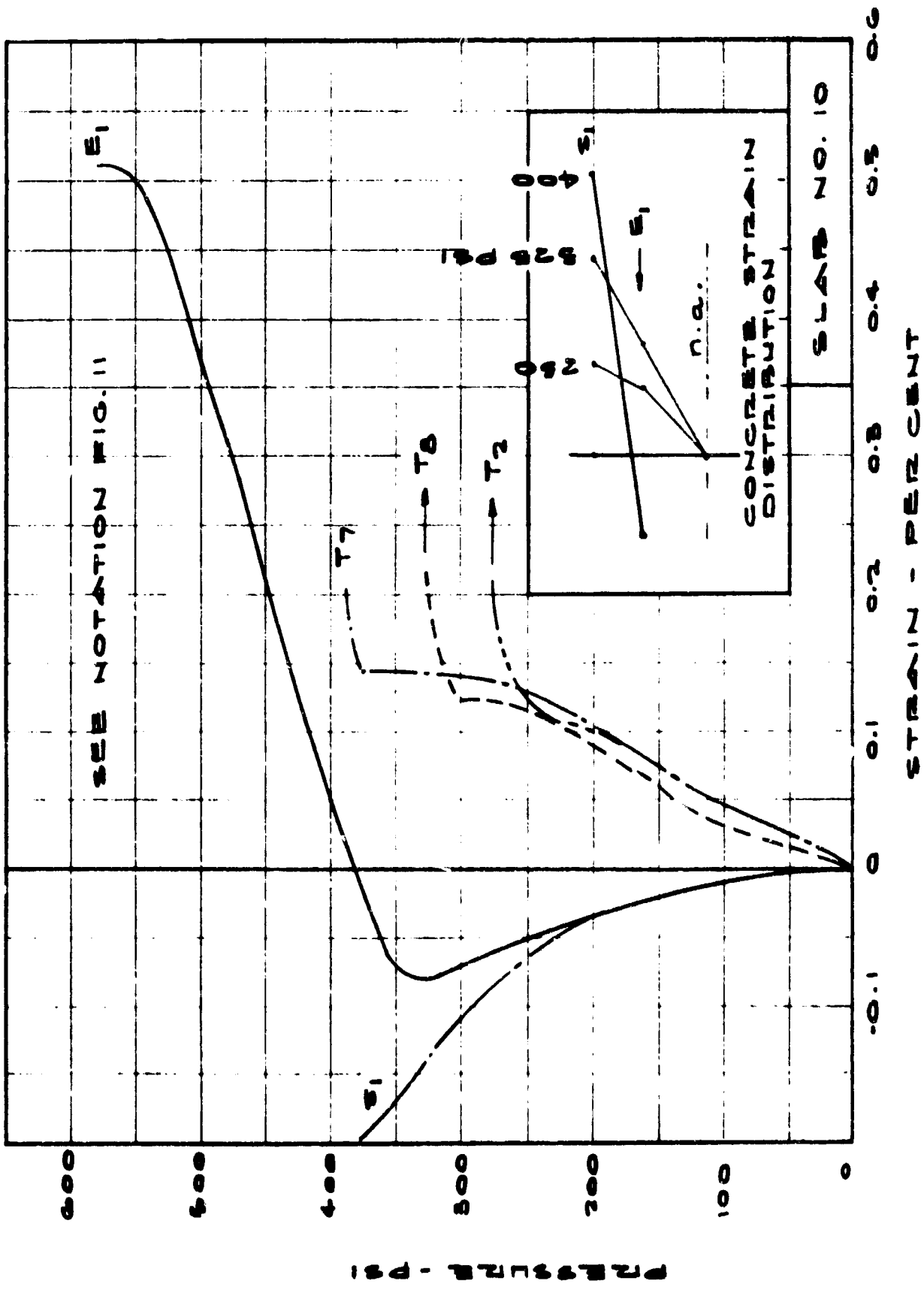


FIGURE 29 PRESSURE VERSUS STRAIN FOR SLAB 10

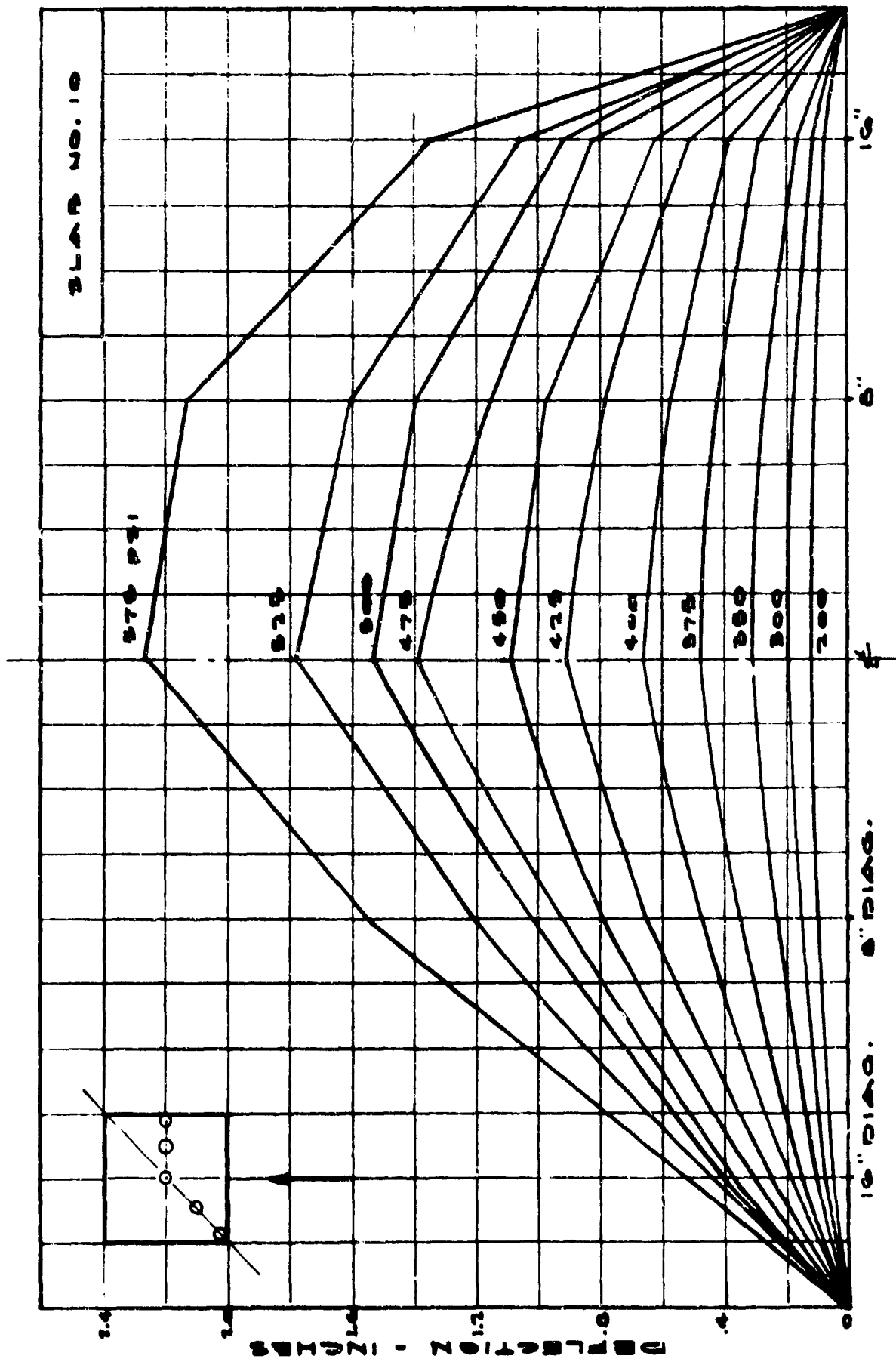


FIGURE 30. PROFILE OF TENSILE SURFACE FOR SLAB 10

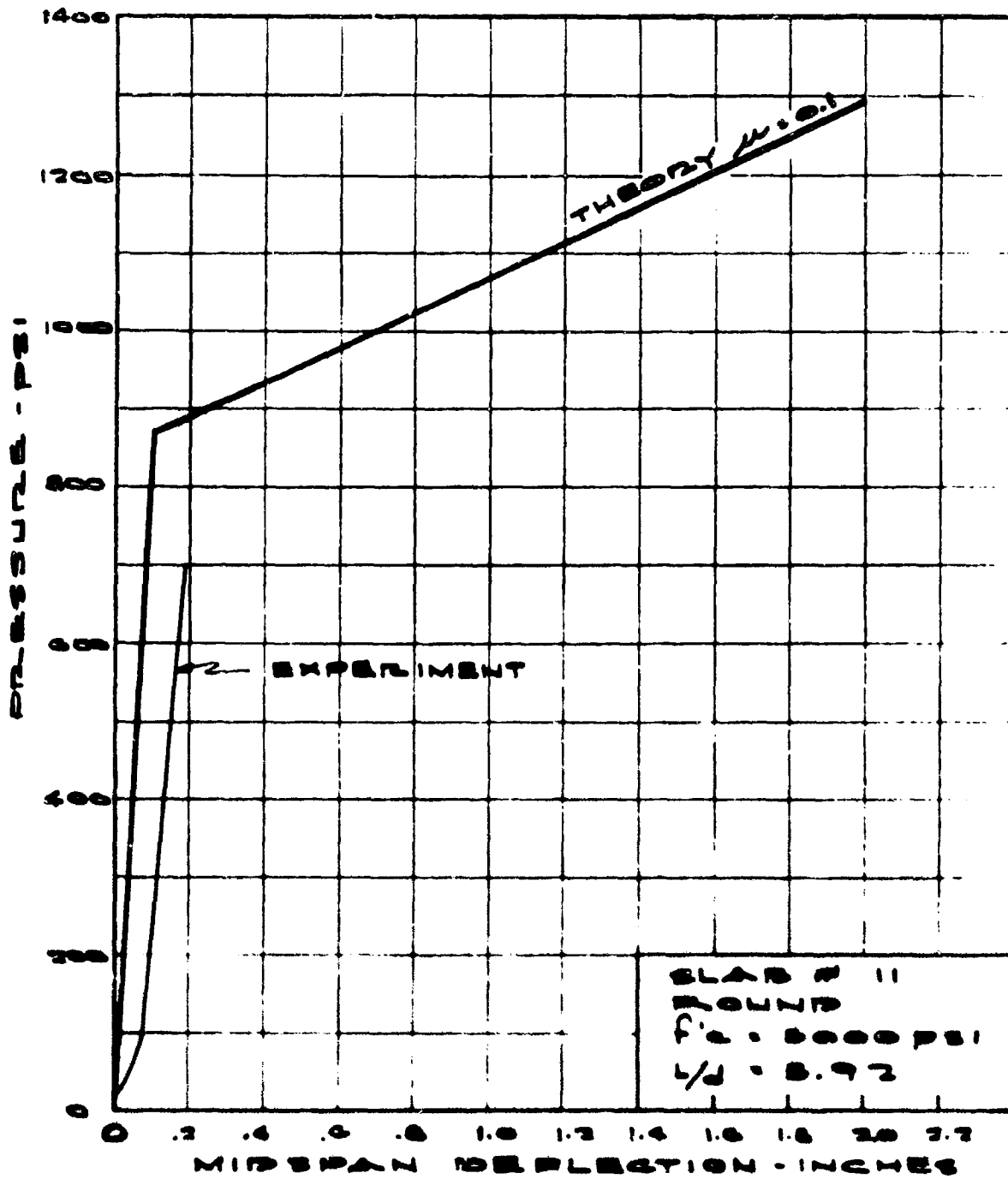


FIGURE 31. PRESSURE VERSUS MIDSPAN DEFLECTION FOR SLAB 11

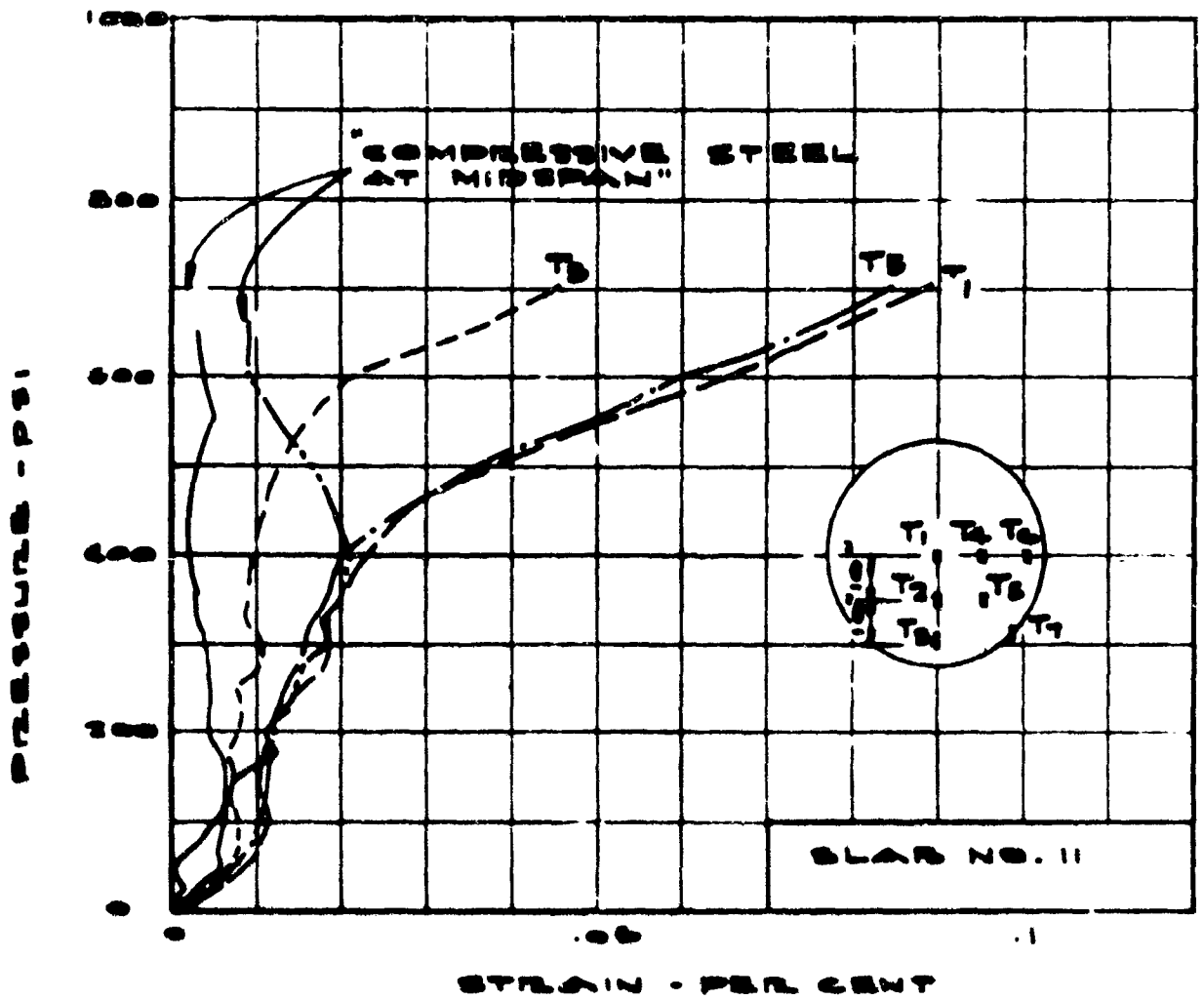


FIGURE 32. PRESSURE VERSUS STRAIN FOR SLAB 11

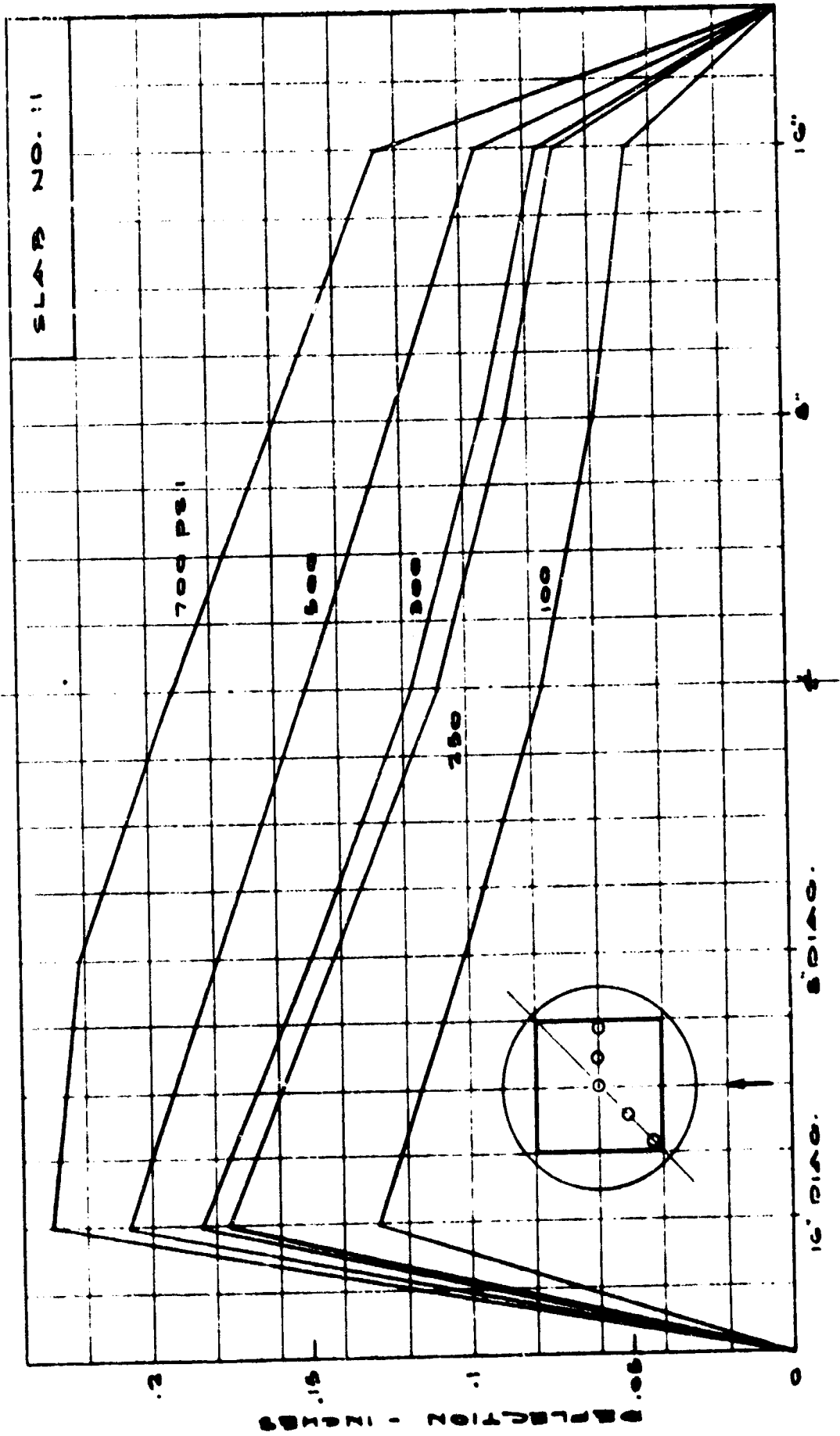


FIGURE 33 PROFILE OF TENSILE SURFACE FOR SLAB 11

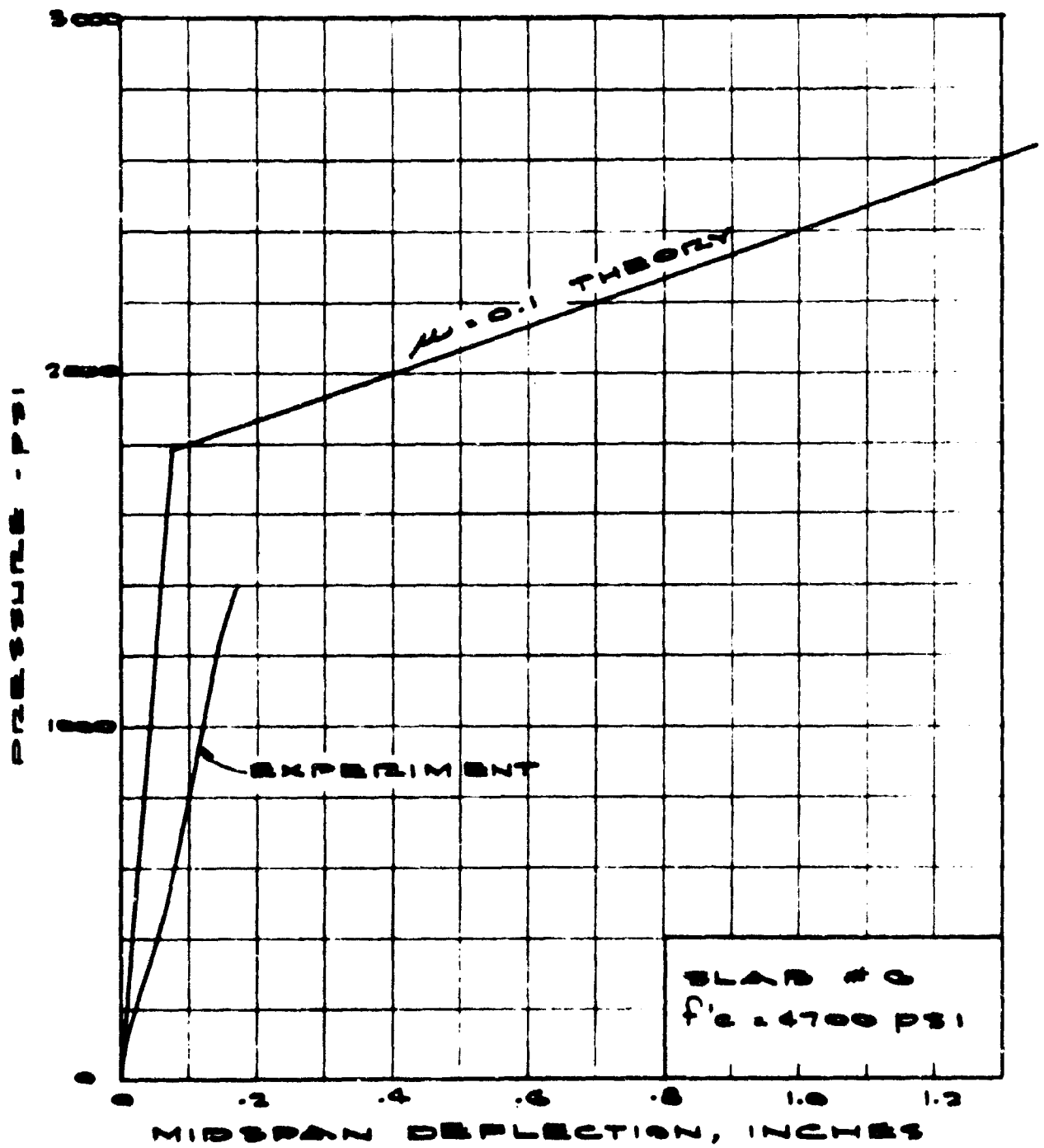


FIGURE 34. PRESSURE VERSUS MIDSPAN DEFLECTION FOR SLAB 6

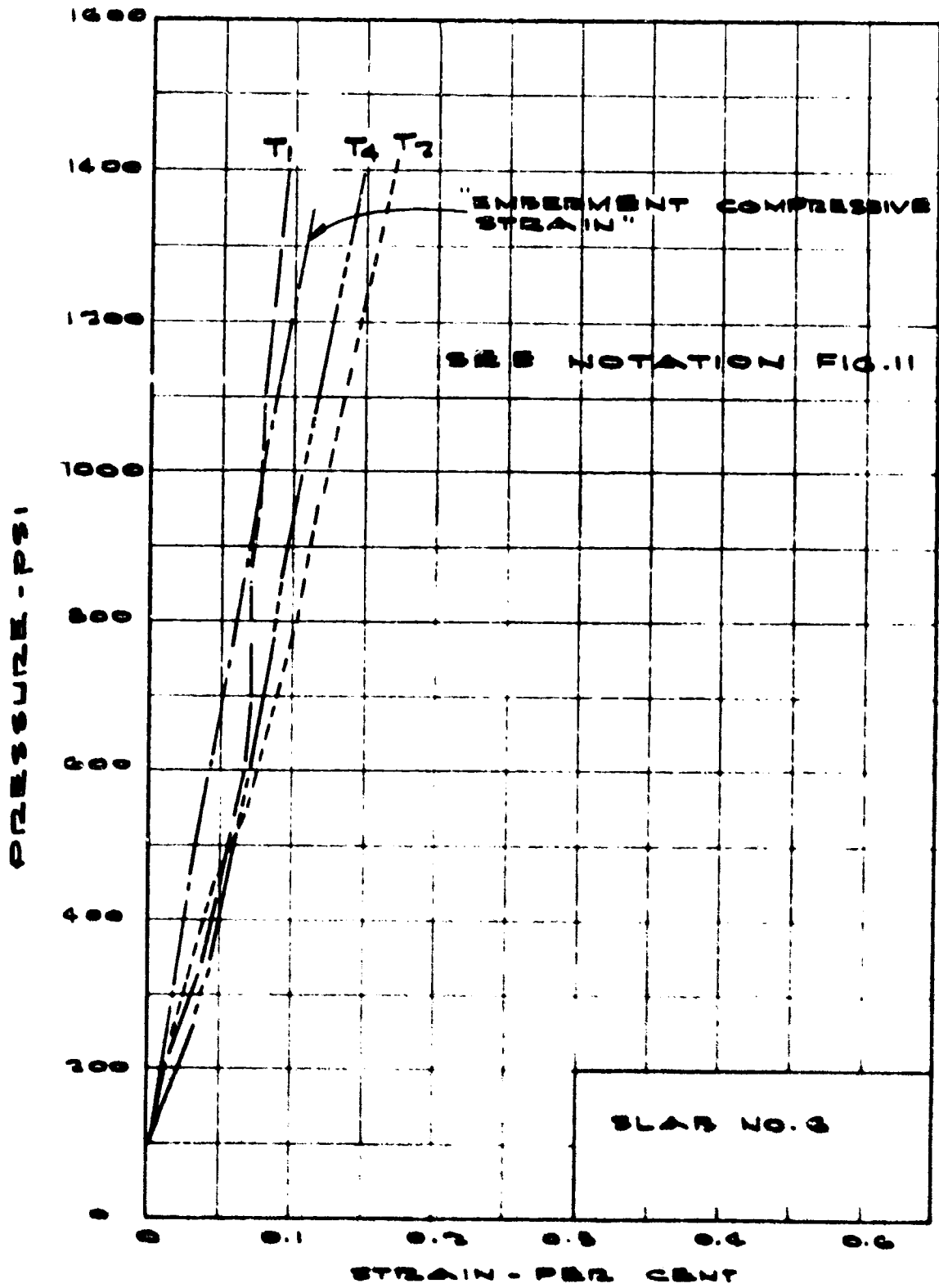


FIGURE 35. PRESSURE VERSUS STRAIN FOR SLAB 6

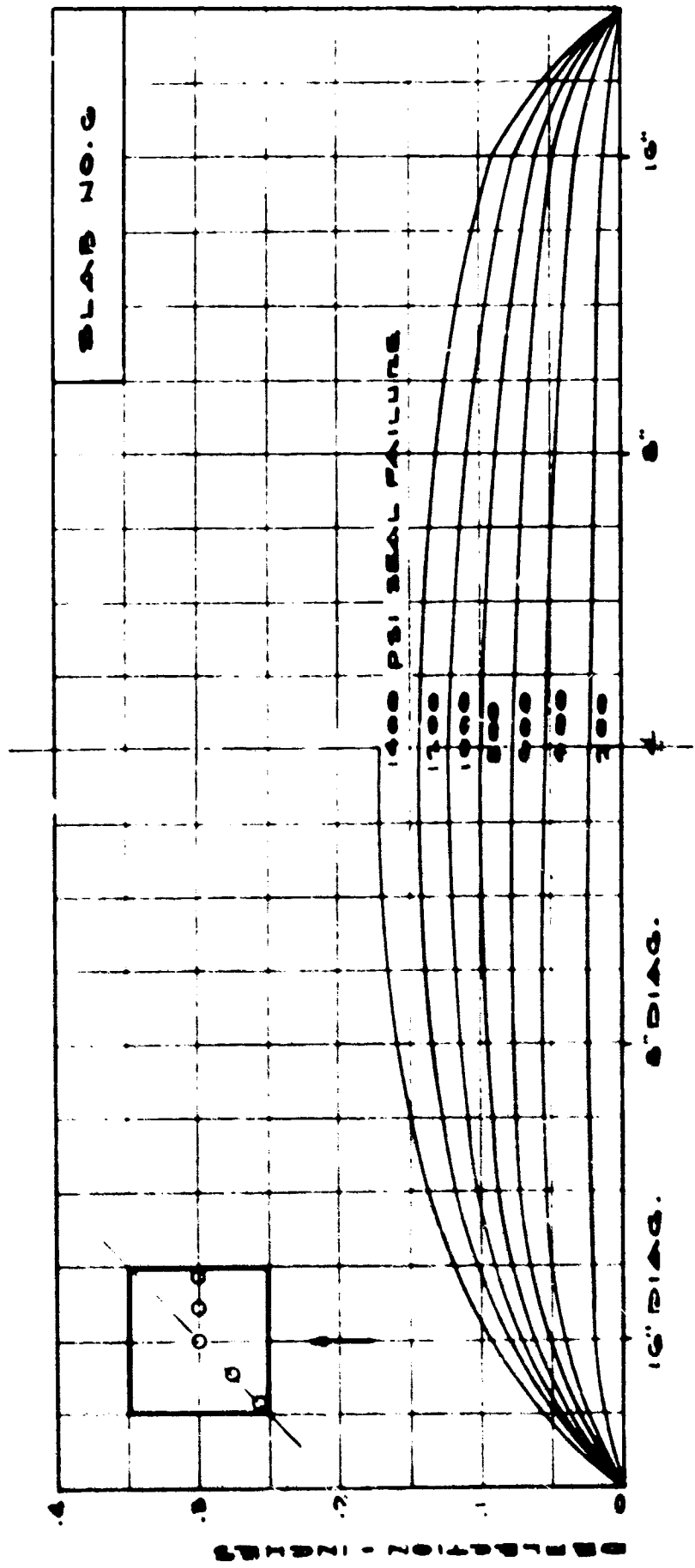


FIGURE 36. PROFILE OF TENSILE SURFACE FOR SLAB 6

J. General Discussion

The observed cracking pattern is indicated in Figure 37 and photographed in Figures 38 and 39. The expected cracking pattern as shown in Appendix B, Figure B2, is very similar. The progressive development of these cracks as the load was being applied was found to be essentially as described in the yield line analysis of Appendix B.

Section A-A, Figure 37, shows the slab cracking observed through the depth of the slab. The concrete in compression formed a dome-like structure, similar to the tied arch behavior found in the deep beam investigations^{1, 2}. The tensile reinforcement bars were the tension ties in this dome; however, the friction forces also supported the dome like an abutment. The diagonal cracks were also bridged with arch action across the corners of the slab as shown by Section B-B of Figure 37. The reinforcement bars in both directions were securely anchored with hooks under the bearing plates thus providing a substantial planar tie for the dome-like structure.

When the deflections of the slab become large with respect to the span-depth ratio, the edge of the slab tends to slip inward which is in the opposite direction from the tendency associated with small deflections. This, in effect, puts a tensile force on the edge of the slab and a positive edge moment. The net effect appears to reduce the compressive strains in the concrete. Since crushing of the concrete was the assumed failure criterion, the reduction in compressive strains would have the end result of increasing the magnitude of predicted deflections and ultimate pressure. The equations in Appendix B do not consider the possibility of such behavior. It is to be noted that the concrete surface strain gages in several of the slabs (1, 2, 4, 5 and 7) behaved at large deflections in a manner suggesting a reduced rate of compressive strain. Some of the gages indicated no compressive strain increase or even showed a reduction in compressive strain magnitude.

The predicted failure mechanism (Appendix B) of crushing of the concrete in compression was not observed at midspan. Although crushing on the diagonals was observed, this did not lead immediately to collapse of the slab. Even Slab 10 did not evidence crushing of the concrete at midspan even though the maximum deflection was twice the predicted "ultimate" deflection, and the maximum pressure was 35 percent greater than the predicted "ultimate" pressure.

The failure mechanism was found (Figure 40) to be that experienced by the previous investigations⁸. This mechanism is described as crushing on the diagonals that changes to tensile cracks which cut right through the slab. The tensile cracks cutting through to the "compressive"

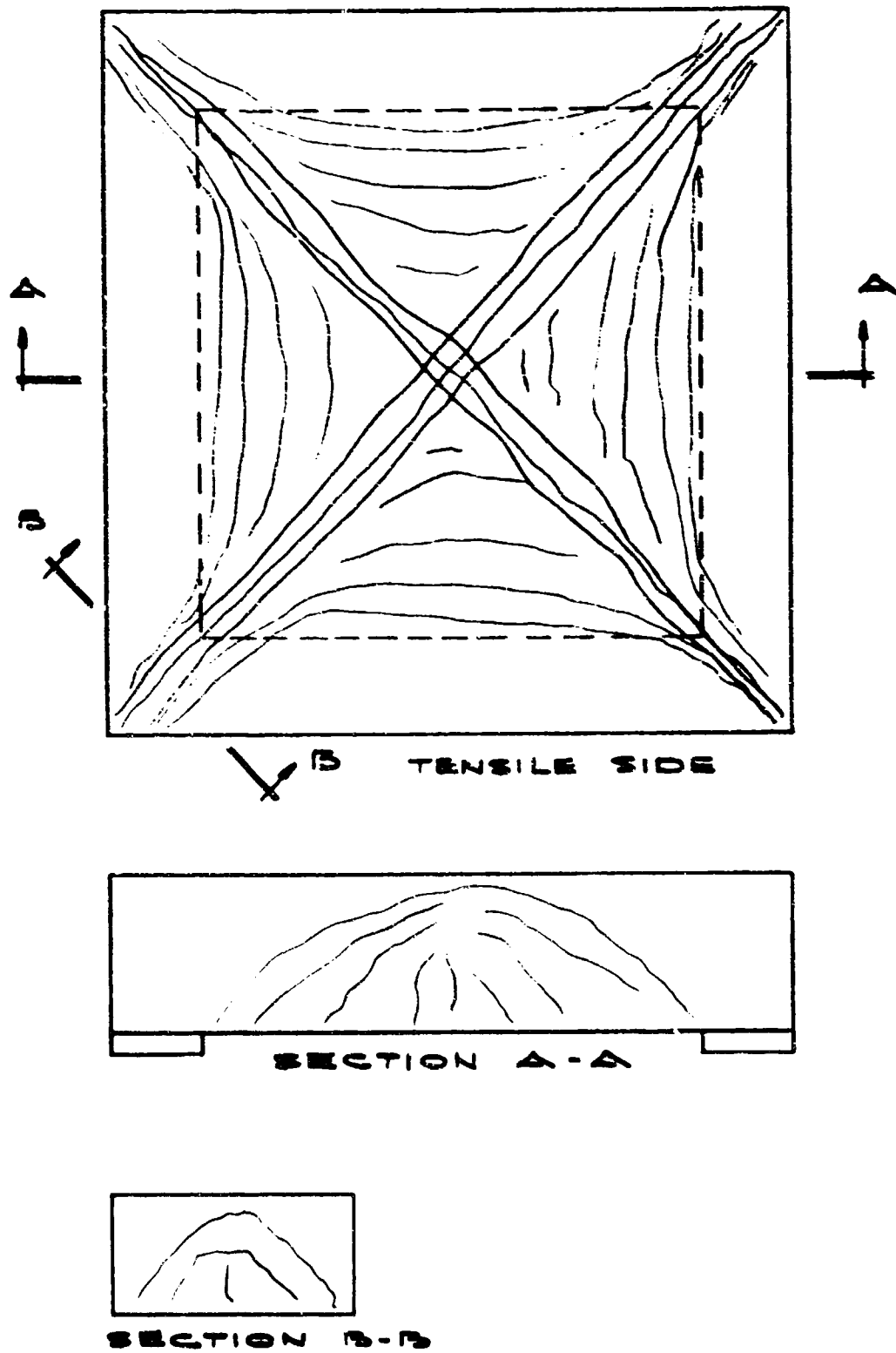


FIGURE 37. OBSERVED CRACKING PATTERN FOR SLAB 7

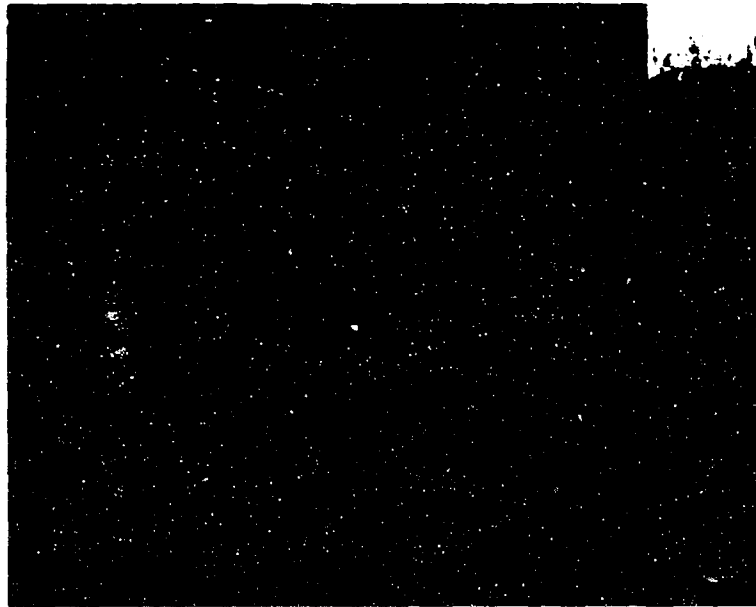
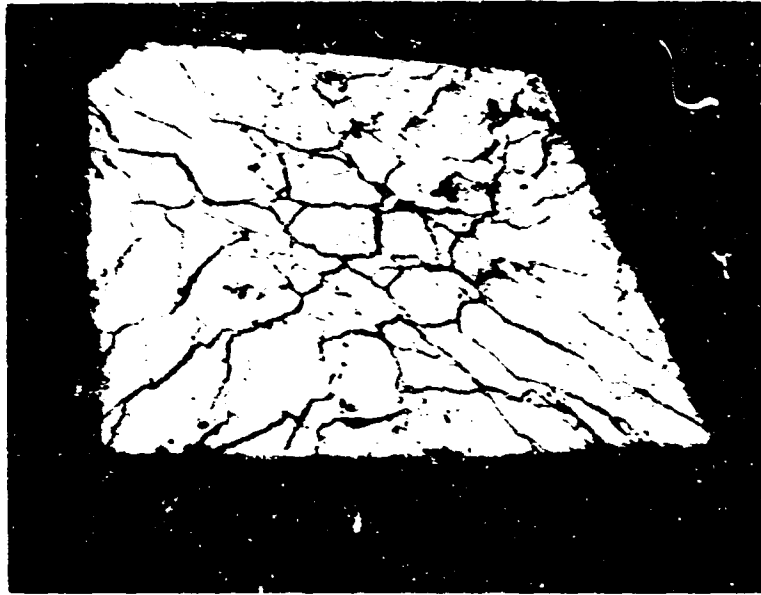


FIGURE 38. POST-TEST PHOTOGRAPH OF TENSILE SIDE
FOR SLABS 7 AND 2

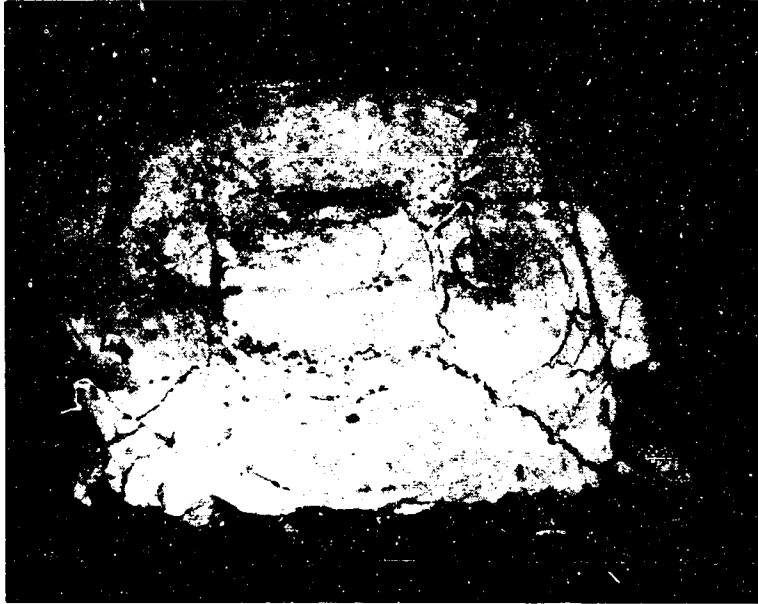


During Test at 865 psi



After Test

FIGURE 39. CRACKS AT 865 PSI AND AFTER TEST FOR SLAB 5



Slab 5



Slab 10

FIGURE 40. COMPRESSIVE SURFACE AFTER TEST FOR
SLABS 5 AND 10

side can be seen in Figure 40 for Slabs 5 and 10. Plate III of Reference 8 shows the same results.

Since most of the slabs were tested only to the maximum pressure attainable on each particular membrane and seal, the real "ultimate" or "failure" load was probably not actually reached on any specimen, even Slab 10. Table XVII of Reference 8 describes simply supported slabs as having no definite collapse load but having continuously increasing load due to tensile membrane action. This tensile action is not due to the tensile edge forces but is due to elongation at the neutral axis of the slab. One such specimen that behaved in this continuous manner was the slab shown in Plate III⁸.

The equations used in Appendix B for predicting yield and ultimate deflection at midspan were based on experience with deep beams.¹ Such a basis was the only one reasonable; however, observations indicate yield deflections about 100 percent greater than predicted. Although mechanical slack might contribute to this, as is apparent by initial nonlinearity in some of the deflection diagrams, it seems that the predicted yield and ultimate deflections are generally low by a considerable amount. Additional theoretical and experimental investigations would be required to develop accurate deflection equations.

The equations used for predicting "ultimate" pressure in the plastic analysis do not consider the "compressive" reinforcement on the tensile side of the neutral axis as was observed on both Slabs 7 and 10; however, the effect of this would be negligible because the moment arm is small.

The relative behavior of slabs having various properties has been measured and compared with the predicted behavior. Since some of the tests were not conducted to deflections and loads that would fully corroborate the theory, it will be assumed for the purpose of evaluating the various parameters that the present theory is reasonably correct.

The span-depth ratio is the primary parameter governing slab behavior. Slabs 1, 6 and 7 were designed to evaluate span-depth ratio. Figure B13 shows the deflection diagrams of Slabs 1, 6 and 7 as predicted by Reference 9, and Figure B19 shows predictions for the same slabs using the analysis in Appendix B corrected to the actual test conditions. Both figures illustrate that a decrease in span-depth ratio by a factor of 2 increases yield pressure by a factor of 4.5, ultimate pressure by a factor of 5.0, and ultimate deflection by a factor of about 1.5.

The reinforcement content is the secondary parameter governing slab behavior. Figure B12 illustrates the relative behavior of Slabs 1

through 5, all of which have the same depth and span. Slabs 2, 1 and 3 all have half percent compressive reinforcement but varying amounts of tensile reinforcement. Slab 1 has twice the reinforcement of Slab 2, thus is about twice as strong but about 75 percent as ductile, etc. Slab 5 is similar to Slab 2 except for the compressive reinforcement and the diagrams are essentially the same. The same is true for Slab 4 and Slab 1. It can be seen that compressive reinforcement has negligible effect on slab behavior except for a slight increase in ductility.

The effect of the shape of the slab has already been discussed. The effect is graphically illustrated in Figure B19 in which deflection diagrams of Slabs 1, 9 and 11 are compared. Comparisons are also made in Figure B19 of Slab 7 with Slab 10 and Slab 6 with Slab 8.

The effect of strain hardening on the reload behavior of the slab has been experimentally demonstrated as shown in Figures 10, 16, 19 and 20. This behavior is essentially as would be expected. The reload behavior is linear up to the level of the previous load. This was found to be true of localized strains as well as overall deflections.

Analytically, the effect of edge pressure on slab behavior was evaluated. Appendix B contains the derivation and the graphic results (Figure B16). It can be seen that having the lateral pressure on the edge acting axially has the net effect of increasing the strength of the slab but decreases the ductility. This is because the axial compression decreases the tensile strains but increases the compression strains. On Slab 1 the yield pressure is doubled, the ultimate pressure is increased by 50 percent, but the ultimate deflection is decreased by a factor of 4. The effect is less on thinner slabs and greater on thicker slabs.

The friction between the slab and the bearing plate was expected to be critical. The friction forces have the same effect on the slab behavior as the tensile reinforcement; therefore, friction reducing devices were used. It had been expected that plastic sheets and lubrication could reduce the coefficient of friction to 0.05; however, this proved to be optimistic. Although simple experiments indicated coefficients of 0.3 to 0.4, coefficients of 0.1 to 0.2 produce the best agreement between predicted and observed slab response. Independent evaluation of the friction coefficient was not within the scope of this investigation.

The effect of friction on the predicted deflection diagrams is shown in Figure 25, in which theoretical predictions are plotted using three different friction coefficients. In the test of Slab 7, the plastic sheet and lubricant had been omitted, thus the observed behavior compares with the coefficient of 0.3. Figure 10, Slab 1, shows similar friction effects, but observed behavior compares with a coefficient of 0.1 since means of

reducing friction were used. Some observed data compare best with a coefficient of 0.2. The reason for this is not evident.

Concrete cylinder tests were conducted on samples taken from the mix used for each specimen. The results of these tests are summarized in Table III. In some cases, the cylinder strength was significantly different from the strength that had been used in the predictions. In such cases, revised predictions have been made. The theoretical effect of variations in concrete strength is shown on Figure 25, Slab 7. As can be seen, the main effect on the slab behavior is a linear extension of the plastic portion of the pressure-deflection diagram.

The reinforcement bars were tensile tested. The results were very similar to the expected stress-strain curve shown in Figure B5.

No bearing failures were observed. The bearing plates, at first, were welded at the corners which resulted in a torsional restraint along the edges (Appendix A). The effect of this was observed near the maximum load on Slab 5 when the plate began digging into the slab along the inner edge of the plate. On Slab 9 the bearing plate was not centered on the pivot, causing crushing of the concrete on the inner edge. These incidents were not classed as bearing failures.

Shear failures were not observed. This may be due, in part at least, to the fact that the deepest slab was not loaded beyond its elastic range.

Since the reinforcing steel was provided with adequate hooks, no bond failures were expected and none occurred.

5. RESULTS OF DYNAMIC TESTS

The results of each dynamic test generally consist of records of (1) pressure in the lower reservoir, (2) pressure in the upper reservoir, (3) midspan deflection of the slab, (4) midspan strain of the tensile reinforcement, all as functions of time, and (5) postload permanent deformation and residual strain. These dynamic results represent the slab response under a dynamic loading superimposed on an initial static loading. This is due to the initial static pressure differential between the upper and lower reservoirs as described in Section 3B.

The fundamental periods of the slabs were computed to be 4.0 ms for Slab 15, 3.75 ms for Slabs 17 and 18, and 3.5 ms for Slab 6. The rise time of the load varied from about 1-1/2 times the period to several times the period.

A. First Dynamic Test, Slab 15

The first dynamic test, Slab 15, was conducted with 700 psi in the lower reservoir and with 500 psi in the upper reservoir. The lower pressure was not vented so that a square load pulse on the slab was generated. This also gave an independent measure of the pressure decrease in the lower reservoir due only to slab deflection (Figure 41). Nitrogen gas was used to minimize this pressure drop. Although the volume of the reservoir containing the gas was more than 3 cubic feet, the pressure dropped from 700 psi to 570 psi, which indicated a volume increase of 20 percent. Unfortunately, the deflection and strain measurements were not recorded successfully during this pressure variation. Therefore, such a volume increase was not corroborated by measured dynamic data. However, the extensive cracking, the residual strain of 4200 microinches/inch, and the permanent deformation of 1-7/16 inches at midspan indicated that a deflection of at least 1-1/2 inches was experienced. The volume change due to 1-1/2 inches midspan deflection was approximately 0.67 cubic feet or 22 percent of the original volume of 3 cubic feet.

The intensity of the square load pulse experienced by the slab was the pressure differential between the lower reservoir and the upper reservoir. The load curve, which was this pressure differential ($q_2 - q_1$), has been added to the recorded data (Figure 41). The post-test condition of Slab 15 is shown in Figure 42.

B. Second Dynamic Test, Slab 16

The second dynamic test, Slab 16, was unsuccessful. The upper seal blew, cracking the specimen edges but without dynamically loading the specimen.

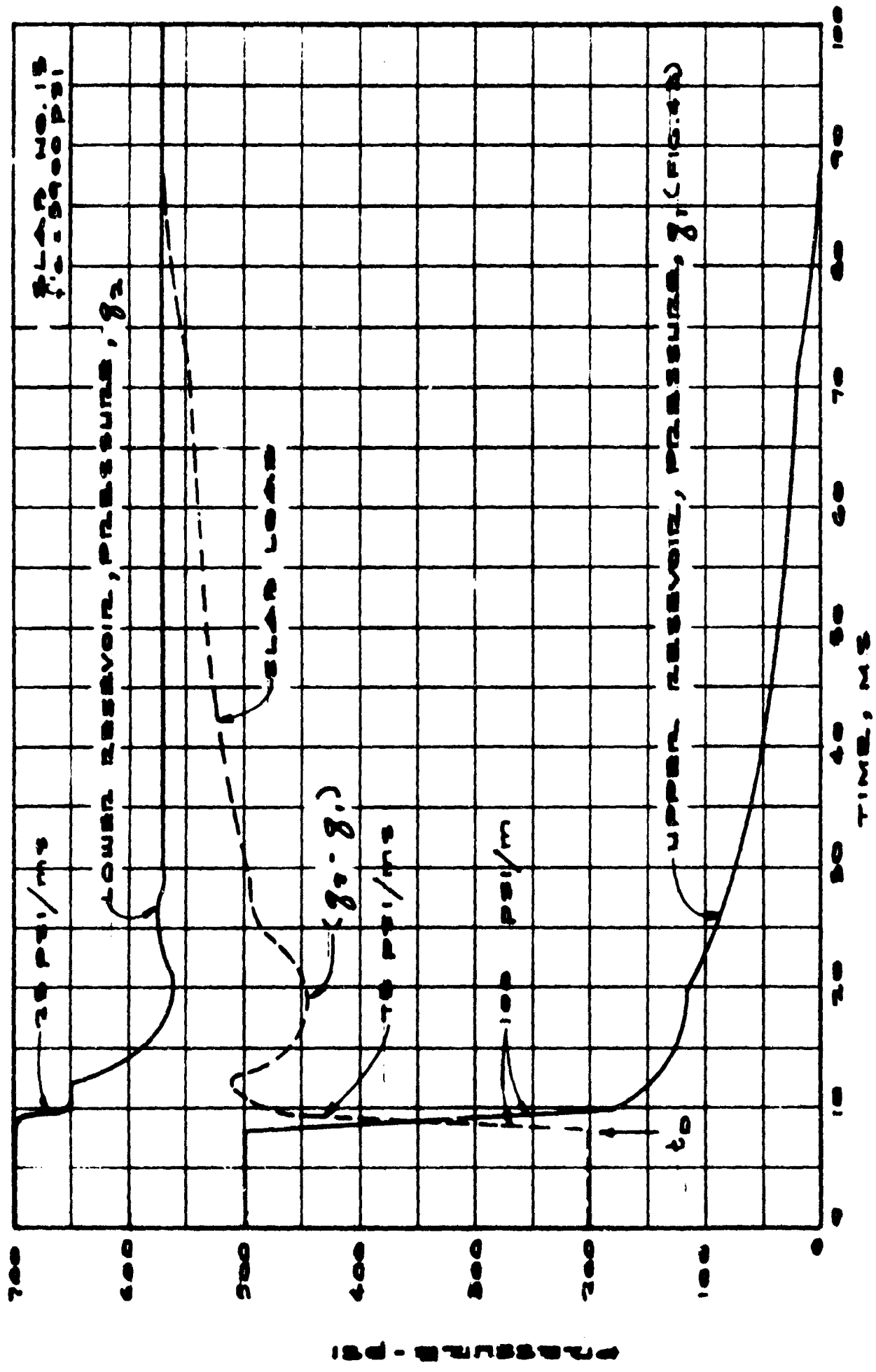


FIGURE 41. DYNAMIC TEST. SLAB 15, SHOWING TIME HISTORY DATA



View of Tensile Surface



Edge View
Slab 15

FIGURE 42. POST-TEST PHOTOGRAPH OF SLAB 15

C. Third Dynamic Test, Slab 17

The third dynamic test, Slab 17, was conducted with 750 psi in the lower reservoir and with 535 psi in the upper reservoir. Again, a square load pulse was generated by not venting the lower reservoir (Figure 43). The reservoir had been two-thirds filled with water, leaving 1 cubic foot of gas. The 8-percent volume increase indicated by the pressure drop from 750 psi to 690 psi was compatible with the magnitudes of the measured deflections and strains. The deflection response was typical of that found in deep beams¹ where the peak deflection occurs later than the peak load because of the time required for the yielding to take place.

The measured residual strain at midspan was 900 micro-inches/inch. The midspan permanent set was about 0.04 inch. There were no cracks. These residual values are comparable with the peak values recorded (Figure 43). Slab 17 was exactly like Slab 1, the static companion specimen. Both slabs were 11-inch deep specimens having one percent tensile and one-half percent compressive reinforcement.

D. Fourth Dynamic Test, Slab 18

To generate load pulses similar to blast waves, the lower pressure reservoir was vented on the fourth dynamic test. The pressure decay was premeasured with only the lower reservoir pressurized. The reservoir was filled with water, leaving only 0.5 cubic foot of gas at pressure. When the 550-psi reservoir was bled through a 1-1/4-inch valve, the exponential pressure decay shown in Figure 44 was produced. This 5-second duration was excessively long, so a 2-inch diameter blow-off disc was installed as shown in Figure 45. The 550-psi reservoir was vented through the 2-inch discharge giving the 2-1/2-second decay shown in Figure 46.

The fourth dynamic test, Slab 18, was conducted with 900 psi in the lower reservoir and with 600 psi in the upper reservoir. The lower reservoir was vented through the 2-inch blow-off disc. The disc was explosively removed at the same time the upper diaphragm was explosively removed. The resultant pressure and strain records are shown in Figure 47. The peak strain intensity was 2470 microinches/inch. The residual strain was 850 microinches/inch. and the permanent set was 0.16 inch at midspan. There were no cracks in the slab.

Slab 18 and the static companion, Slab 4, were 11-inch deep specimens having one percent tensile but no compressive reinforcement.

Prior to the fifth dynamic test, the pressure decay was measured again with more water in the reservoir than previously. The

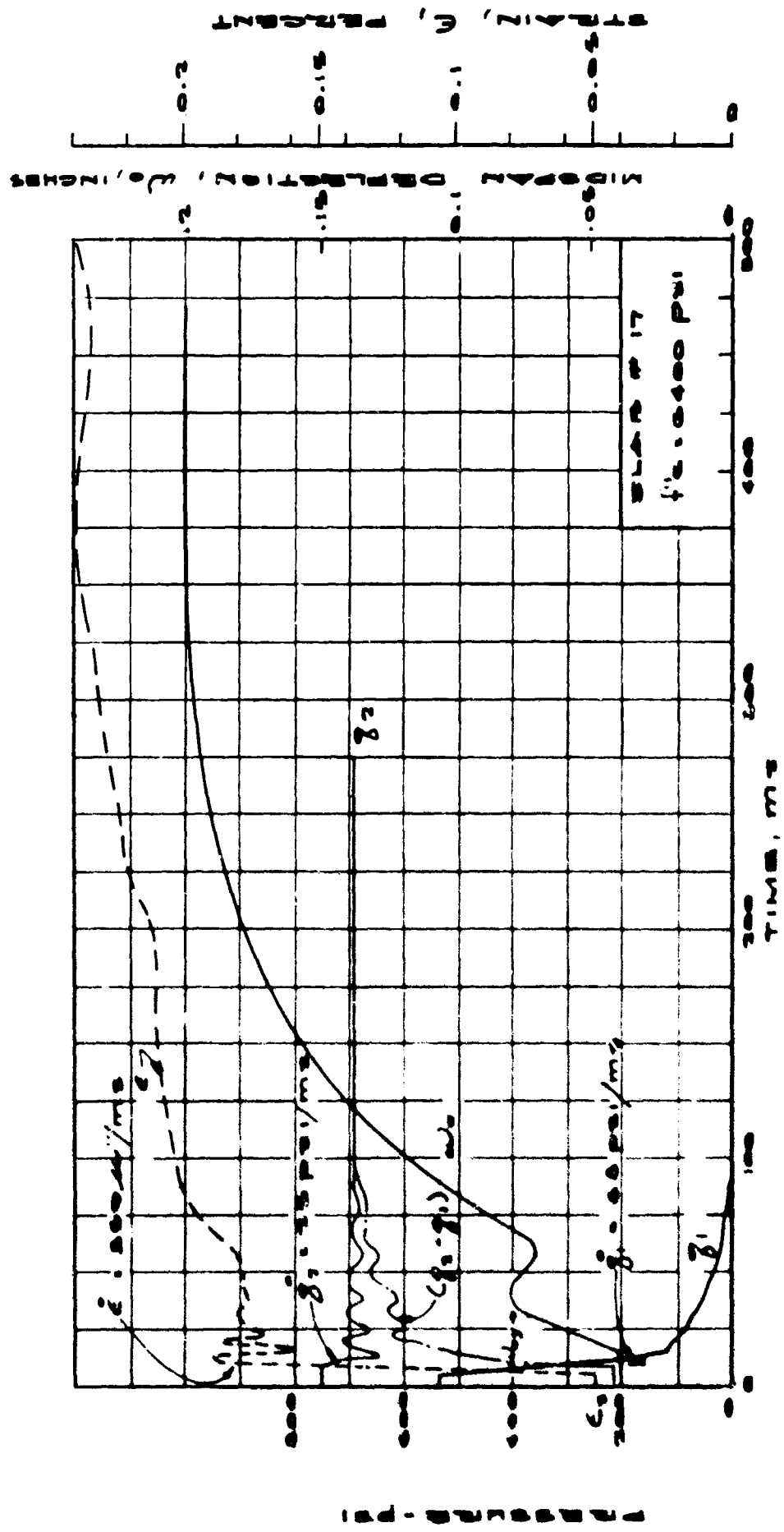


FIGURE 43. DYNAMIC TEST, SLAB 17, SHOWING TIME HISTORY DATA



Pressure = 121 psi/cm
Time = 0.5 sec/cm

FIGURE 44. PRESSURE DECAY THROUGH A 1-1/4-INCH DIAMETER VALVE



FIGURE 45. LOWER CAVITY PRESSURE RELEASE BLOW-OFF DISC



92
—

Pressure = 121 psi/cm
Time = 0.5 sec/cm

FIGURE 46. PRESSURE DECAY THROUGH A 2-INCH DIAMETER BLOW-OFF DISC

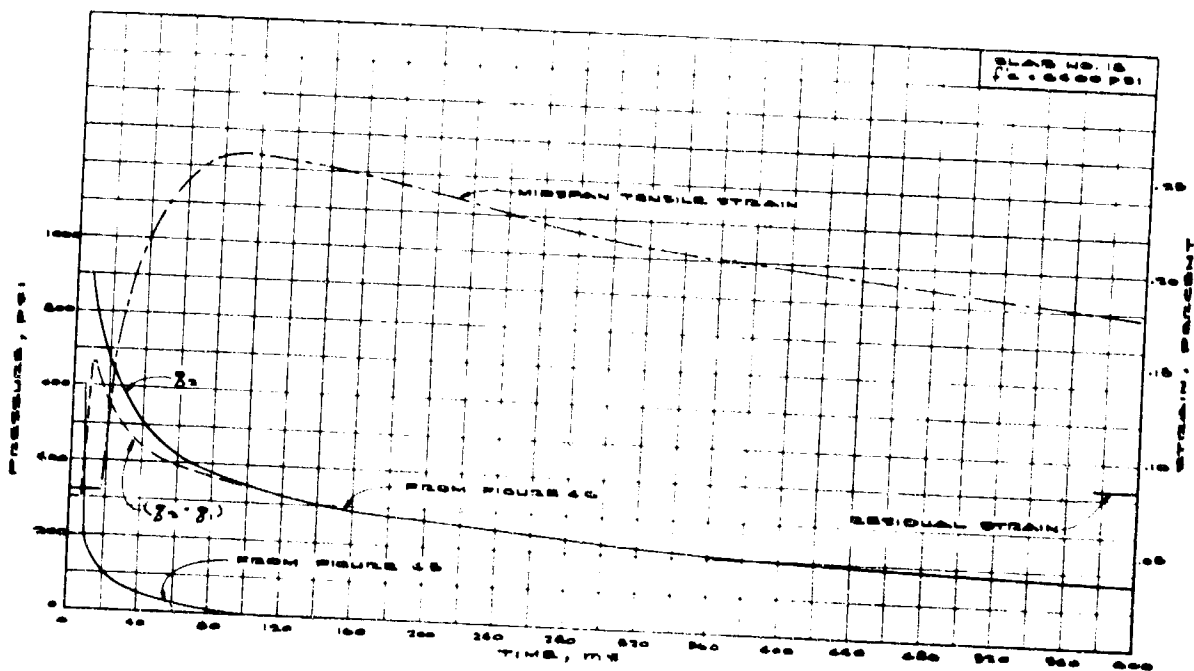


FIGURE 47. DYNAMIC TEST, SLAB 18, SHOWING TIME HISTORY STRAIN DATA

water-filled reservoir was pressurized to 390 psi and, when vented, a decay duration of one second was produced (Figure 48). The strain and deflection were also recorded as the pressure decayed to show the elastic recovery of the slab (Figure 48).

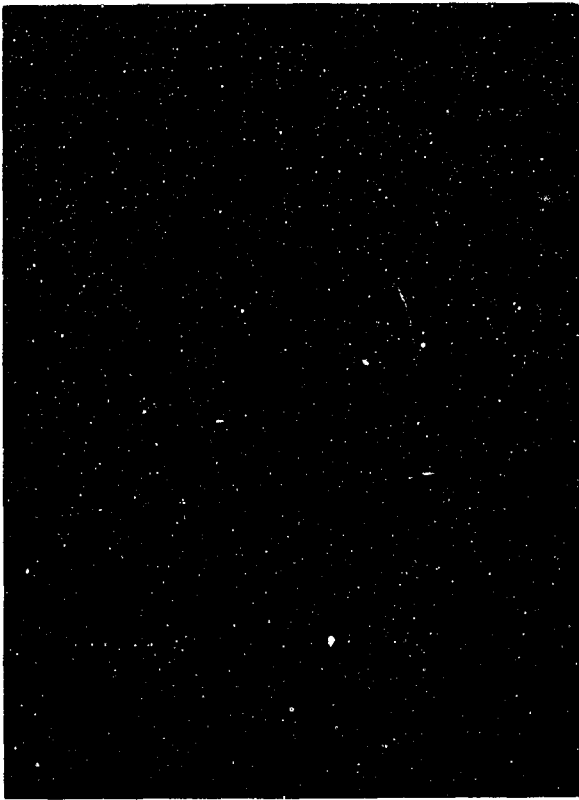
E. Fifth Dynamic Test, Slab 20

The fifth dynamic test, Slab 20, was conducted with 750 psi in the lower reservoir and 500 psi in the upper reservoir. The water-filled lower reservoir was vented as in the fourth dynamic test. When the upper pressure was released, the pressure drop in the lower reservoir was severe, as was expected with a water-filled reservoir (Figures 49 and 50).

The measured decay duration of 1-1/2 seconds was longer than the one second measured in Figure 48 primarily because of the higher pressure. Also, there was a thin layer of gas on top of the water-filled reservoir because bottled nitrogen was used to pressurize. This gas layer was estimated to be about 1/4-inch thick, which was about 0.2 cubic foot of gas at 765 psia. Upon decompression of this gas layer to ambient pressure, a gas volume of 10 cubic feet was discharged. The discharge of such a gas volume through a 2-inch diameter orifice was probably the predominant cause of the 1-1/2-second decay duration.

This test made it apparent that the quantity of air required in the reservoir to prevent large pressure drop from slab deflection alone was too large a quantity to be evacuated through a 2-inch orifice within one second. Higher intensity pressures were possible but only with longer durations. Obviously, a much larger vent capacity was required so that a gaseous pressure medium could be used. The desired exponential decay is inherent with a gaseous pressure medium:

The response of the specimen, Slab 20, to this loading was measured (Figure 49). The residual strain was 1600 microinches/inch, and the midspan deformation was 0.31 inch. The cracking pattern (Figure 51) was the typical diagonal pattern.



30



30

30

Pressure = 100 psi/cm
Time = 0.5 sec/cm
Pressure Decay

$\epsilon = 125 \mu\text{''/''/cm}$
 $\Delta = 0.067 \text{ in/cm}$
Time = 0.2 sec/cm
Strain and Deflection Recovery

FIGURE 48. PRESSURE DECAY THROUGH 2-INCH BLOW-OUT DISC
WITH WATER-FILLED RESERVOIR

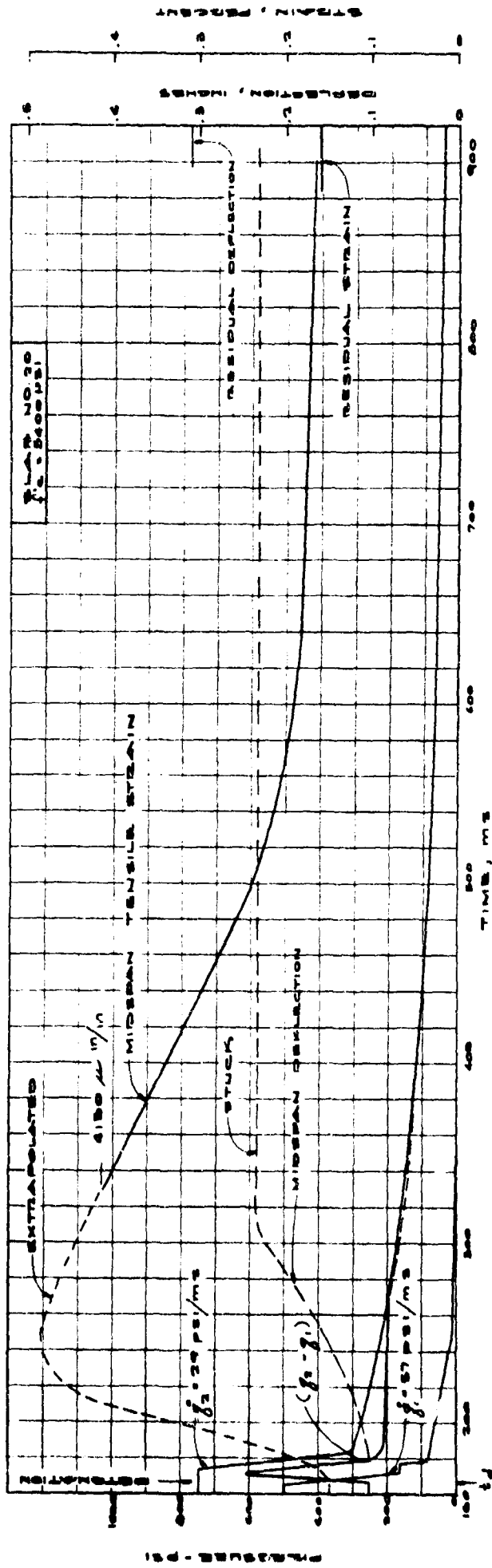
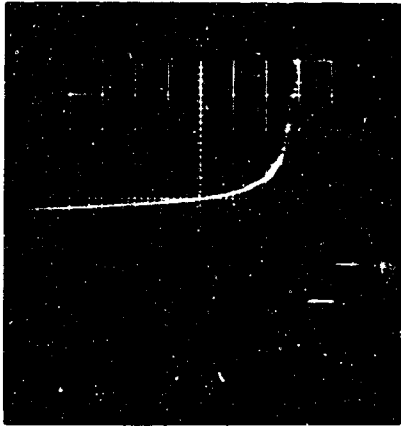


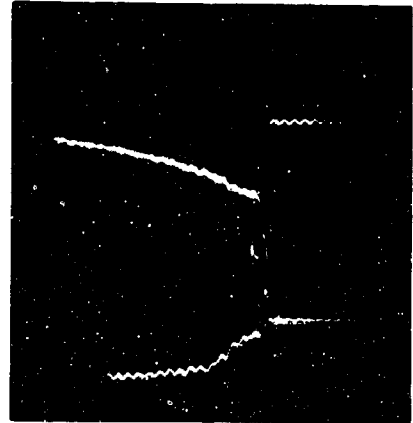
FIGURE 49. DYNAMIC TEST, SLAB 20, SHOWING TIME HISTORY DATA



ε

Scope 1 - Strain

ε = 500 μ"/"/cm
t = 200 ms/cm



q₁

q₂

Scope 2 - Pressure

q₁ = 65 psi/cm
q₂ = 121 psi/cm
t = 50 ms/cm



q₂

Δ

Scope 3 - Pressure

Δ = .33"/cm
q₂ = 135 psi/cm
t = 200 ms/cm

q₁ = Upper Cavity Pressure
q₂ = Lower Cavity Pressure
t = Time, milliseconds
ε = Midspan Tensile Steel, microinches/inch
Δ = Midspan Deflection, inches

FIGURE 50. OSCILLOGRAMS FOR SLAB 20

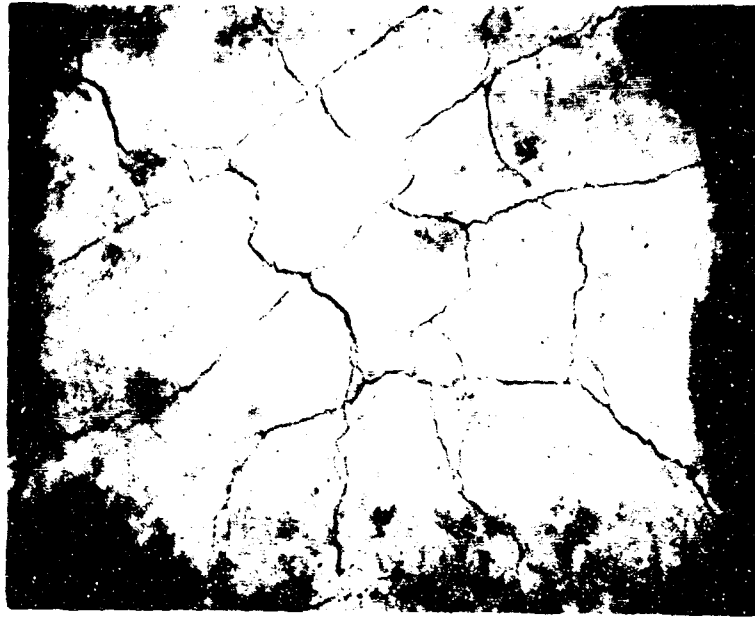


FIGURE 51. POST-TEST PHOTOGRAPHS OF SLAB 20

6. COMPARISON OF DYNAMIC TEST RESULTS WITH STATIC TEST RESULTS

Comparison of dynamic test data with companion static test data is difficult. Known differences such as friction reducing devices or concrete strength must be considered. Based on the experience developed in the static test, the quantitative effect of friction on dynamic behavior can be evaluated assuming the friction factor is the same for dynamic loading as for static loading. Since it has been shown for these specimens that the concrete strength has no effect on the static slab behavior except the ultimate pressure and deflection, the differences in concrete strength can be neglected except when the deformations become large.

A. Comparison of the Dynamic Response of Slab 15 with the Static Behavior of Slab 7

A comparison of the behavior of Slab 15 with that of its static companion, Slab 7 (the 8-inch deep slabs having one percent tensile and one-half percent compressive reinforcement), is based on the only data available, the residual deformation, residual strain, and the cracking of the specimen (Figure 42). These data which for the dynamic test represent the result of a dynamic loading superimposed on an initial static loading are comparable to the corresponding data that would be produced by a 600-psi static load on Slab 7. This is an extrapolation of Slab 7 predicted deflection behavior using a friction coefficient of 0.1 and f'_c of 5900 psi. Such extrapolation is required because no attempt was made to reduce the friction for Slab 7, whereas for Slab 15 friction reducing material was used. Also, Slab 7 had not been deflected to 1-1/2 inches. This analysis is reasonable in the light of the behavior of all the static tests, especially Slab 10.

The cracking pattern produced by the dynamic load on Slab 15 (Figure 42) was very similar to the pattern produced by the static load on Slab 7.

B. Comparison of the Dynamic Response of Slab 17 with the Static Behavior of Slab 1

A comparison of the dynamic strains and deflections and the residual strain and deflection of slab 17 with the static behavior of slab 1 shows that measurements of about the same magnitude were produced by a static load on slab 1 of the same intensity as the maximum intensity of the square pulse on Slab 17.

C. Comparison of the Dynamic Response of Slab 18 with the Static Behavior of Slab 4

Comparison of Slab 18 behavior with that of its static companion specimen (Figure 52) shows that a static pressure of 770 psi would be required to produce the measured dynamic data. This suggests that the actual load was higher than the peak of 660 psi (Figure 47), or that the dynamic coefficient of friction was essentially zero. The load could have been higher due to the location of the pressure transducers. The upper transducer was such that the upper pressure was probably decaying faster than that measured. The lower transducer was such that the lower pressure was probably decaying slower than that measured. The net result would have been a higher peak pressure than that shown in Figure 47.

However, this same anomaly existed for the previous dynamic test, Slab 17, for which the pressures were more reliable. It is quite likely then that for the dynamic loading the frictional edge forces and edge moments do not develop to the same magnitude as for a static loading.

The difference in f'_c between Slabs 4 and 18 would have no effect on the above comparison because the deflections were not very large as discussed in Section 5A.

D. Comparison of the Dynamic Response of Slab 20 with the Static Behavior of Slab 5

Slab 20 and its static companion, Slab 5, were 11-inch deep specimens having one-half percent tensile but no compressive reinforcement. However, Slab 5 was tested with the bearing plate frame that exerted edge moments on the slab (Section 4C), whereas Slab 20 had bearing plates that were free of edge restraint. Therefore, in comparing Slab 20 behavior with Slab 5 behavior, the strength of Slab 5 must be reduced by about 8 percent.

Comparison of the above data with the static companion specimen, Slab 5, shows that the measured peak strain, the residual strain and the permanent set would have been produced by a 450-psi static pressure.

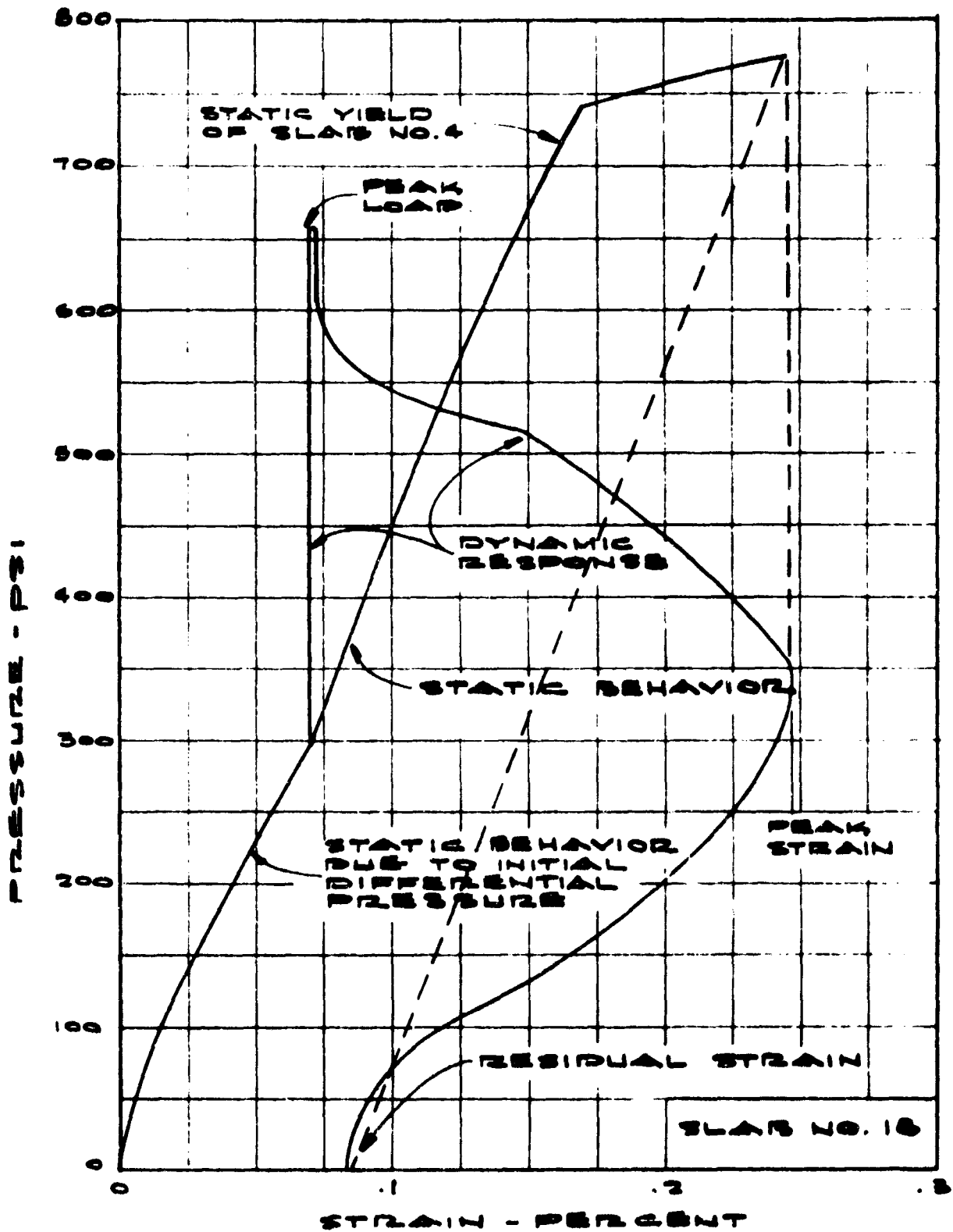


FIGURE 52 COMPARISON OF DYNAMIC STRAIN RESPONSE OF SLAB 18 WITH THE STATIC BEHAVIOR OF SLAB 4

7. SUMMARY AND CONCLUSIONS

The static behavior of deep slabs under uniform load was investigated analytically and experimentally. Deflections, strains, and crack development were observed with various intensity loads on ten slab specimens. The slab specimens were tested with **nominal span-depth ratios of 3, 4 and 6**. The specimens had reinforcement **content** varying from 0.5 percent to 1.5 percent. Square, rectangular, and round shape specimens were investigated. The reload behavior was observed as well as the first load behavior.

Equations were formulated for the static test conditions for yield and failure loads. Predictions of the static pressure required to cause yielding of the slab, the deflection at that pressure, and the ultimate pressure and deflection were made for the test specimens (Tables IV and V). Graphic comparison of predicted and observed deflection behavior for each test shows the correlation. Correlation at yield pressures was generally within 10 percent, but correlations of yield deflections and ultimate pressures and deflections were not good. Loads as much as 35 percent higher than predicted ultimate were observed. Yield deflections were observed to be generally 100 percent higher than predicted. Maximum deflections were as much as two times the predicted ones.

The dynamic behavior of deep slabs under uniformly distributed load was also measured on four slabs. To generate the high intensity dynamic load with a rise time in milliseconds and a duration of about one second, a special test facility was developed. The measured rate of pressure rise was 100 psi per millisecond. A peak pressure of 600 psi was generated. The duration of the pressure was variable from about 1-1/2 seconds up.

The slabs tested dynamically were companion specimens to the statically tested slabs.

A dynamic peak load of 1.5 times the static yield load was sustained by one specimen, Slab 20. On the other three slab tests, there appeared to be little difference between the static and the dynamic response.

Analytical evaluation of the effect of various parameters on slab behavior was conducted and discussed. It was shown that the primary strength parameter was the span-depth ratio and that the second most critical parameter was the amount of tensile reinforcement. It was also shown that compressive reinforcement had little effect on slab behavior. The effect of the shape of the slab was discussed and the conclusion drawn that the circular and square shapes had essentially the same strength but the rectangular shapes were weaker.

Analytically it was shown that friction between the slab and the bearing surface had a significant effect on slab behavior. For example, increase in friction factor from 0.05 to 0.2 increased the pressure required to yield Slab 1 by 30 percent.

Analytically it was also shown that the concrete strength does not affect the strength of the slab but affects the ductility slightly.

Analytically it was also shown that pressure acting axially on the vertical edge of the slab, as well as laterally, increases the strength considerably.

APPENDIX A

DESCRIPTION OF TEST FACILITY

The test facility that meets the desired conditions is shown in Figures A1, A2 and A3. The square, rectangular, and round slabs are shown, respectively.

A. Static Loading

The pressure vessel, along with the specially designed lid, served as the structure that held the huge loads. The pressure was applied upward on the specimen from the lower reservoir. The reservoir was sealed with a thin flexible membrane that conformed to the surface irregularities of the concrete and that stretched with the slab movement, see Figure A4. The membrane had to have enough ductility to take the 1 to 2 inches of slab flexure at midspan and the 1/4 inch of vertical displacement as the lid elastically deformed under the 2 to 3 million pounds of load. The O-ring seal between the membrane and the plate was changed to fit the square, rectangular, and round slabs. The plan dimensions of the seal were selected so the load was applied on the span only, thereby avoiding load on the overhanging edge.

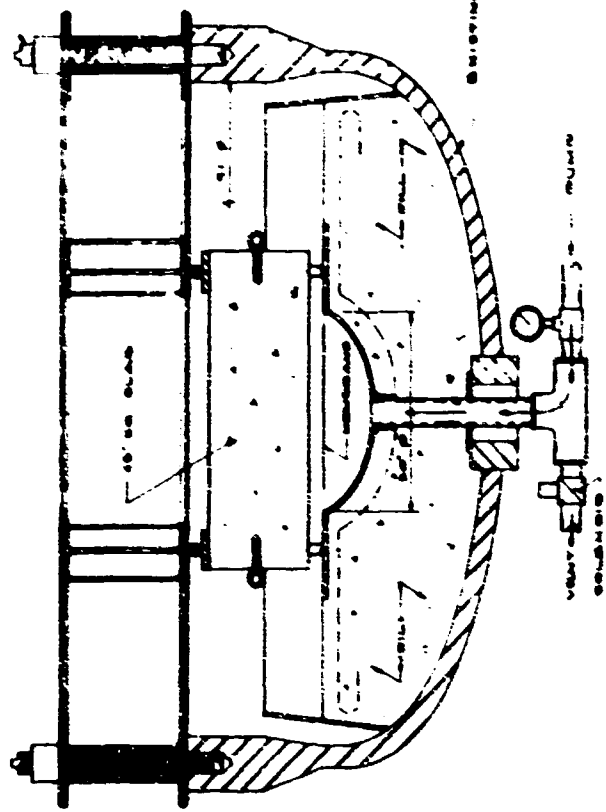
The specimen transferred the load through a 6-inch wide, 1-inch thick bearing plate to the round pivot frame, thence into the lid. In the beginning, the bearing plates for each edge were welded at the corners. Slabs 2, 5, 7 and 4 (first loading) were tested in this manner. The torsional restraint on the edge of the slab is treated analytically in Appendix B. All other tests were conducted with bearing plates free to rotate at the corners.

The three slab depths that give the desired variation in span/depth fit into the structure with a separate concrete filler poured to fit each of the three slab thicknesses.

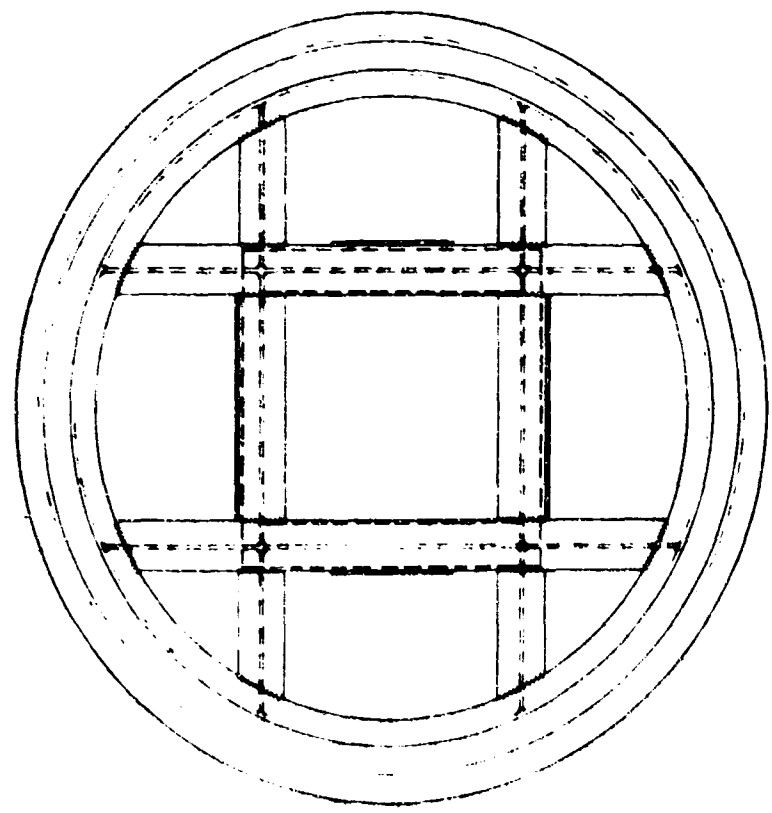
B. Dynamic Loading

The dynamic load was generated by also pressurizing above the slab in a pressure chamber formed by a steel diaphragm (see Figure A3), then, at a preselected pressure level, the restraining diaphragm was cut away with a special linear shaped charge explosive. As the diaphragm was cut away, the upper pressure exhausted rapidly. The net pressure was the load on the slab since the lower pressure was still applied. Thus, the rise time of the slab load was the exhaust time of the upper pressure cavity.

8742

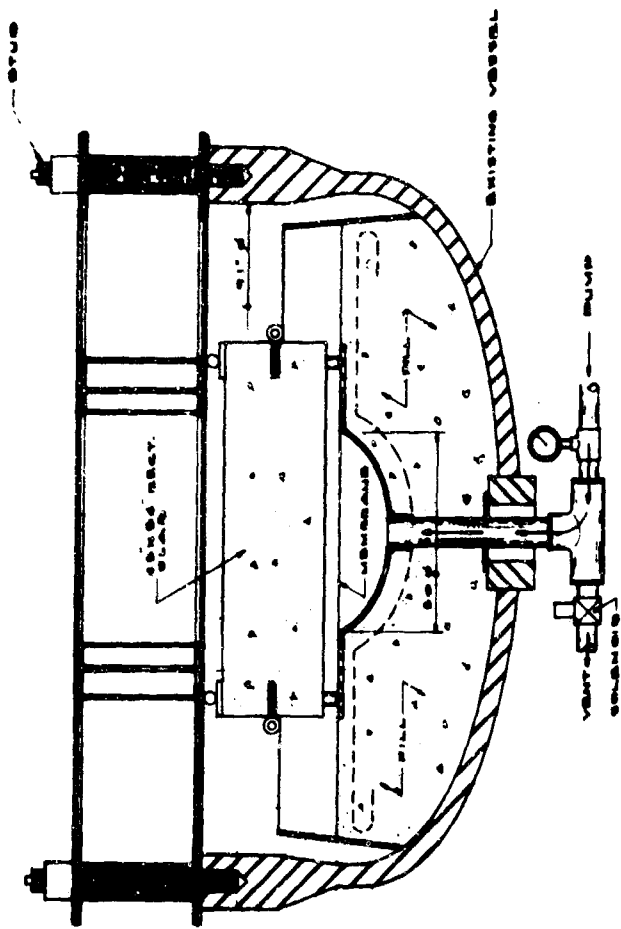


SECTION

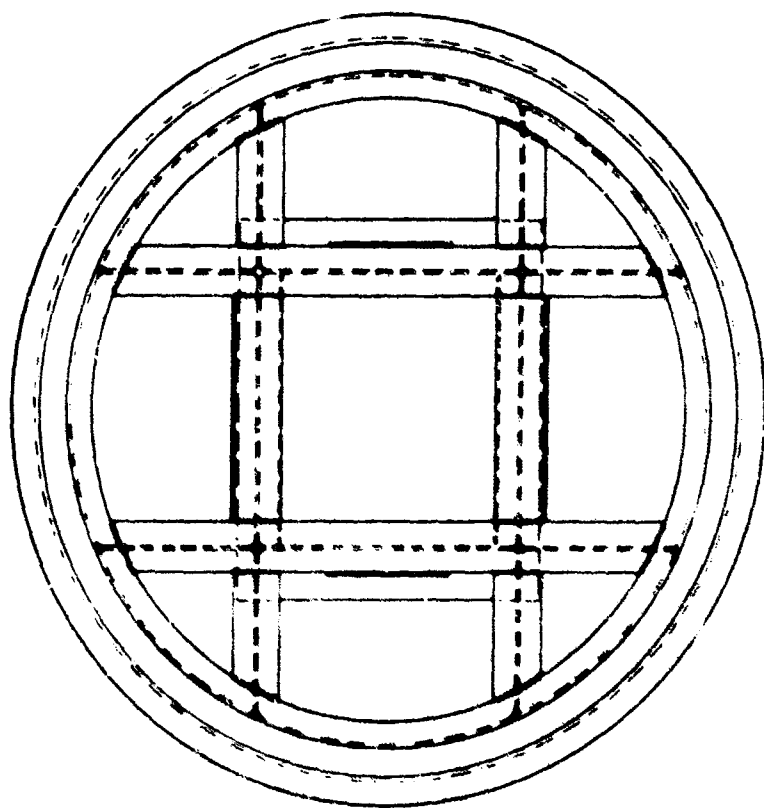


PLAN
COVER PLATE REMOVED

FIGURE A1. SQUARE SLAB TEST FIXTURE

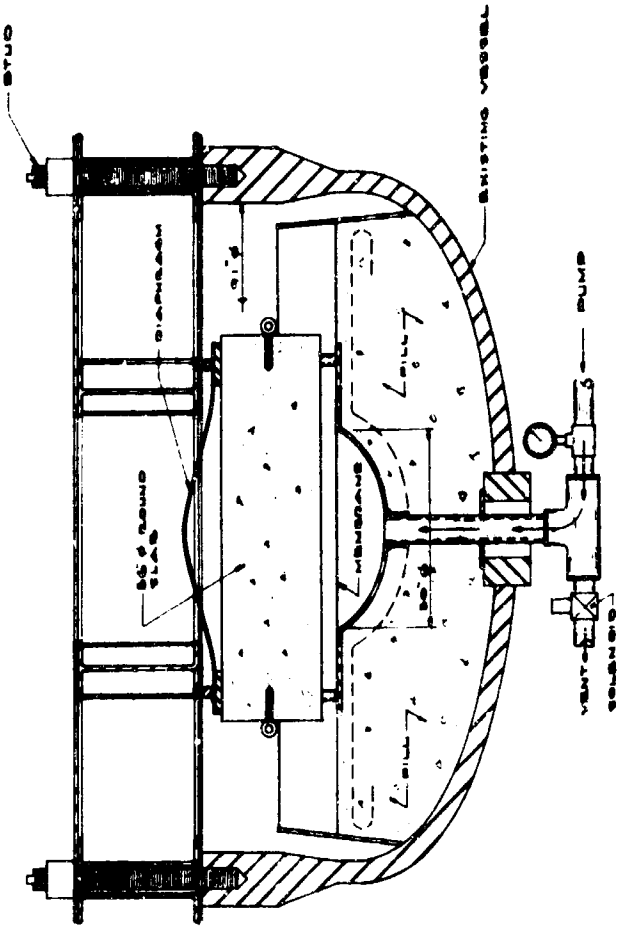


SECTION

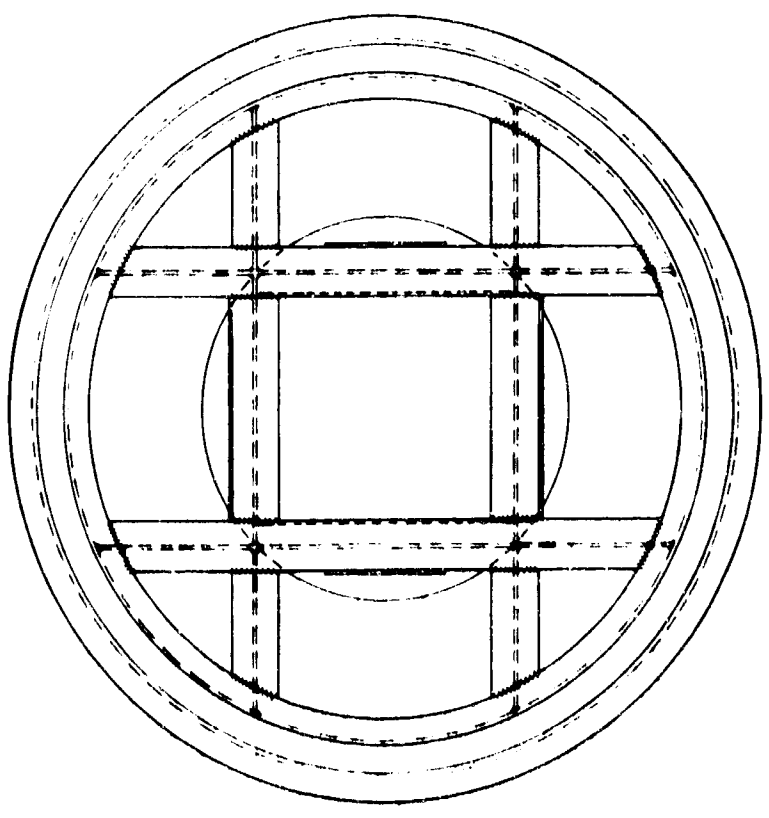


PLAN
 FROM PRESSURE GAUGE

FIGURE A2. RECTANGULAR SLAB TEST FIXTURE



SECTION



PLAN
COVER PLATE REMOVER

FIGURE A3. ROUND SLAB TEST FIXTURE

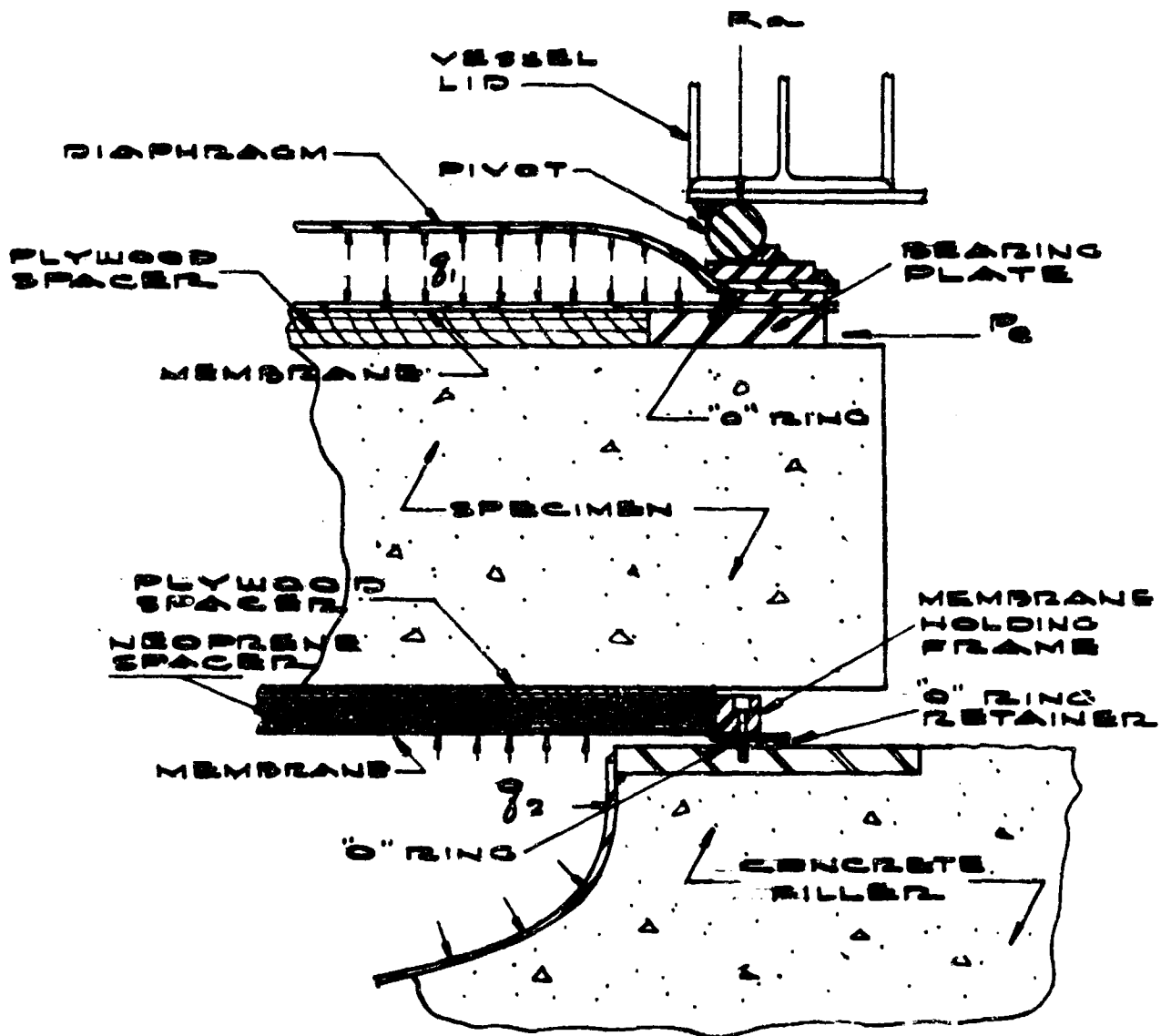


FIGURE A4. SCHEMATIC OF SPECIMEN LOADING AND SUPPORTING ARRANGEMENT

The decay of the dynamic load was produced by draining the pressure in the lower cavity. By programming multiple solenoid valves, the rate of the flow could be controlled to obtain various decay functions and durations.

It was expected, however, that, as the upper pressure was exhausted and the slab loaded, the resultant slab deflection would increase the volume of the lower cavity; this would cause the lower cavity pressure to decrease. A gaseous pressurizing medium would minimize this pressure decrease; however, a liquid medium would minimize the decay duration. By providing a moderate reservoir size and a large venting capacity, it was expected that an optimum combination of these two effects could be produced.

To avoid the mass effects of a fluid pressure medium on top of the slab, nitrogen gas was used. The expansive energy of the compressed gas plus some of the explosive energy would have dangerously propelled the cutaway diaphragm, so a 1200-pound cable blasting mat was suspended over the test facility to catch the steel diaphragm and any spalling concrete.

A fluid pressure medium in the upper reservoir would have given a faster pressure decay, thus a shorter rise time of the resultant dynamic load on the specimen. This possibility was not evaluated.

APPENDIX B

PREDICTION OF STATIC BEHAVIOR

The phenomenological behavior of a slab subjected to uniform pressure is essentially defined by the pressure-midspan deflection diagram. The purpose here, in essence, is to develop theories for the prediction of the pressure-deflection diagram, sometimes called the "resistance diagram," for the static loading on deeply proportioned slabs.

The analysis now to be described was published as Interim Reports, Part I⁹ and Part II¹⁰, and in Progress Reports. For continuity, that material is now duplicated with appropriate corrections.

A. Square Slabs

The pressure-midspan deflection diagram is expected to be shaped in the manner shown in Figure B1. Before the concrete cracks, the slab behaves as an elastic isotropic slab. The diagram is, therefore, initially linear, but only for a short range as the concrete begins to crack at a low pressure. As the cracks form and grow larger, the slope of the pressure-deflection diagram progressively decreases as shown. At about one-half of the pressure required to cause yielding of the tensile steel, the major cracks will be well developed, and the pressure-deflection diagram will become fairly straight and with a slope which corresponds to the full cracked condition. Yielding begins at the lowest level of steel reinforcement and gradually progresses, causing a rounded transition from the fully cracked linear region to the fully inelastic state. After considerable yielding strain, hardening will occur in some cases. For the specimens planned, the deep slab is expected to fail by crushing of the concrete around midspan.

The deflection surface will be smoothly curved at very low loads before cracking, but the cracking will significantly influence the deflected shape. The major cracks which are observed on the tensile side of the slab are expected to appear somewhat as they do for medium-thick slabs. The expected cracking pattern is shown in Figure B2 for a square slab with square mesh reinforcement. The major cracks will be vertical diagonal cracks and circumferential cracks roughly parallel to the edges. The cracks parallel to the edges will propagate upward and toward midspan, nearly reaching midspan and the loaded surface for the deeper slabs.

The vertical diagonal cracks divide the slab into essentially four triangular segments, as shown in Figure B2. Along these cracks, the torsional resistance is fairly well destroyed. Therefore, after these

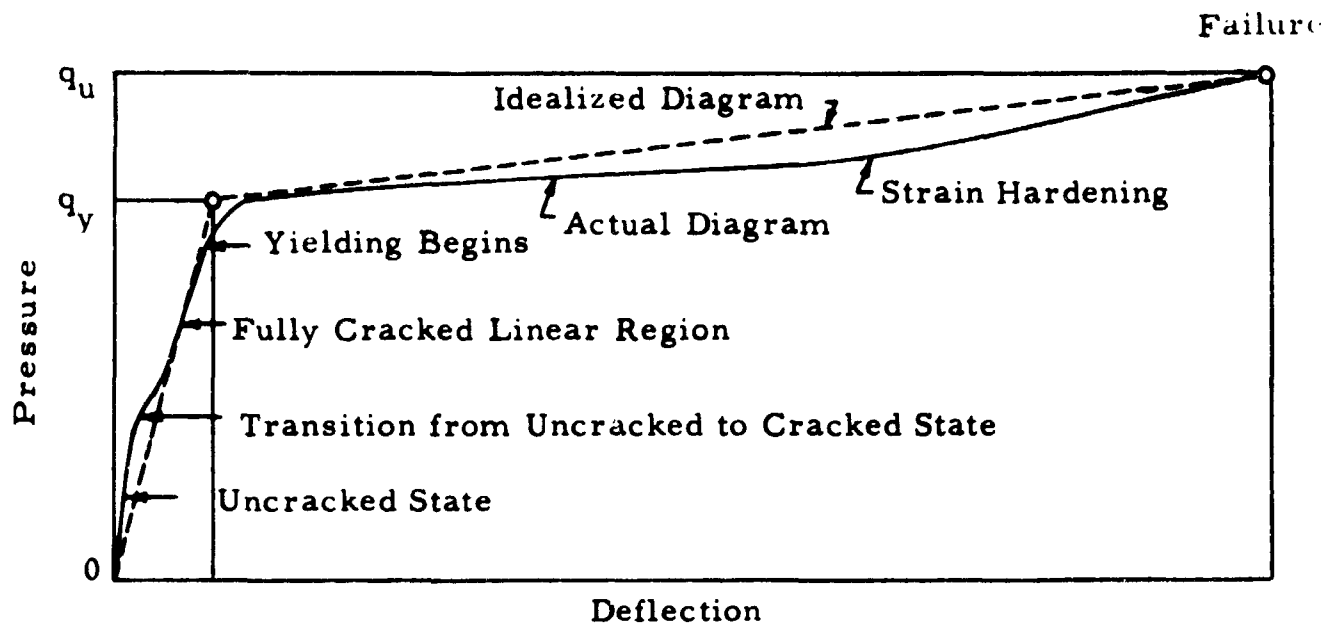


FIGURE B1. TYPICAL PRESSURE-DEFLECTION DIAGRAM

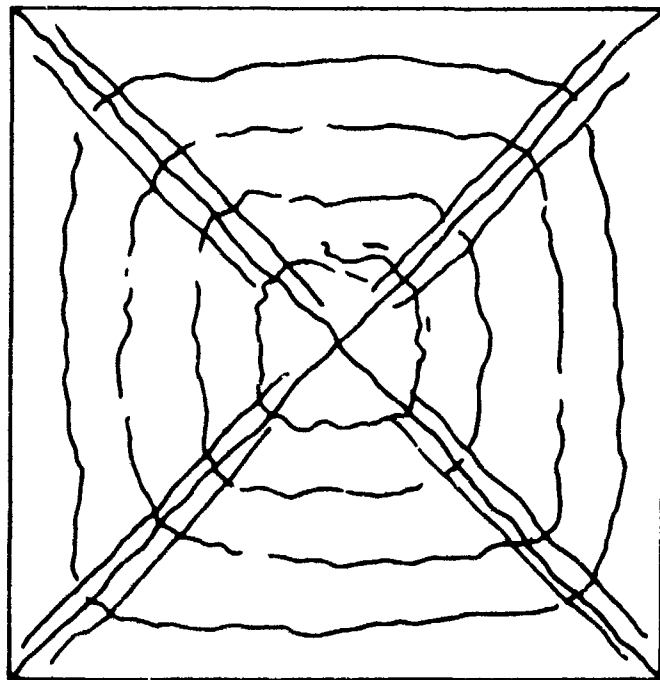


FIGURE B2. EXPECTED CRACKING PATTERN FOR SQUARE SLABS

cracks develop, the slab will tend to deflect in a piecewise mode. That is, large pieces of the slab are expected to act as essentially rigid bodies. The deflected shape of the loaded surface will then be composed of flat triangular segments joined along sharply defined bend lines, also called "yield lines" or "fracture lines." This shape can be defined by the position of the bend lines, and the magnitude is defined by the deflection at midspan as this is essentially a one degree of freedom system. It will be assumed that the fracture lines will have the same position for deep slabs as for medium thick slabs. Their position may be determined theoretically by the well-known fracture line theory of slabs.

The expected pressure-deflection diagram can be closely approximated by two straight lines, as shown on Figure B1. These lines are defined by the origin and the pressure and midspan deflection coordinates for the yield point and the ultimate point. The following method, therefore, is for the prediction of the latter two points.

Although splitting and shear failures are quite possible, especially for the deeper slabs, no consideration has been given herein to these modes of failure primarily because so little information is available. This study is predicated on the assumption that the failure is by bending and, therefore, that other forms of failure do not occur first.

B. Analysis of Deep Beam Strips

A slab may be thought of as composed of many narrow beam strips running parallel to each set of reinforcement plus torsional resistance between beam strips. The flexural properties of each beam strip are considered to be independent of the existence of other beam strips even though they may be crossing and using the same concrete as part of each strip. In this procedure, at any point on any of the fracture lines in the slab, the bending moment at yield or ultimate in the direction of one of the sets of reinforcement is assumed to be equal to the yield or ultimate moment per unit width of the corresponding beam strip. Therefore, one of the first steps in this method is to determine the yield and ultimate moments per unit width of the typical beam strips. These are determined in the usual manner for flexural members.

Consider a typical cross section subjected to combined axial compression P and bending moment M as shown in Figure B3. Note that the axial load is considered to act at mid-depth of the beam strip. This position is rather arbitrary but some position must be chosen and adhered to in order to avoid confusion; the usual choice, the centroid, is not convenient because it is not fixed in position but depends upon the relative values of M and P since the concrete is assumed to have no strength in

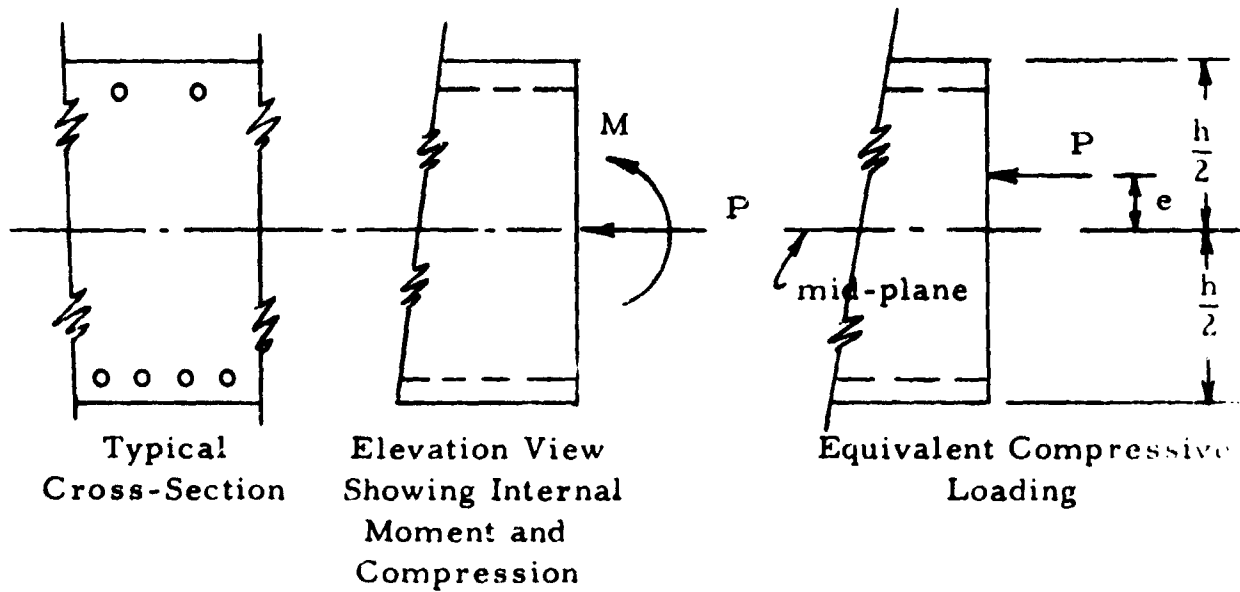


FIGURE B3. INTERNAL FORCES ON THE SLAB

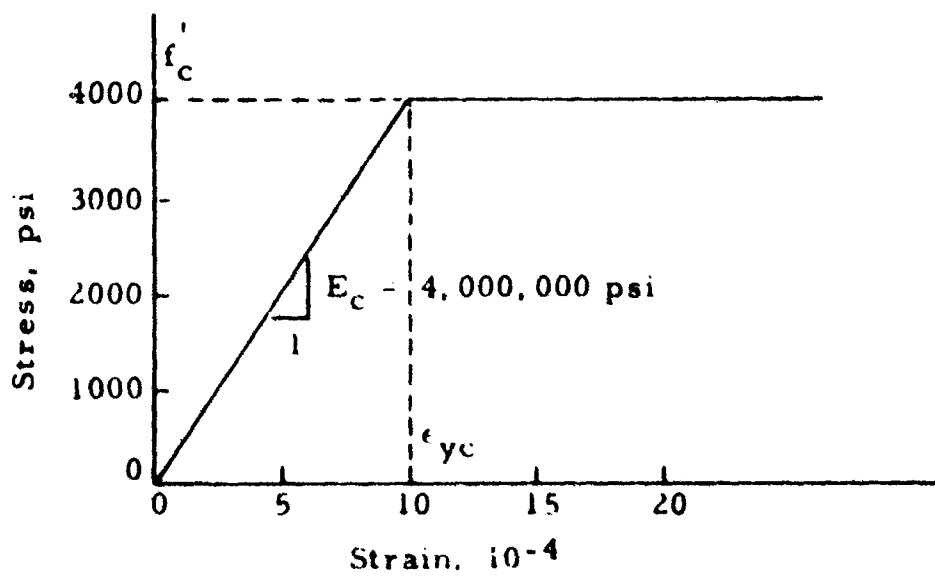


FIGURE B4. ASSUMED STRESS-STRAIN CURVE FOR CONCRETE

tension. Define the ratio M/P as an equivalent eccentricity e . Thus, as illustrated in Figure B3

$$e = \frac{M}{P} \quad (1)$$

The usual problem is as follows: given e , to find the values of P and M at yield and ultimate.

1. Material Properties

The concrete and steel reinforcement are considered to have the typical properties shown in Figures B4 and B5. The idealized stress-strain curve for concrete shown in Figure B4 was recommended by Jensen¹¹ for 4000-psi concrete on the basis of extensive studies of cylinder and beam tests. The steel stress-strain curve of Figure B5 was found by de Paiva and Austin¹ to be typical of intermediate grade reinforcing steel. These properties will be used in calculating the probable strengths of the specimens in this test series.

2. Fundamental Considerations

The analysis of the strength of a beam subjected to moment and axial load is based upon three assumptions:

- (1) The strains are linear through the depth
- (2) The relationship between stress and strain for a fiber of the beam is the same as for a coupon specimen
- (3) The tensile stresses in the concrete are negligible

and the condition that for equilibrium the sum of the stresses over the cross section must equal the applied axial load P and the moment of the stresses about mid-depth must equal the applied bending moment. These assumptions lead to the following developments.

3. Initial Yield State

The beam strip is assumed to yield when the computed stress in the tensile reinforcement reaches the yield point. Thus, the criterion for yielding is:

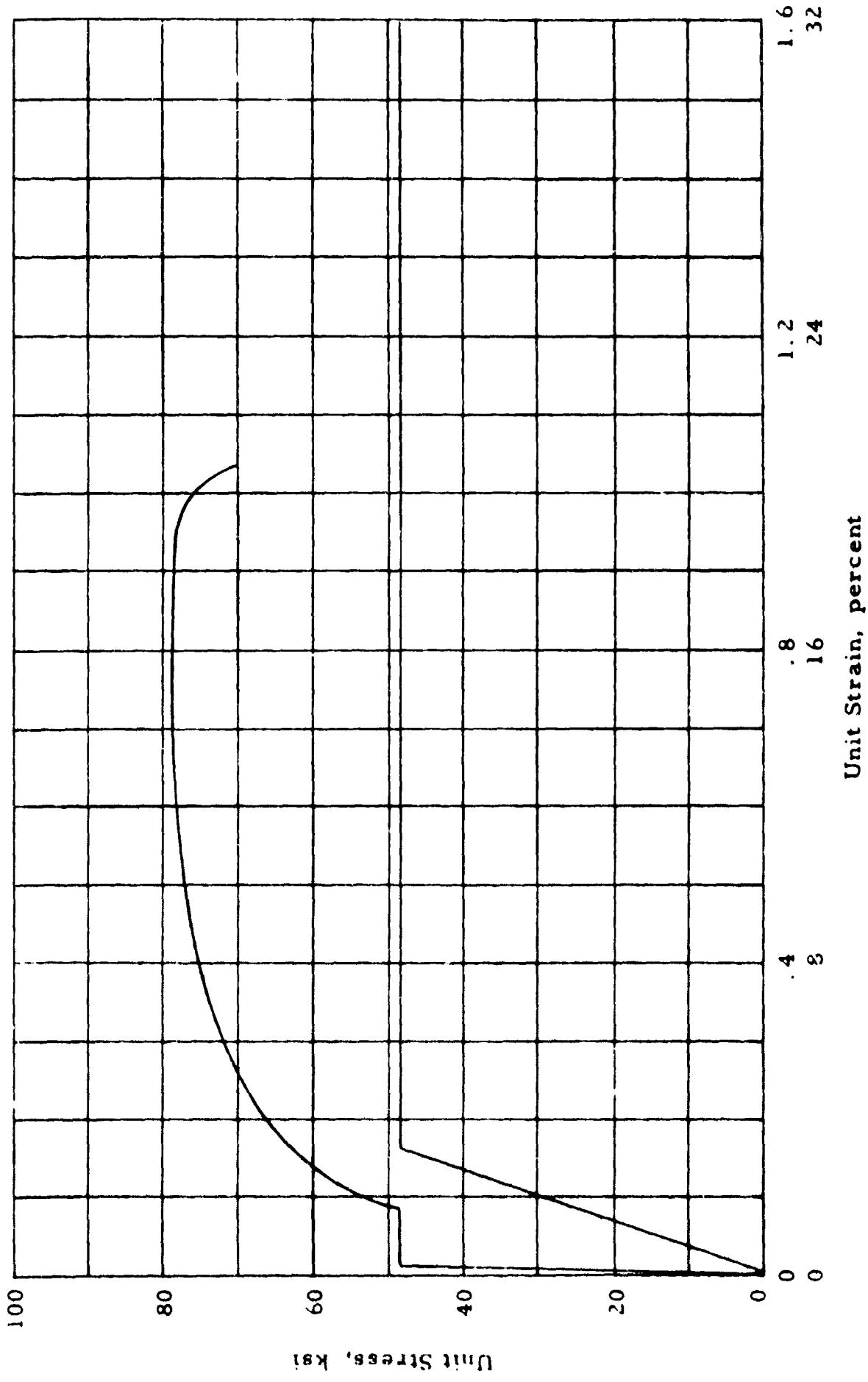


FIGURE B5. TYPICAL STRESS-STRAIN CURVE FOR THE REINFORCING STEEL

$$\epsilon_s = \epsilon_y$$

in which ϵ_y is the yield point of the tensile reinforcement, assumed equal to 0.0016 for the studies herein.

If the maximum concrete stress is less than the cylinder strength f'_c , the strain and stress distributions shown in Figure B6 are assumed to exist. The equilibrium requirement then is as follows

$$P_y = C_1 + C_s - T \quad (2a)$$

and

$$M_y = C_1 \left(\frac{h}{2} - \frac{kd}{3} \right) + C_s \left(\frac{h}{2} - g \right) + T \left(d - \frac{h}{2} \right) \quad (2b)$$

in which the values of the compressive and tensile force resultants, C_1 , C_s and T are defined on Figure B6. If the maximum concrete strain is greater than the yield strain, then the strain and stress distributions shown in Figure B7 are assumed to exist. In this case, the equilibrium requirements are as follows

$$P_y = C_1 + C_2 + C_s - T \quad (3a)$$

and

$$M_y = C_1 \left[\frac{h}{2} - \frac{1}{2} \left(kd - \frac{\epsilon_{cy}}{\alpha} \right) \right] + C_2 \left[\frac{h}{2} - \left(kd - \frac{2}{3} \frac{\epsilon_{cy}}{\alpha} \right) \right] + C_s \left[\frac{h}{2} - g \right] + T \left[d - \frac{h}{2} \right] \quad (3b)$$

It may be noted that all of the quantities in Equations (2) and (3) may be determined directly if the depth of the compression zone, kd , or the parameter, k , is known. If there is no axial load, the value of k may be determined from the following conventional elastic equation

$$k = \sqrt{2 \left[np + (n-1)p' \left(1 - \frac{d'}{d} \right) \right] + [(n-1)p' + np]^2} - [(n-1)p' + np] \quad (4)$$

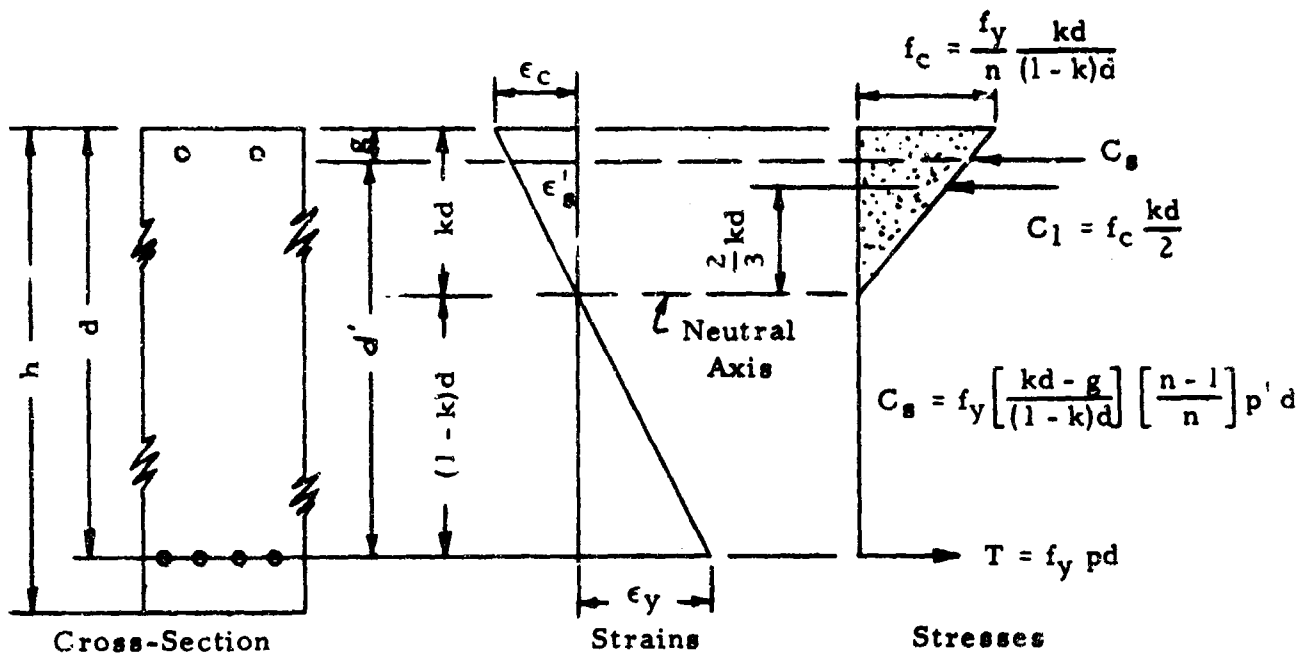


FIGURE B6. STRAIN AND STRESS RELATIONSHIPS AT YIELDING OF TENSILE REINFORCEMENT CONCRETE NOT YIELDED

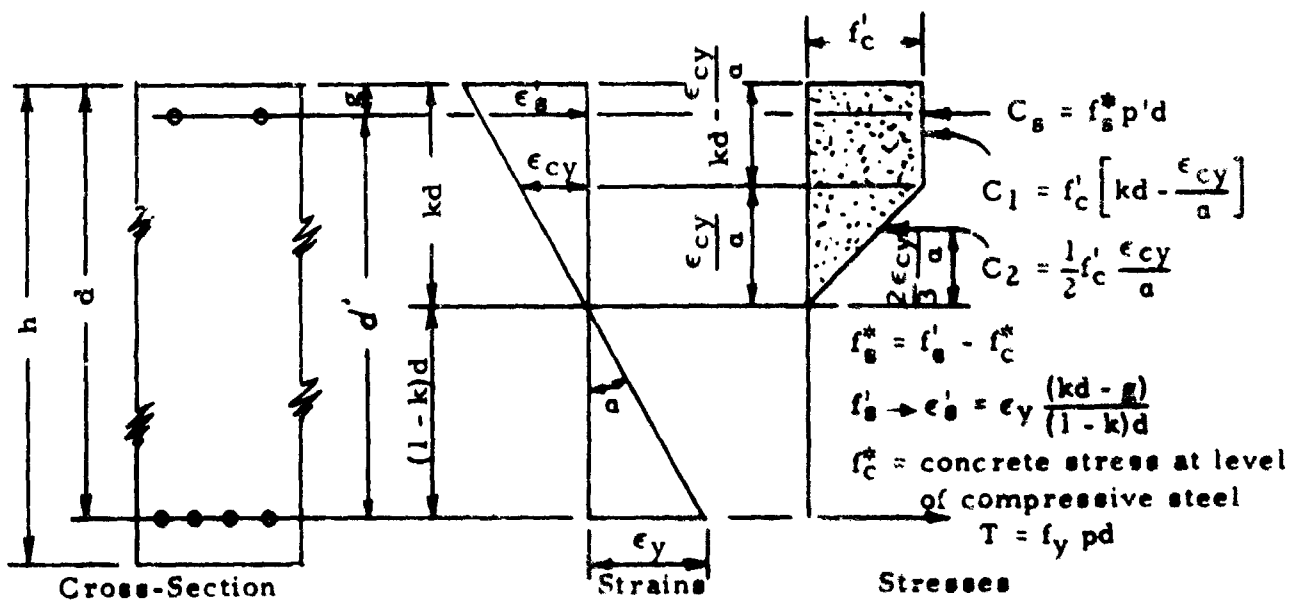


FIGURE B7. STRAIN AND STRESS RELATIONSHIPS AT YIELDING OF TENSILE REINFORCEMENT CONCRETE YIELDED

However, if the axial load is not zero, then the solution is most easily determined by a successive approximations procedure in which various values of kd , or k , are assumed and the values of P_y , M_y , and e determined. To assist in assuming reasonable values of kd , the value of e , or $1/3$, can be plotted as a function of kd , or k .

4. Ultimate State

The ultimate strength of a beam which fails by crushing of the concrete after initial yielding of the tensile reinforcement can be predicted through consideration of the distribution of stresses and strains shown in Figure B8. It is assumed that the concrete crushes when the maximum strain reaches a limiting value given by Equation (5), determined in previous beam studies

$$\epsilon_{cu} = 0.008 \quad \text{when } \frac{L}{d} \leq 3 \quad (5a)$$

$$\epsilon_{cu} = 0.001 \left(11 - \frac{L}{d} \right) \quad \text{when } 3 \leq \frac{L}{d} \leq 7 \quad (5b)$$

$$\epsilon_{cu} = 0.004 \quad \text{when } \frac{L}{d} \geq 7 \quad (5c)$$

The parameter $k_1 k_3$ has been found in previous studies to be suitably approximated by the following expression

$$k_1 k_3 = 1.37 - 0.000108 f'_c \quad (6)$$

in which f'_c is expressed in pounds per square inch.

The equilibrium requirements are as follows

$$P_u = C_1 + C_s - T \quad (7a)$$

$$M_u = C_1 \left(\frac{h}{2} - 0.42a \right) + C_s \left(\frac{h}{2} - g \right) + T \left(d - \frac{h}{2} \right) \quad (7b)$$

Note that all quantities in Figure B8 and Equations (7a) and (7b) can be evaluated once the depth of the compression zone "a" is known. The tensile steel stress at ultimate, f_{su} , must be found by use of the stress-strain curve if the corresponding strain, ϵ_{su} , exceeds the strain at the beginning of strain hardening, which is often the case. The solution may be made by a successive approximations procedure as outlined in the

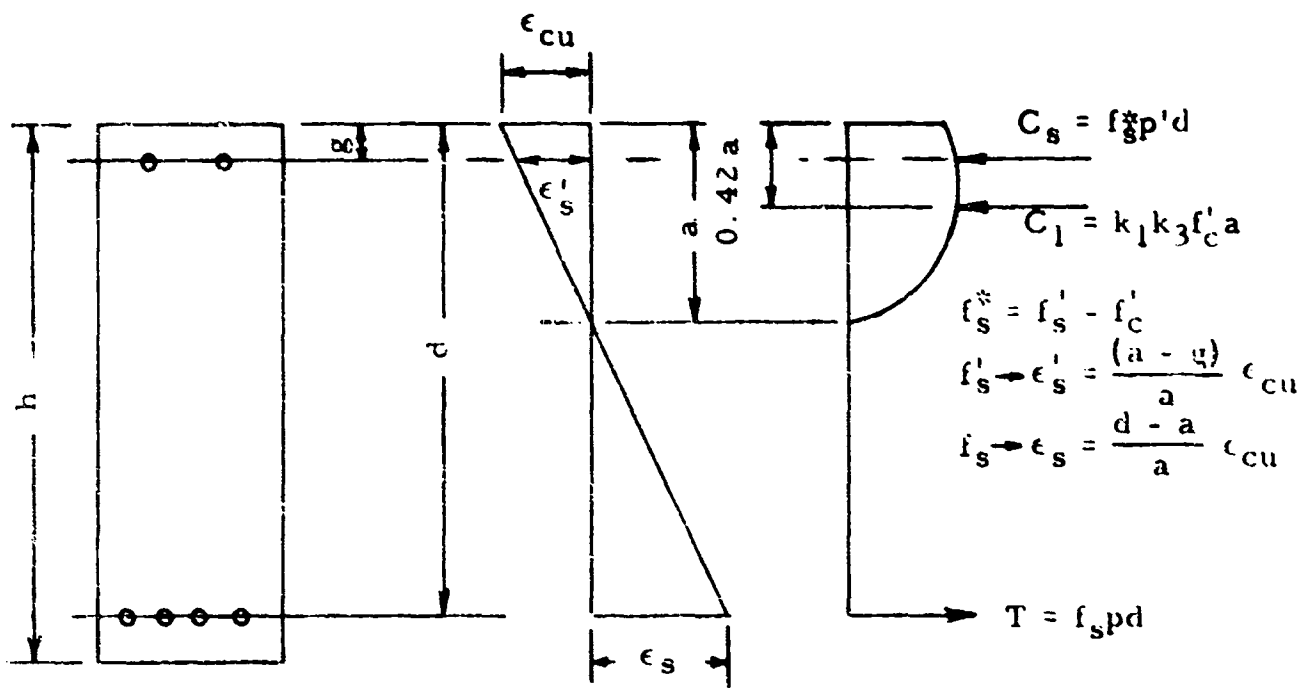


FIGURE B8. STRESS AND STRAIN RELATIONSHIPS AT ULTIMATE

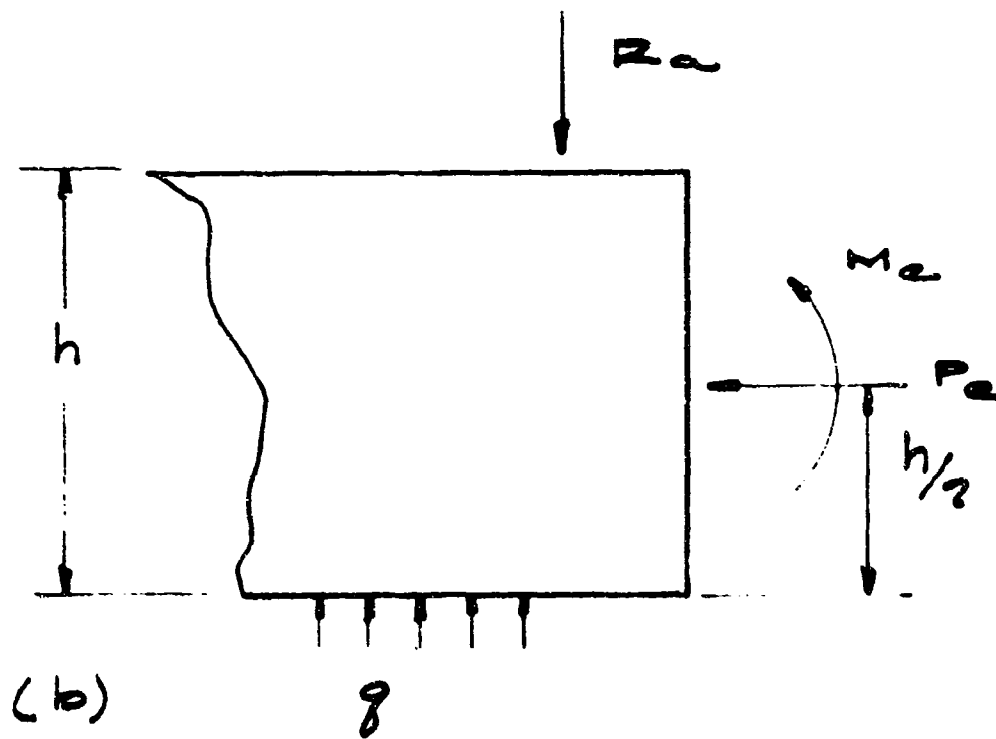


FIGURE B9. ASSUMED EDGE FORCES AT MIDEDEGE FOR DEFLECTED POSITION

previous section, starting with assumed values of the depth of the compression zone.

C. Application of Analysis for Square Slabs with Square Mesh Reinforcement

In this section are presented the results of the analyses of square concrete slabs with square mesh tensile and compressive reinforcement, with the individual reinforcing bars running parallel to the supports. The actual edge conditions of the test are discussed first. Then the theories for both elastic and plastic analyses are presented. Formulas for predicting the yield and ultimate points on the load-deflection curves are recommended, and then these formulas are applied to predict the flexural behavior of the slabs of this series of tests. Finally, a short discussion is presented of the expected results if the full pressure were allowed to act on the edges of these slabs.

1. Edge Conditions

The supporting and loading arrangements are shown in Figure A1. A simplified sketch of the supporting arrangements is shown in Figure A4. The slab is supported on the tensile, or upper, side by a steel bearing plate which will rotate on pivot A.

When the slab deflects under the pressure q , the ends will rotate about the pivots, A. Therefore, the slab will be considered to be supported from center to center of the pivots. The reaction at this point will be the reaction for a simply supported edge of a plate. The reaction at midedge of a simply supported plate, for Poisson's ratio, ν , equal to 0.13, can be found to be approximately as follows¹²

$$\text{Reaction at midedge} \cong 0.44 qL = 17 q \quad (8)$$

in which L is the inside span, equal to 39 inches, which is the total reaction at A. The reaction will vary roughly as a parabola or sine wave with a maximum at midedge and a small value at the corners.

The reaction formula of Equation (8) should be considered as a reasonable estimate for a rather ideal, closely mated slab and supports. Small variations in the fit of the slab on the supports in the preload condition may cause large discrepancies from these values. The reactions are shown in Figure B9.

When the slab deflects, the slab in contact with the bearing at point A will move outward. There should be slipping of the slab relative to the support. To reduce the coefficient of friction, a thin

plastic sheet will be inserted between the inserts and the support and seal. It is expected that the coefficient of friction μ will be reduced to a value of about 0.10 in this way. The estimated frictional forces at midedges are shown in Figure B9. These forces will vary from a maximum at midspan to small forces near the corners.

The frictional forces can be replaced by equivalent compressive forces acting in the middle plane and couples acting about the horizontal axis at mid-depth. At midedge these have the following values

$$\begin{aligned} \text{Edge Compressive Force} &= 17 \mu q \\ \text{Moment at Midedge} &= M_e = -8.5 \mu q h \end{aligned} \quad (9)$$

in which h is the total depth of the slab.

2. Elastic Analysis

Consider now the bending moments in a square, isotropic, elastic slab which is simply supported on the edges and subjected to a uniform pressure q and the edge forces described above. The maximum bending moments, which occur at midspan, are determined below. Consider that the slab has a Poisson's ratio of 0.13, as before.

The maximum bending moment due to the uniform pressure q can be found from the solutions given in Timoshenko and Woinowsky-Krieger¹² to be as follows

$$M_q = 1/24 qL^2 = 0.0417 qL^2 = 63.4 q \quad (10)$$

in which M_q denotes the bending moment at midspan due to the pressure, equal in all directions. It may be noted that the moments across a diagonal section are almost uniformly distributed, varying from this value at midspan to a value of $0.0403 qL^2$ at the corners.

The calculation of the bending moments at midspan caused by the edge moments is based upon the assumption that the applied edge moments vary along the edge as a half sine wave, with maximum value at midedge and zero values at the corners. The bending moment at midspan, equal in all directions, has been calculated from the coefficients tabulated by Newmark¹³; it is as follows

$$M_m = 0.450 M_e$$

Evaluating M_e from Equation (9), we obtain the following expression

$$M_m = -3.82 \mu q h \quad (11)$$

Additional bending moment is caused by the interaction of the compressive forces in the middle plane of the plate and the deflections. It has been determined that the frictional forces at each edge cause compressive forces which vary approximately as a parabola or sine wave along the edge. However, to simplify the calculations, it will be assumed that the actual compressive forces can be replaced by an equivalent uniform compression which has a magnitude such that the total force on the edge will be the same as for the true distribution. The force exerted on the slab by the seal and resisted by the bearing causes only moment. Therefore, the total compressive force on one edge is simply equal to the coefficient of friction μ multiplied by one-fourth of the total load on the plate. That is, if P_e is the average force per unit length on the edge

$$LP_e = 0.25 qL^2 \mu$$

or

$$P_e = 9.75 \mu q \quad (12)$$

This compressive force, in dimensions of force per unit width, will act at every point in the plate and in all directions. This is a condition of "hydrostatic compression."

The interaction of the compressive force P_e with the deflection produces the same moments as a lateral force, q_i , given by the following expression

$$q_i = -P_e \left(\frac{\partial^2 w}{\partial x^2} + \frac{\partial^2 w}{\partial y^2} \right)$$

in which w is the deflection, positive downwards, and x and y are Cartesian coordinates in the plane of the plate, parallel to the edges. If the deflected shape is assumed to have approximately the shape of a double sine wave

$$w = w_0 \sin \frac{\pi x}{L} \sin \frac{\pi y}{L}$$

in which w_0 is the deflection at midspan, then the lateral force is given by the following expression

$$q_i = 2 \frac{\pi^2}{L^2} P_e w_0 \sin \frac{\pi x}{L} \sin \frac{\pi y}{L}$$

This lateral force causes a maximum moment at midspan, for $\nu = 0.13$, as follows, as shown by Timoshenko and Woinowsky-Krieger¹²:

$$M_a = 0.565 w_o P_e$$

Evaluating P_e from Equation (12), one obtains the following expression for the maximum moment at midspan

$$M_a = 5.51 q \mu w_o \quad (13)$$

The total moment at midspan is the sum of the three components given in Equations (10), (11) and (13)

$$\text{Total Moment at Midspan} = M_o = M_q + M_m + M_a$$

or

$$M_o = 63.4 q - 3.82 q \mu h + 5.51 q \mu w_o \quad (14)$$

If the coefficient of friction μ is assumed to be equal to 0.05, Equation (14) reduces to the following form

$$M_o = 63.4 q - 0.191 q h + 0.275 q w_o \quad (15)$$

The elastic formulas of this article are expected to be applicable to the prediction of the pressure at yielding. They should not be used for the prediction of the pressure at failure.

3. Plastic Analysis

The well-known fracture-line theory, also called the yield-line theory, described in detail by Wood⁸ is expected to give approximately correct relationships between the internal forces and pressure at both yield and at failure.

Consider again the square slab subjected to uniform load, edge moments, and edge compression as described previously. The moment normal to the fracture lines is considered to be distributed uniformly along the fracture lines, and it is assumed that twisting moments parallel to the fracture lines cannot be resisted along the fracture lines. The moment normal to the fracture lines, M_f , has three components

$$M_f = M_{fq} + M_{fm} + M_{fa} \quad (16)$$

in which M_{fq} is the component due to the pressure on the slab, M_{fm} is the component due to the edge moments, and M_{fa} is the component due to the compressive forces in the plane of the plate.

Consider first the moment component due to the lateral pressure, M_{fq} . If the yield lines are taken as the two diagonals, the moment caused by the pressure q is, by statics, as follows

$$M_{fq} = \frac{1}{24} qL^2 = 0.0417 qL^2 = 63.4 q \quad (17)$$

If it is considered that the yield lines have the shape of those shown in Figure B2, with "fans" at the corners, the moment is theoretically slightly increased for the optimum position of the yield lines. Thus

$$\max. M_{fq} \cong \frac{1}{22} qL^2 = 0.0455 qL^2 = 69.1 q$$

However, experiments with reinforced concrete slabs show that the fans at the corners usually do not develop and that Equation (17) best describes the behavior. Therefore, Equation (17) is adopted herein.

Consider next the component moment M_{fm} caused by the edge moments. The fracture lines for this loading are assumed to be the diagonals, as shown in Figure B10(a). No vertical shear acts along these fracture lines because of symmetry. Consider the external and internal forces acting on the triangular segment ABO, shown in Figure B10(b). The external edge moment $M_e \sin \pi y/L$ acts along the edge AB, and the uniformly distributed moments M_{fm} act normal to the edges OA and OB. For moment equilibrium about edge AB, clearly

$$2 \left(M_{fm} \frac{L}{\sqrt{2}} \right) \frac{1}{\sqrt{2}} = \int_0^L M_e \sin \frac{\pi y}{L} dy$$

or

$$M_{fm} = \frac{2}{\pi} M_e = - 5.42 \mu qh \quad (18)$$

in which M_e was evaluated from Equation (9).

Consider now the moment component due to the uniform compressive edge forces P_e which act in the plane of the slab, as shown in Figure B11(a). The same diagonal fracture lines must be considered for this loading as for the other loadings; the position of these fracture lines is governed mainly by the primary loading q . The slab is considered to deflect due to bending along the fracture lines with each triangular segment rigid. The deflection at the center, point O, is denoted as w_o . Considering the triangular segment ABO shown in Figure B11(b), the uniform edge

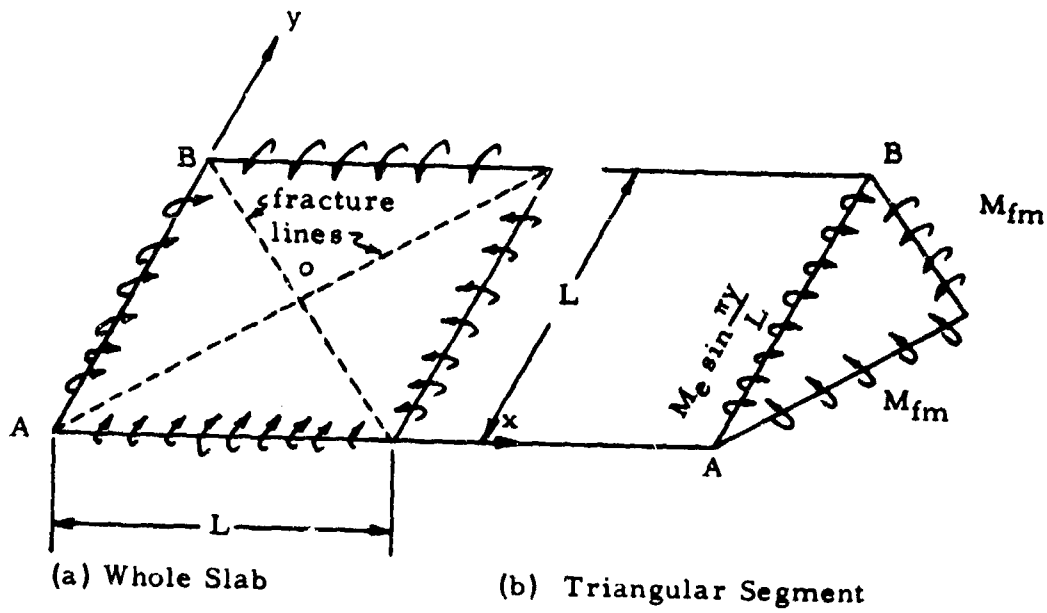


FIGURE B10. SLAB SUBJECTED TO EDGE MOMENTS

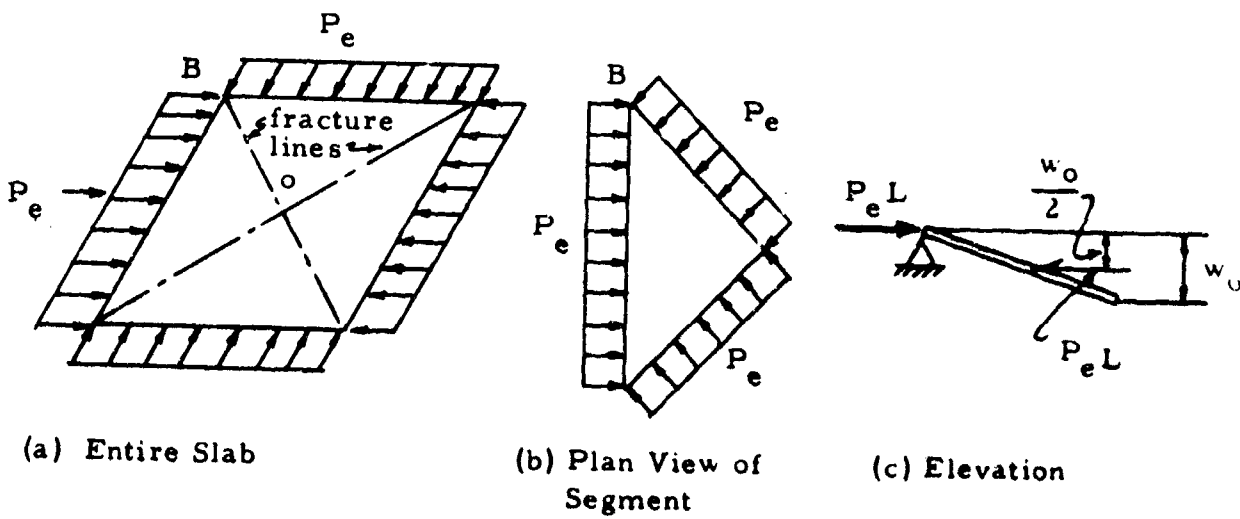


FIGURE B11. SLAB SUBJECTED TO HORIZONTAL EDGE COMPRESSIVE FORCES

compression P_e acts normal to the edge AB, and the internal compressive forces which act normal to the fracture lines OA and OB are also equal to the magnitude of P_e . These compressive forces are considered to act horizontally at all points. The resultant of the compressive forces on the two fracture lines OA and OB is a force $P_e L$ acting normal to edge AB, horizontally, and at a distance below the undeflected position of $w_o/2$, the average deflection of the fracture lines, as shown in Figure B11(c). Therefore, the moment about edge AB of the horizontal compressive force is equal to $P_e L w_o/2$. It is also clear that the moment about edge AB of the uniformly distributed moment M_{fa} which acts on the fracture lines OA and OB is equal to $M_{fa} L$. Therefore, for equilibrium of moments about AB

$$M_{fa} = P_e \frac{w_o}{2} = 4.88 \mu q w_o \quad (19)$$

in which P_e was evaluated from Equation (12).

The total uniform moment along the fracture lines is obtained by summing the components defined in Equations (17), (18) and (19)

$$M_f = 63.4 q - 5.42 \mu q h + 4.88 \mu q w_o \quad (20)$$

For a coefficient of friction, μ , of 0.05, Equation (20) takes the following form

$$M_f = 63.4 q - 0.271 q h + 0.244 q w_o \quad (21)$$

4. Prediction of Yield State

The pressure at initial yielding may be determined from the elastic Equation (15) by setting the moment at midspan, M_o , equal to the yield moment for the beam strips, M_y , as determined in Section B3. Thus

$$M_y = q_y (63.4 - 0.191 h + 0.275 w_{oy}) \quad (22)$$

In addition to the moment, a distributed force acts in the plane of the slab. It is assumed that this planar force per unit width is the average edge force P_e given by Equation (12). With the coefficient of friction assumed equal to 0.05, the distributed planar force is given by Equation (23)

$$P_y = 0.488 q_y \quad (23)$$

Equations (22) and (23) can be solved simultaneously with Equations (2) or (3), as fits the case.

The prediction of the pressure at yield may also be based upon the fracture line theory. In this case, the uniform moment along the diagonal fracture line, M_f , at yield is assumed to be equal to the yield moment for the beam strips, M_y . Thus, one obtains Equation (24)

$$M_y = q_y (63.4 - 0.271 h + 0.244 w_{oy}) \quad (24)$$

In this case, also, the distributed planar force is assumed to be equal to P_e and, hence, is given by Equation (23). Thus, Equations (23) and (24) can be solved simultaneously with Equations (2) or (3).

There is very little difference between the predictions of these two theories. Since this investigation is more concerned with determining the knee in the pressure-deflection curve than the exact point at which yielding is initiated, Equations (23) and (24) have been adopted as they are expected to give a closer estimate than Equations (22) and (23).

The deflection of the deep slab at midspan at yielding is assumed to be about the same as for a typical mid-section beam strip of the slab. Therefore, from the report by de Paiva and Austin¹, the deflection at midspan is expected to be given, roughly, by the following formula

$$w_{oy} = a \frac{\epsilon_y L^2}{(1 - k) d} \quad (25a)$$

in which

$$a = 0.250 \quad \text{for } \frac{L}{d} \leq 3 \quad (25b)$$

$$a = 0.250 - 0.0365 \left(\frac{L}{d} - 3 \right) \quad \text{for } 3 \leq \frac{L}{d} \leq 7 \quad (25c)$$

$$a = 0.104 \quad \text{for } 7 \leq \frac{L}{d} \quad (25d)$$

5. Prediction of Ultimate State

The ultimate load point ordinarily bounds the usable strength. The pressure-deflection diagram beyond this point usually has a considerable negative slope; the member in this state is not considered to be structurally dependable. In some cases, however, the maximum load may be reached considerably before the load starts to fall off rapidly. Possibly a small amount of spalling causes a premature small dip in the pressure-deflection diagram. In cases such as this, the ultimate load

point is considered to be the point just before the load starts to fall off rapidly.

It is believed that the slab will fail by crushing of the concrete in compression near midspan. The pressure coordinate of the ultimate load point can be determined from the fracture line theory. At collapse, the uniform moment along the diagonal, given by Equation (21), is expected to be equal to the ultimate moment for the beam strips, M_u , as determined in Section B5. Hence, Equation (26) can be used to determine the pressure at collapse

$$M_u = q_u (63.4 - 0.271 h + 0.244 w_{ou}) \quad (26a)$$

The planar compressive force at ultimate is given by an expression similar to Equation (23)

$$P_u = 0.488 q_u \quad (26b)$$

Equations (26) can be solved simultaneously with Equation (7) to obtain the pressure at ultimate, q_u .

The deflection at ultimate is expected to be equal to that of a typical mid-section beam strip. Therefore, the following formula, from de Paiva and Austin, is used to estimate this value

$$w_{ou} = \beta \frac{\epsilon_{su} L^2}{(1 - k_u) d} \quad (27a)$$

and

$$\beta = \alpha - 0.030 \quad (27b)$$

in which α is given by Equation (25).

6. Prediction of Test Results

The yield and ultimate states have been computed by the procedure described in Sections C4 and C5 for the static test specimens previously described and listed in Table II. The results of these computations are given in Tables IV and V and are plotted in Figures B12, B13 and B14. It should be remembered that these results are theoretical; the observed results were previously described.

In Figure B14, the pressure at yield and ultimate is plotted versus the span/depth for Specimens 1, 6 and 7, which have the

TABLE IV. SUMMARY OF PREDICTED AND OBSERVED RESULTS

Slab No.	Predicted				Observed				Ult/ Max.
	Yield		Ultimate		Yield		Ultimate		
	q_y , psi	w_y , inches	q_u , psi	w_u , inches	q_y , psi	w_y , inches	q_u , psi	w_u , inches	
1	792	0.080	1116	1.32	720	0.15	1000	0.8	Max.
2	533	0.071	825	1.82	450	0.17	850	1.2	Max.
3	1500	0.086	1900	0.99	1200	0.23	-		Max.
4	788	0.079	1085	1.15	750	0.15	920	1.08	Ult
5	512	0.073	770	1.72	450	0.17	875	2.25	Ult
6	1783	0.067	2630	1.35	1400	0.17	-	-	Max.
7	528	0.078	682	0.84	420	0.10	670	0.86	Max.
9	610	0.073	842	1.02	575	0.15	775	1.0	Max
10	298	0.067	434	1.18	300	0.2	575	2.2	Ult
11	875	0.092	1290	2.0			700	0.19	Max.

TABLE V. THEORETICAL SOLUTIONS

Specimen No.	Effective Depth, d inches	Shape	Span/Depth, L/d	Tensile Reinforcement Ratio p, percent	Compressive Reinforcement Ratio, p', percent	Depth of Neutral Axis, kd, inches	Yield		Ultimate		Coefficient of Friction, f	Concrete Strength f_c , psi
							Pressure q_y , psi	Depth of Neutral Axis, kd, inches	Deflection at Midspan, w_y , inches	Pressure, q_u , psi		
1	9.25	Square	4.22	1.0	0.5	3.00	792	.080	1116	1.32	0.1	4000
2	9.25	Square	4.22	0.5	0.5	2.20	533	.071	825	1.82	0.2	5400
3	9.25	Square	4.22	1.5	0.5	3.45	1500	.086	1900	0.99	0.2	5400
4	9.25	Square	4.22	1.0	0	2.95	788	.079	1085	1.15	0.1	4700
5	9.25	Square	4.22	0.5	0	2.38	512	.073	770	1.72	0.2	4700
6	13.25	Square	2.94	1.0	0.5	4.16	1783	.067	2630	1.35	0.1	4700
7	6.50	Square	6.00	1.0	0.5	2.12	528	.078	682	0.84	0.3	5200
8	13.25	Rect. 0.73	2.64	1.0*	0.5*	4.00	360	.053	2060	1.16	0.1	5000
9	9.25	Rect. 0.73	3.79	1.0*	0.5*	2.74	627	.067	932	1.37	0.1	3000
10	6.50	Rect. 0.73	5.38	1.0*	0.5*	1.72	298	.067	417	1.06	0.1	6400
11	12.25	Circular	3.92	1.0	0.5	3.63	875	.092	1290	2.00	0.1	5000

*Rectangular Specimens have 1/2 as much reinforcement in the long direction.

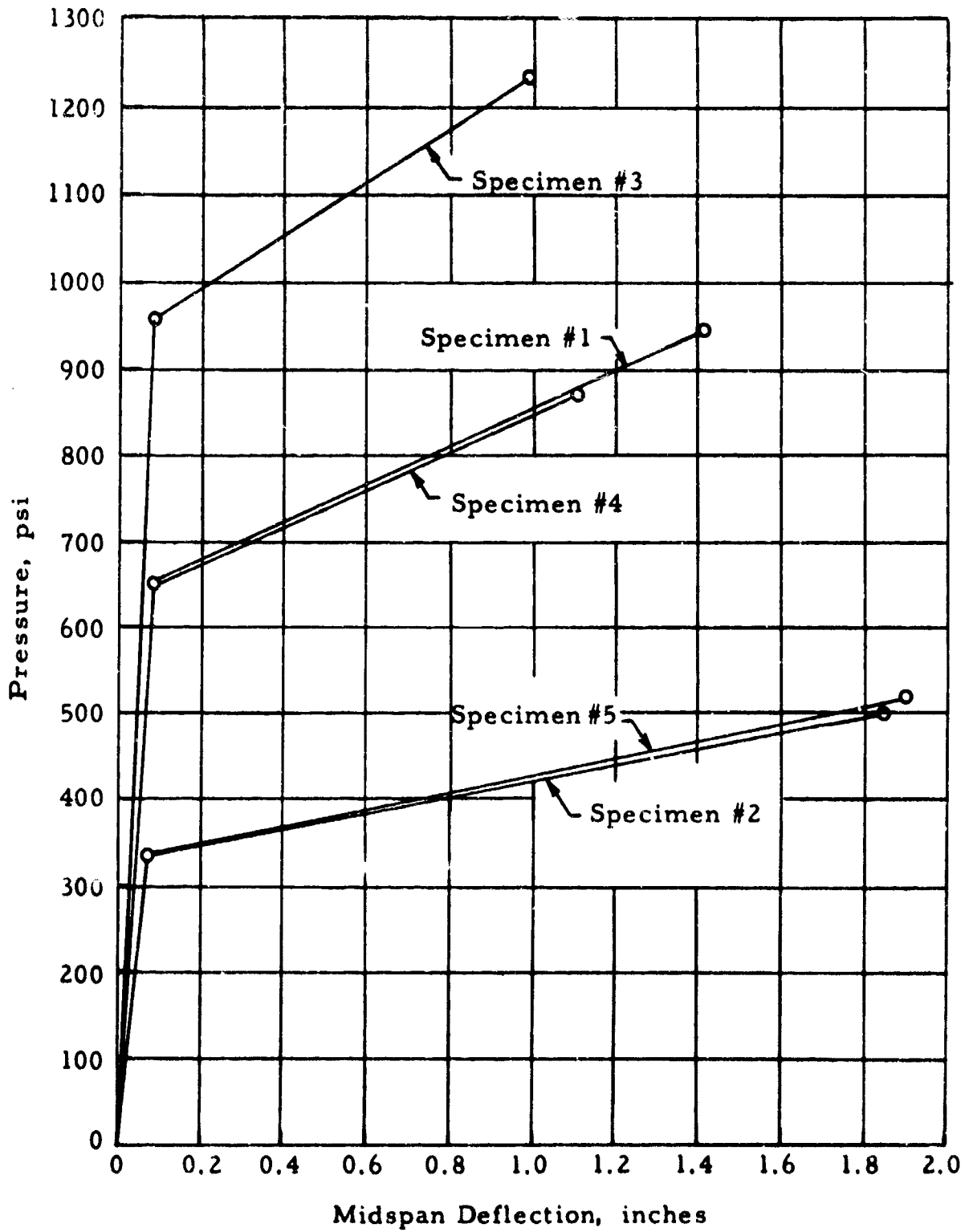


FIGURE B12. PREDICTED PRESSURE-DEFLECTION DIAGRAMS FOR SLABS WITH SPAN-DEPTH RATIOS OF 4.22

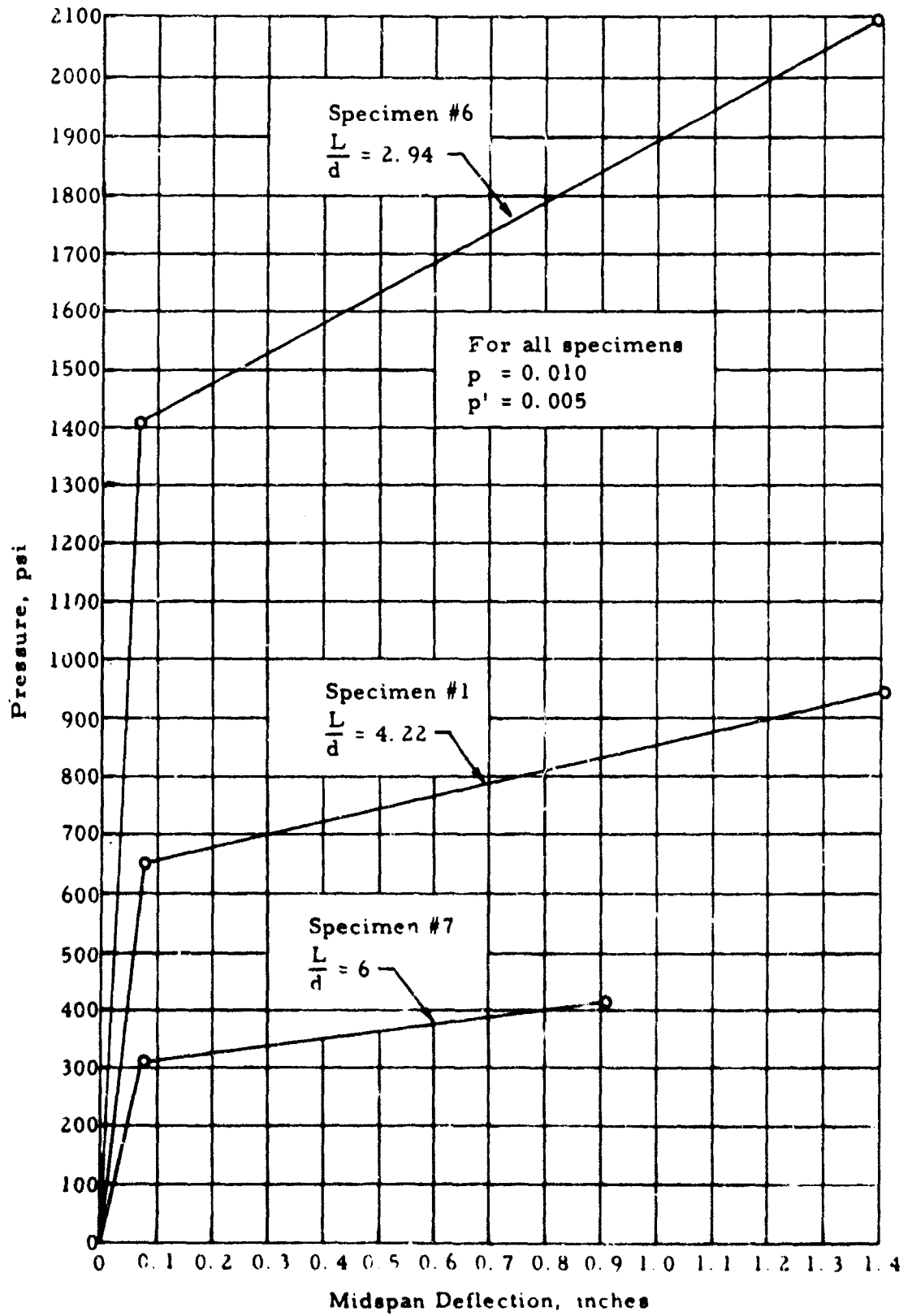


FIGURE B13. EFFECT OF SPAN-DEPTH RATIO ON PRESSURE DIAGRAMS

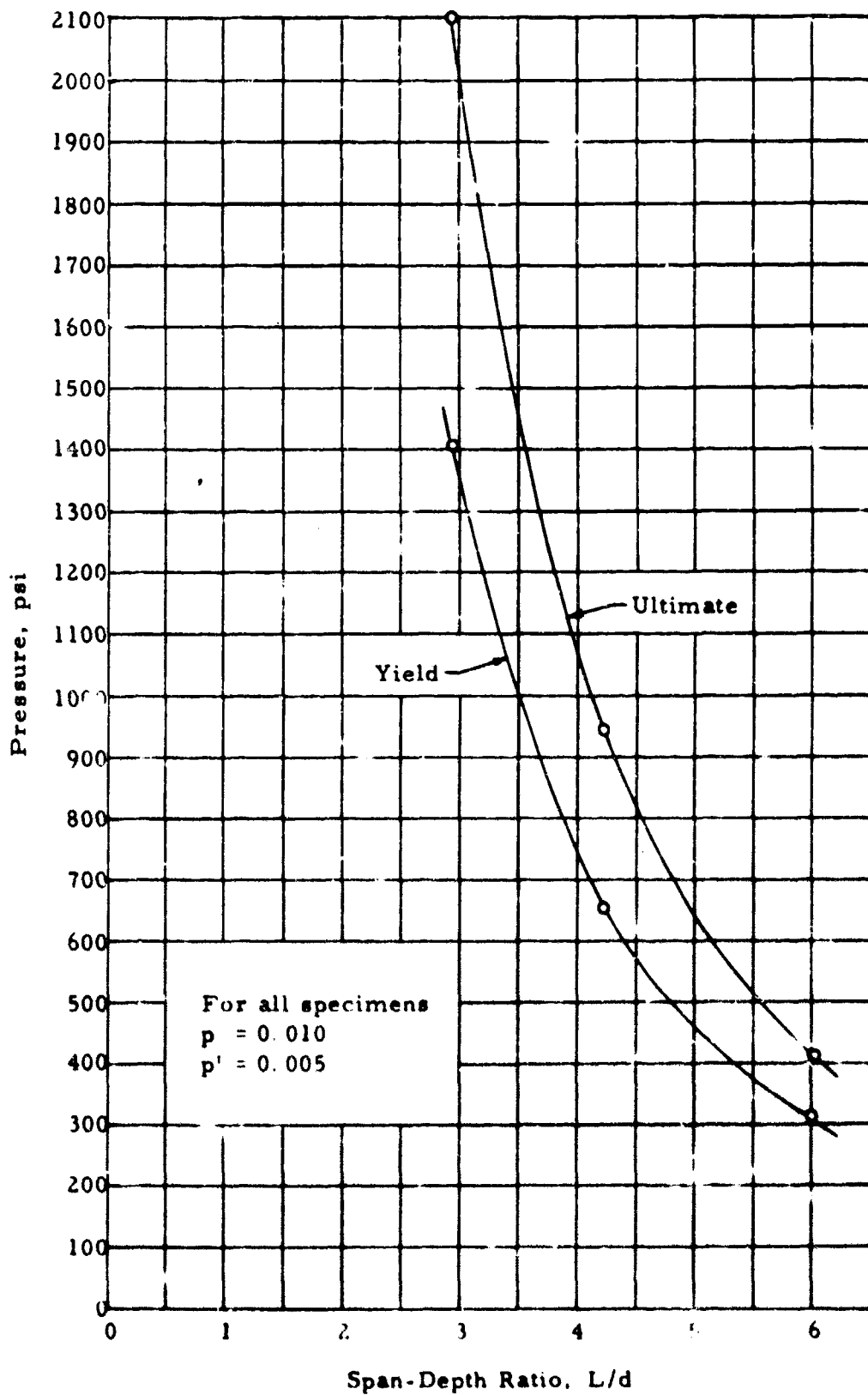


FIGURE B14. EFFECT OF SPAN-DEPTH RATIO ON PRESSURE AT YIELD AND ULTIMATE

same percentages of tensile and compressive reinforcement but different span/depth ratios. The strength of the slabs is seen to rise very rapidly as the span/depth decreases. In Figure B13, it may be noted that the deflections at ultimate did not decrease as the span/depth decreased. Hence, the energy-absorbing capacity of the deep slabs, measured by the area under the pressure-deflection curve, increased rapidly as the span/depth decreased.

In Figure B12 are shown the pressure-deflection curves for the five specimens with span/depth of 4.22. It is clear from this diagram that the strength increases as the tensile reinforcement increases. However, the ultimate deflections decrease. Thus, the energy-absorbing capacity of Specimen 3 with $p = 0.015$ is about the same as for Specimen 1, with $p = 0.010$. In Figure B12, it is also clear that the compression reinforcement is not very helpful since the diagram for Specimens 4 and 5 which do not contain compression reinforcement are almost identical with the diagrams for Specimens 1 and 2 which are identical with 4 and 5, respectively, except that they contain compression reinforcement. It is very questionable here as to whether the proposed theory adequately accounts for the beneficial effects of compression steel. The deep beam series did not give much information on the beneficial effects of compressive reinforcement. In any case, compressive reinforcement is used mainly to provide for rebound.

7. Effect of Slab Overhang and Loading Not on the Whole Span

Since the uniform load is transmitted to the slab with a flexible membrane, the loaded area is significantly less than the area enclosed by the clear spans. This reduction of loaded area is now treated as correction to the more general case of load on the entire span area.

The slab specimen overhangs the clear span by the amount of the bearing width. This overhang provides some additional strength that may be significant.

Both of these corrections enter Equation (10). Figure A4 shows this effect. Equation (10) becomes

$$M_q = \frac{qa^2}{24} \left(\frac{3L - 2a}{R} \right) \quad (28)$$

For the square specimen, the loaded area is 36 in. \times 36 in., the span area is 39 in. \times 39 in., and the reinforcement is effective over an area 43 in. \times 43 in. These dimensions give

$$M_q = 56.7 q \quad (29)$$

This correction has already been included in the predicted pressure-deflection diagrams shown in Figures 7 through 36.

This correction is not applicable to the case where pressure acts on the edges, Section C9.

8. Effect of Torsional Restraint of the Bearing Plates

Slabs 2, 5, 7 and 4 (first loading) were supported on bearing plates welded at the corners, whereas all the other slabs were supported on plates free to rotate at the corners. The torsional resistance of the plates imposes an edge moment on the slab. This edge moment has not been considered in the equations heretofore. By equating the torsional rotation relation of a rectangular bar with the edge slope relation of a simply-supported square slab, an expression for the additional edge moment is found. Thus, for the square slabs, the edge slope is

$$\begin{aligned}\theta &= 23.5 \times 10^{-4} q/h^3 \\ \theta &= 4.60 \times 10^{-6} q \quad \text{for 8-in. slabs}\end{aligned}\tag{30}$$

and for 1 in. \times 6 in. steel bearing plates, 39 in. long, twisted θ at the center

$$\theta = \frac{T \ 19.5}{41.4 \times 10^6} = 0.471 \times 10^{-6} T$$

Then, assuming the plate rotation and slab rotation are equal at the center of the edge

$$T = 9.76 q = M_e \quad \text{for 8-in. slabs}\tag{31}$$

which is the edge moment imposed by the torsional resistance of the bearing plate frame.

The torsional moment acts on the slab similar to the frictional edge moment, so Equation (31) is an additional term in Equation (15). Therefore, for the 8-in. thick slabs

$$\begin{aligned}M_m &= 0.450 M_e = 4.40 q \\ M_o &= 56.7 q - 3.82 q\mu h + 5.51 q\mu w_o - 4.40 q\end{aligned}\tag{32}$$

Similarly, for the 11-in. slabs:

$$M_e = 3.75 q$$

$$M_m = 0.450 M_e = 1.69 q$$

Therefore

$$M_o = 56.7 q - 3.82 q\mu h + 5.51 q\mu w_o - 1.69 q \quad (33)$$

For $\mu = 0.05$ and for 8-in. slabs, the moment equation becomes $M_y = 50.2 q$ instead of $M_y = 54.6 q$. This is a 9-percent increase in yield pressure. Of course, for higher friction coefficients, the percentage is higher. For example, for $\mu = 0.2$ on 8-in. slabs

$$M_y = 48.1 q \text{ without the torsion moment}$$

and

$$M_y = 43.7 q \text{ with the torsion moment}$$

which is a 10 percent increase in yield pressure. For stiffer slabs, the effect is less. For Slab 2 and $\mu = 0.1$, $M_y = 49.1 q$ instead of $M_y = 50.8 q$, which is only 3-1/2 percent increase in yield pressure.

9. Effect of Edge Pressure

Cases may arise in practice where the pressure acts on the edges of deep slabs. Therefore, the following brief study has been made to determine the approximate effect of pressure on the edges.

The edge forces for this case are shown in Figure B15. The reaction is assumed to be concentrated at the center of the pivot, as before. The magnitude of the distributed reaction at midedge is that for the slab only. Thus,

$$R_A = 17 q$$

in which q is the applied pressure acting on the slab. The distributed reaction varies along the edge roughly as a sine wave or parabola with maximum value at midedge.

When the slab deforms under load, a frictional force is induced at the reaction, as shown in Figure B15. The distributed frictional force at midedge is equal to $17 q\mu$, in which μ is the coefficient of friction. This causes the following distributed edge moment about the middle surface of the slab

$$\text{Moment at Midedge} = M_e = - 8.5 \mu qh$$

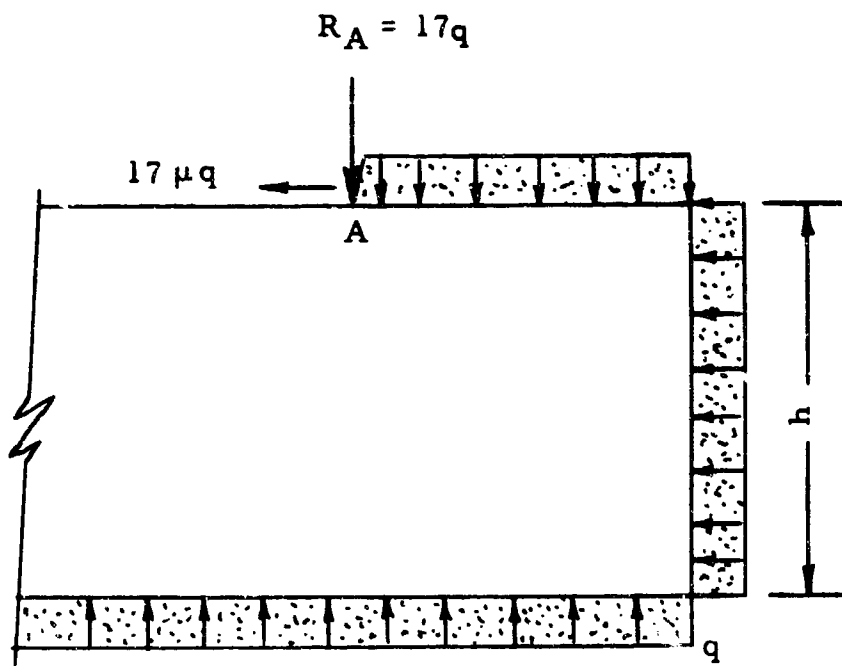


FIGURE B15. ASSUMED EDGE FORCES AT MIDEDEGE FOR SLAB SUBJECTED TO EDGE PRESSURES

in which h is the total depth of the slab. The distributed edge moment also varies along the edge roughly as a sine wave or parabola.

In addition to the edge moment M_e , a distributed edge compressive force acts in the plane of the slab. The edge compressive force is caused by the frictional force at the reactions and the pressure on the ends. The average value of the compressive force due to friction is given by Equation (12), and the compressive force due to the pressure is equal to qh . Therefore, the total average compressive force P_E is given by the following equation

$$P_E = qh + 9.75 \mu q$$

The following analysis of the behavior of the deep slabs is based upon the fracture line theory, as before. The uniformly distributed moment across the fracture lines, M_f , is composed of three components: namely, the moment due to the lateral load, M_{fq} ; the moment due to the edge moments, M_{fm} ; and the moment due to the edge compressive force, M_{fa} ; as indicated in Equation (16).

The fracture line moment due to the lateral load, M_{fq} , is given by Equation (17) as before.

The moment along the fracture lines due to the edge moments, M_{fm} , is given by Equation (18)

$$M_{fm} = \frac{2}{\pi} M_e = -5.42 \mu qh$$

The fracture line moment due to the edge compressive force, M_{fa} , is given by the following expression which is analogous to Equation (19)

$$M_{fa} = P_e \frac{w_o}{2} = qw_o (0.500 h + 4.88 \mu)$$

The total uniform moment along the fracture lines is obtained by summing the three components. The following expression is obtained for $\mu = 0.05$

$$M_f = q \left\{ 63.4 - 0.270 h + w_o (0.500 h + 0.244) \right\} \quad (34)$$

The average compressive force in the slab is given by the following expression for $\mu = 0.05$:

$$P_E = q(h + 0.488) \quad (35)$$

The deflections at yield and ultimate are computed by Equations (25) and (27), as before.

Equations (34) and (35) are used with Equations (2), (3), or (7) to obtain the desired solutions, as described previously.

The yield and ultimate load points have been computed for Specimens 1, 6 and 7. To illustrate the effect of edge pressure, the theoretical pressure-deflection diagrams for Specimens 1, 6 and 7 are shown, both for pressure acting on the edges and for no pressure on the edges, in Figure B16. It can be seen that edge pressure raises substantially the pressures at yield and ultimate but decreases the ductility greatly. Thus, for Specimen 1 with span/depth of 4.22, the pressure at yielding is more than doubled, the pressure at ultimate is raised by 52 percent, and the midspan deflections at failure are decreased from 1.41 inches to 0.36 inch. It may be noted that the deepest slab, Specimen 6, with span/depth of 2.94, fails before the tensile reinforcement yields.

The proposed theory for slabs with edge pressure is considerably more of an extrapolation than the corresponding theory for slabs without edge pressure. Experimental verification is needed before this theory can be relied upon. The current series of tests of slabs without edge pressure are not suitable for this purpose.

D. Rectangular Slabs with Orthotropic Reinforcements

The behavior of rectangular slabs is sufficiently similar to square slabs that only the analysis that departs from the square slab analysis will be presented in this section.

The expected cracking pattern is shown in Figure B17. The crack development is like the square slabs described in Section A.

Heretofore, the slab reinforcement has been a square mesh with reinforcement percentage the same in both directions, or the isotropic reinforcement. For the rectangular slabs, the reinforcement percentage in the long direction has been reduced to half that in the short direction according to the moment requirement for this aspect ratio. This orthotropy and the aspect ratio are treated in the following analysis.

1. Flexural Analysis

The flexural analysis of rectangular slabs with orthotropic tensile and compressive reinforcement is presented in this section.

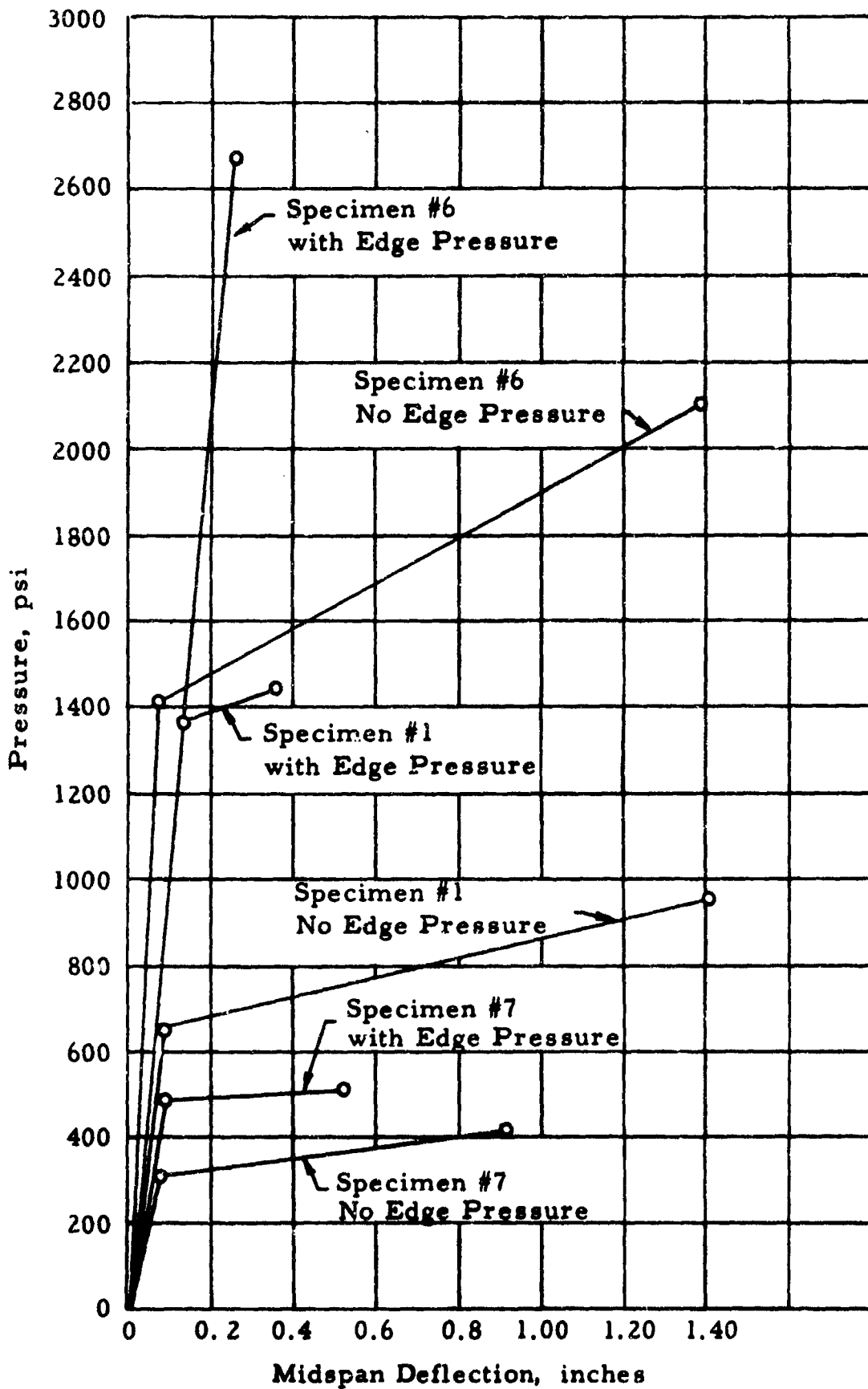


FIGURE B16. PRESSURE-DEFLECTION DIAGRAM FOR SPECIMENS 1, 6, AND 7 WITH AND WITHOUT EDGE PRESSURE

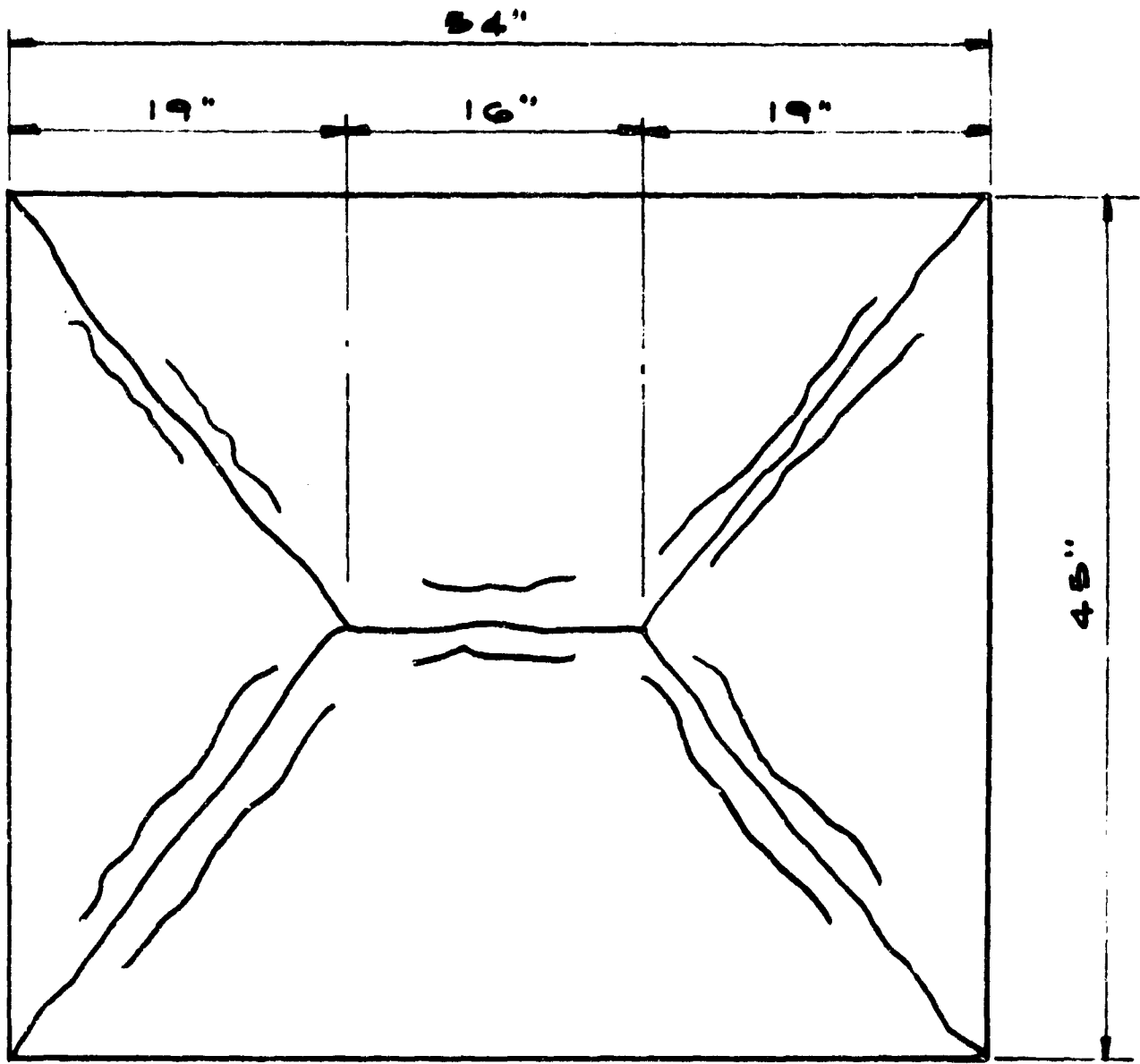


FIGURE B17. EXPECTED CRACKING PATTERN FOR RECTANGULAR SLABS

As the edge conditions define the boundaries of the flexural action, they are discussed first. Equations for predicting the pressure and deflection at which the tensile reinforcement yields and at which the concrete crushes (ultimate point) are given. Solutions to these equations for the slab specimens to be tested in this investigation are given and are plotted as predicted pressure-midspan deflection diagrams, Figures 28, 31, and B19.

a. Edge Conditions

The supporting and loading geometry is shown schematically in Figure A4. The slab reaction is carried through a 6-inch-wide bearing plate that is free to rotate with the slab about the pivot. The uniform load (hydrostatic pressure) is transmitted to the slab by means of a flexible membrane. This loading technique prevents pressure from acting on the slab edges, accommodates slight variation in slab depth, and eliminates any concentrated loads due to fixtures bearing on the slab. This load acts on an area somewhat less than the full slab area as shown in Figure A4; therefore, it must be accounted for in the analysis. This effect, however, is treated as a correction to the more typical case of load on the entire slab. At "miedge," the center of edge of the slab, the approximate reaction, as found by Reference 12, is

$$R_a = 0.49 qL = 17.2 q \text{ (long edge)} \quad (36)$$

These reactions vary along the edge with the above values occurring at the miedges and a smaller value at the corners.

As the slab deflects, the slab in contact with the bearing will move outward. There will be slipping of the slab relative to the bearing plate. The friction generated develops edge compression and moment even though friction reducing devices are used, as shown in Figure B9. The frictional forces can be evaluated as an equivalent compressive force acting in the mid-plane of the slab and a couple acting about the horizontal axis at mid-depth. At miedge these forces have the following values

$$\text{Long Edge Compressive Force} = 17.2 q\mu \quad (37)$$

$$\text{Long Edge Moment} = 8.6 q\mu h \quad (38)$$

where h is the total depth of the slab.

b. Elastic Analysis

The bending moments in a rectangular, orthotropic, elastic slab which is simply supported on the edges and loaded by a uniform pressure, q, and the edge forces described above are now considered. The

maximum bending moment induced by the uniform load will occur at mid-span. For the case of an orthotropic slab, the magnitude of this moment is given by Equation (39)¹⁴

$$M_q = q \frac{L^2 a^2}{24} \left[\sqrt{3 + \beta^2} - a\sqrt{\beta} \right]^2 \quad (39)$$

where

$$a = \text{aspect ratio of rectangle} = \frac{\text{width}}{\text{length}}$$

$$= 35''/48'' = 0.729$$

$$\beta = \text{ratio of orthotropy} -$$

$$= \frac{\text{yield moment in long direction}}{\text{yield moment in short direction}}$$

In this investigation, the rectangular specimens have been designed according to the ACI Code and the U. S. Army Corps of Engineers' practice which results in a $\beta = 1/2$. Equation (39) becomes then

$$M_q = q \frac{L^2}{27.06} \quad \text{for the long direction}$$

$$M_q = q \frac{l^2}{14.39} \quad \text{for the short direction} = 85.3 q$$

for $l = 35''$

(40)

The edge moments are computed in the same manner as for a square slab with appropriate corrections. The complete derivation is described in Section C2 and will not be repeated here. The pertinent resulting relations are as follows

$$M_m = 0.58 M_e = 5.0 q\mu h \quad \begin{array}{l} \text{midspan moment} \\ \text{due to friction} \\ \text{forces on the long} \\ \text{edge with coeffi-} \\ \text{cient of friction } \mu \end{array}$$

(41)

$$M_a = 0.565 w_o P_e$$

the midspan moments induced by the interaction of the edge compressive force P_e with the deflection w_o

(42)

The average edge compressive force P_e is

$$P_e = \mu R$$

From Figure B18

$$R_a = \frac{q(L-l)l/2 + (l/2)^2 q}{L} = 11.1 q$$

so

$$P_e = 11.1 q \mu \quad (43)$$

Therefore, from Equation (42), $M_a = 6.28 q \mu w_o$. Total moment at midspan is

$$M_o = M_q + M_m + M_a$$

or

$$M_o = 85.3 q - 5.0 q \mu h + 6.28 q \mu w_o \quad (44)$$

As in the case of square slabs, the uniform load does not act on the full span width and length as shown in Figure A4. Furthermore, the slab is larger than the span by the amount of the bearing surface. Both of these effects increase the pressure at which yield and failure occur. These two effects are evaluated by appropriate dimension changes in the relations given in Reference 14. Thus

$$R = 16.2 q$$

$$M_o = 69.0 q - 4.7 q \mu h + 5.74 q \mu w_o \quad (45)$$

and

$$P_e = 10.13 q \mu \quad (46)$$

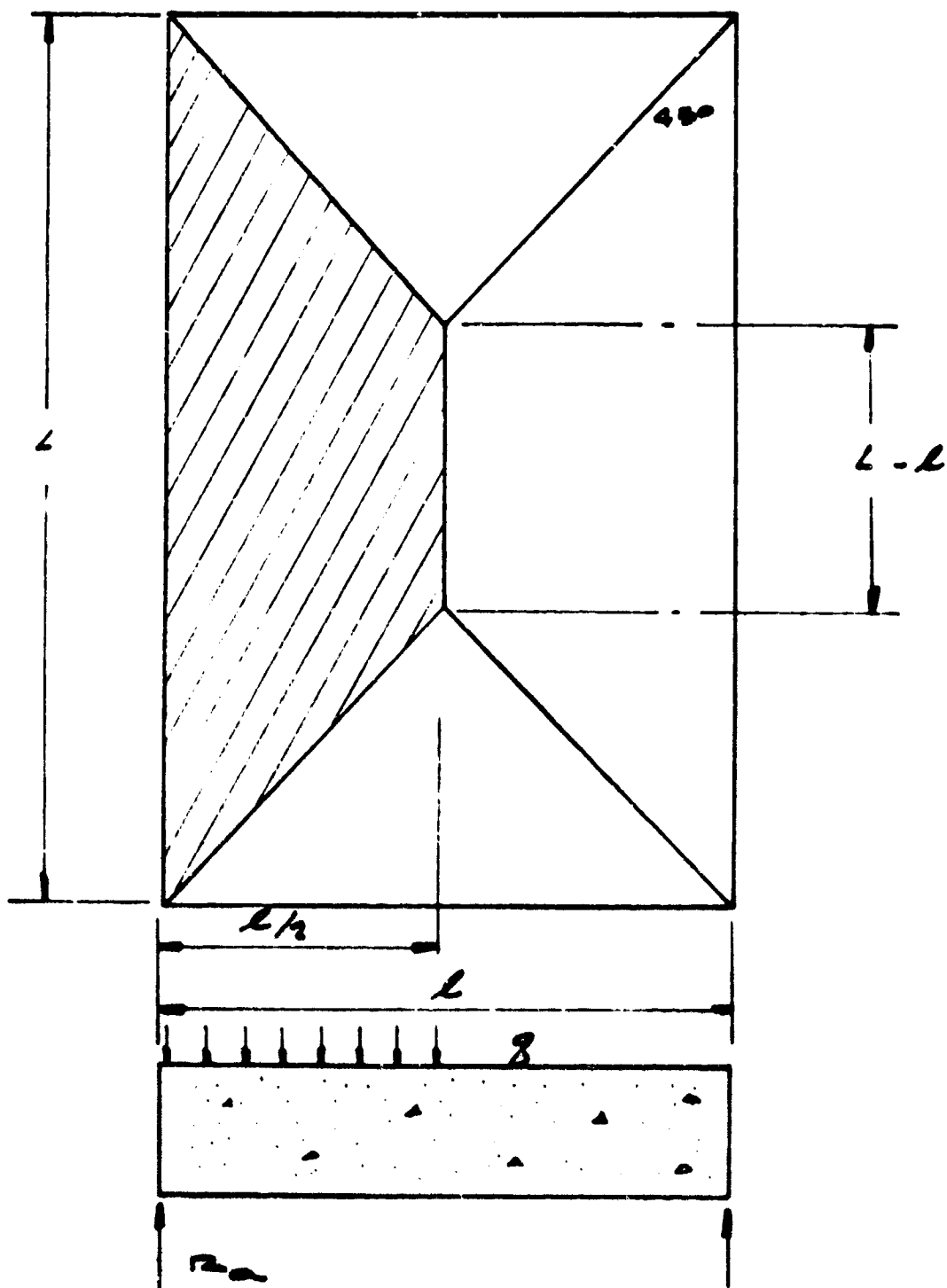


FIGURE B18. DISTRIBUTION OF LOAD ON REACTIONS

These are the relations used to predict the yield pressure coordinate on the load-deflection curves for the rectangular specimens used in this investigation.

c. Plastic Analysis

The fracture-line theory of Wood⁸ is applicable to the plastic response of the slabs. The theory presented in Section C3 while developed for square slabs is generally applicable to all slabs. The resulting equation is

$$M_f = 85.3 q - 5.47 q\mu h + 5.55 q\mu w_{ou} \quad (47)$$

The effect of restricted load area and slab overhang must also be included. Equation (47) thus becomes

$$M_f = 69.0 q - 5.15 q\mu h + 4.05 q\mu w_{ou} \quad (48)$$

d. Prediction of Yield State

The yield pressure may be determined by setting the elastic Equation (45) equal to the equation of equilibrium, Equation (2)

$$\begin{aligned} M_y &= C_1 \left(\frac{h}{2} - \frac{kd}{3} \right) + C_s \left(\frac{h}{2} - g \right) + T \left(d - \frac{h}{2} \right) \\ P_y &= C_1 + C_s - T \end{aligned} \quad (49)$$

in which the values of the compressive and tensile force resultants, C_1 , C_s , and T are defined in Figure B6.

All the quantities in Equation (49) can be determined directly if the depth of the compression zone, kd , is known. The axial load complicates the determination of the value kd ; therefore a successive approximation procedure is used. Values of kd are assumed which determine the values of P_y , M_y , and $e_y = M_y/P_y$. When this e_y approximately equals the "e" required by the ratio of [Equation (45)/Equation (46)], the trial kd is correct. Since

$$M_o = M_y = q_y (69.0 - 4.70 \mu h + 5.74 \mu w_{oy})$$

$$\therefore q_y = M_y / (69.0 - 4.70 \mu h + 5.74 \mu w_{oy})$$

The midspan deflection of the deep slab at yielding of the tensile steel is assumed to be about the same as for a typical mid-section beam strip of the slab. Therefore from the report by de Paiva and Austin¹, the deflection at midspan is expected to be as follows:

$$w_{oy} = \frac{\alpha \epsilon_y l^2}{(1 - k) d} \quad (50)$$

in which

$$\alpha = 0.250 \quad \text{for } \frac{l}{d} \leq 3$$

$$\alpha = 0.250 - 0.0365 \left(\frac{l}{d} - 3 \right) \quad \text{for } 3 \leq \frac{l}{d} \leq 7$$

$$\alpha = 0.104 \quad \text{for } 7 \leq \frac{l}{d}$$

e. Prediction of Ultimate State

The ultimate load point of the pressure-deflection diagram is the upper bound of the usable strength of the slab. The diagram beyond this point usually has a considerable negative slope. The slab in this state is not structurally dependable.

The pressure coordinate of the ultimate load point can be determined from the fracture line theory which is Equation (48). This equation is set equal to the equations of equilibrium

$$M_u = C_1 (h/2 - 0.42a) + C_2 (h/2 - g) + T (d - h/2)$$

$$P_u = C_1 + C_2 - T$$

(51)

Values for M_u and P_u were determined by the successive approximation technique used for the yield state. In this technique, values of "a" are assumed which give values for M_u and P_u , thus, $e_u = M_u/P_u$. When $e_u = e = [\text{Equation (48)}/\text{Equation (46)}]$, then

$$M_o = M_u = q_u (69.0 - 5.15 \mu h + 4.05 \mu w_{ou})$$

Therefore

$$q_u = M_u / (69.0 - 5.15 \mu h + 4.05 \mu w_{ou})$$

Midspan deflection at ultimate is expected to be equal to that of a typical mid-section beam strip. Therefore, the formula from de Paiva and Austin¹ is used to estimate deflection as follows:

$$w_{ou} = \beta \frac{\epsilon_{su} l^2}{(1 - k_v) d} \quad (52)$$

and

$$\beta = \alpha - 0.030$$

where α is given in Equation (50).

2. Prediction of Static Response of Rectangular Slab Specimens

The analysis described above is to be experimentally evaluated with the loading and supporting technique indicated. The test specimens are described in Table II. Specific predictions for those specimens are presented in this section as well as a brief comparison between the behavior of the square and rectangular specimens.

a. Prediction of Pressure-Deflection Diagram for Test Slabs

The yield and ultimate states have been computed by the procedure described in Sections D1d and D1e for the rectangular static specimens listed in Table II. The results of these computations are given in Tables IV and V and plotted in Figure B19. The experiments on the square slabs demonstrated that the coefficient of friction between the slab and bearing plate could not be reduced to 0.05. A realistic friction factor of 0.1 has been used to predict the rectangular slab behavior.

b. Comparison between Square and Rectangular Slabs

For comparison between the square isotropic slab specimens predicted in Section C6 and the rectangular orthotropic slab specimens predicted in this section, Figure B19 also contains the square diagrams. Specimen 1 is the square companion to Specimen 9, and Specimen 7 is the mate to Specimen 10, etc. Each pair has the same depth and contains the same percentage of reinforcement. The square span is 39 inches, whereas the rectangular span is 35 in. \times 48 in. It should be noted that the rectangular slab is weaker primarily because it is rectangular, not because it is orthotropic. The yield pressure for an isotropic rectangular slab is only 2-1/2 percent greater; whereas the yield pressure for a square orthotropic slab with $\beta = 1/2$ is 38 percent greater than the yield pressure of the rectangular orthotropic slab.

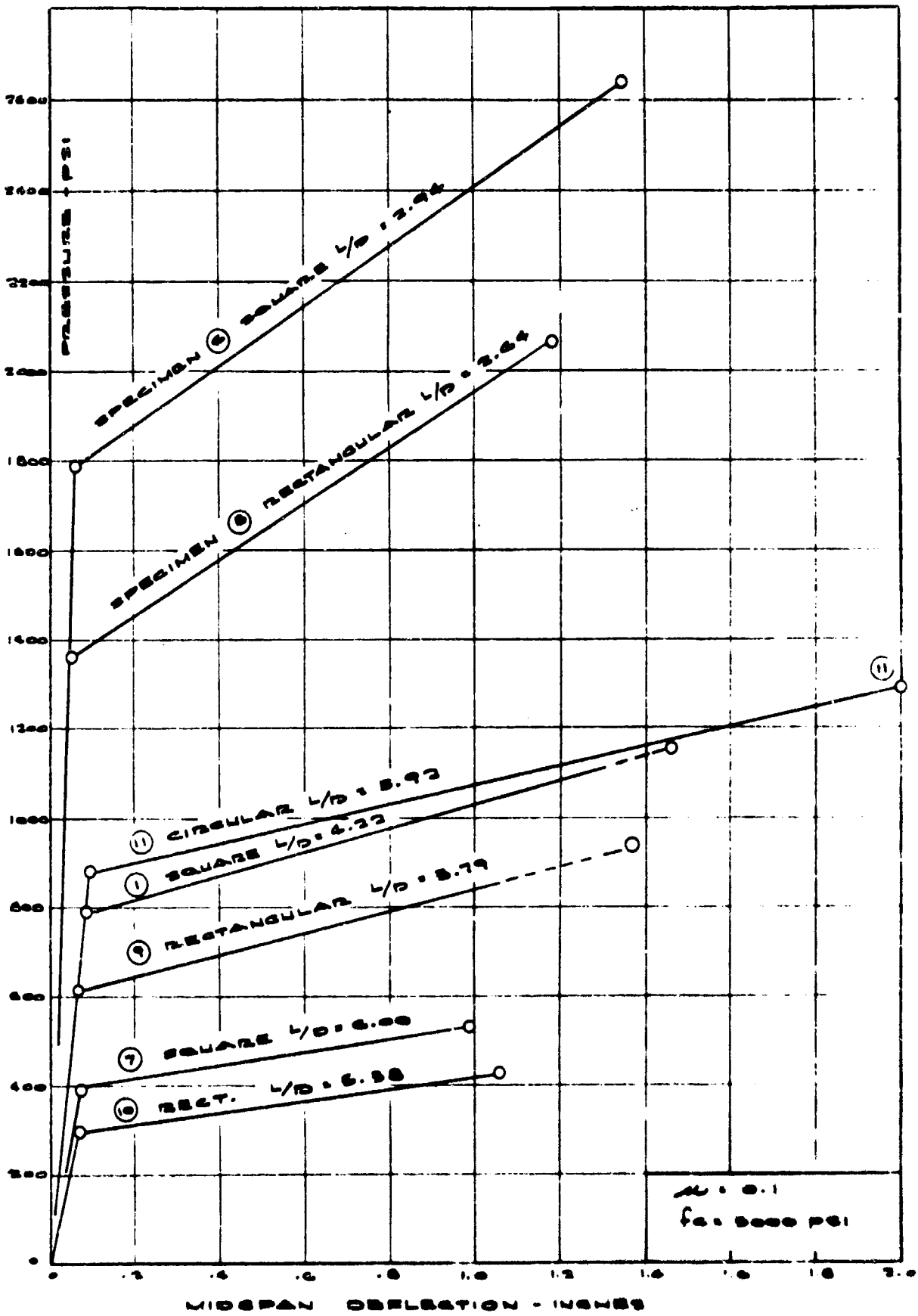


FIGURE B19. PREDICTED PRESSURE-DEFLECTION DIAGRAMS
 COMPARING RECTANGULAR, SQUARE
 AND CIRCULAR SPECIMENS

E. Circular Slabs

For the circular slabs, the essential change in the theory occurs in the yield line analysis which is summarized in the following paragraphs. Figure B20 shows the expected cracking pattern, the essential terms and the radial wedge being analyzed. The resultant load on the wedge is $Q = \theta a^2 q / 2$, which acts at the centroid of the circular sector. The distance of the centroid from the center of the circle is $aa = (2a \sin \theta / 2) / (3\theta / 2)$, which depends on the angle θ . For small angles, the sector approaches a triangle. Therefore

$$a = 2/3$$

For equilibrium of moment on the radial wedge

$$\begin{aligned} Mc\theta + mc\theta &= Q(b - 2/3 a) \\ &= \frac{\theta a^2 q}{2} (b - 2/3 a) \end{aligned}$$

or

$$M + m = q \frac{a^2 (3b - 2a)}{6c} \quad (53)$$

Equation (53) for the test specimen described in Table II is

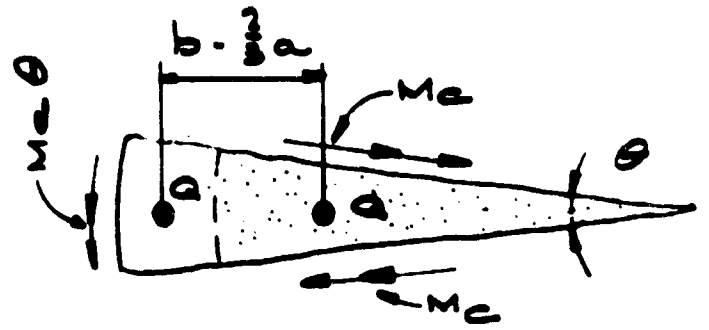
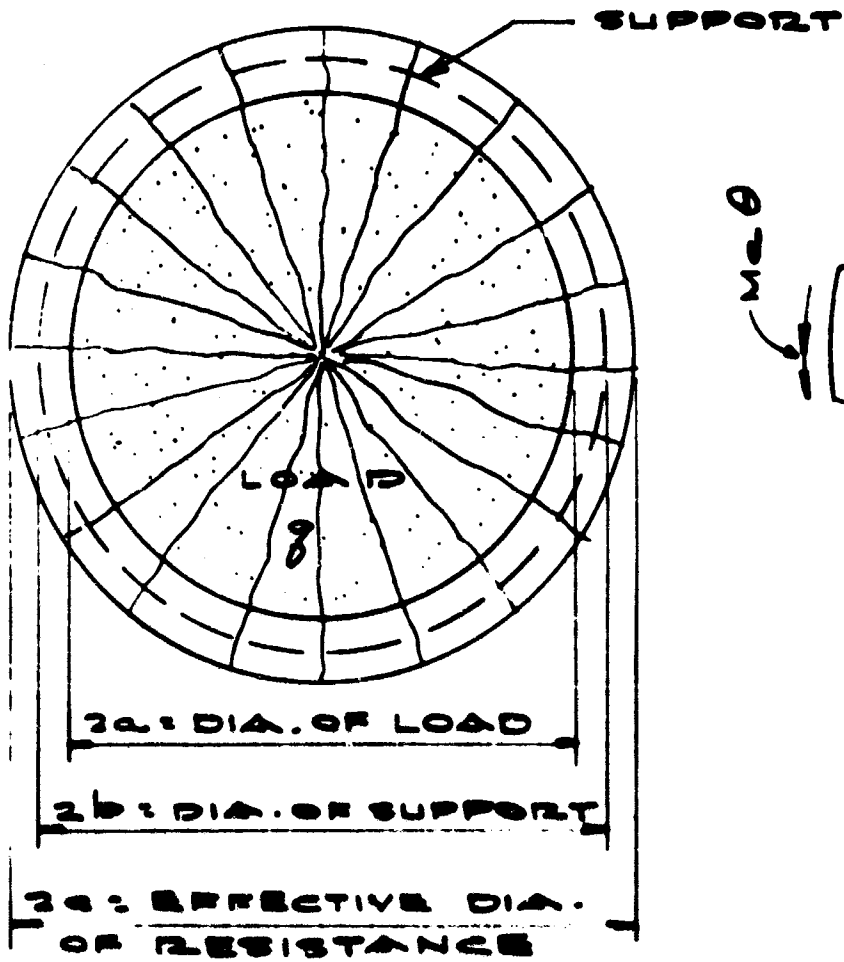
$$M + m = 84.4 q \quad (54)$$

The edge conditions are the same as the square and rectangular slabs. The frictional forces are

$$\begin{aligned} P_e &= \mu R \\ R &= \frac{a^2}{2b} q = 10.55 q \\ \therefore P_e &= 10.55 q\mu \\ M_e &= 10.55 q\mu h / 2 \end{aligned} \quad (55)$$

For circular slabs, the center moment, M_m , due to the edge moment, M_e , is

$$M_m = M_e = 5.28 q\mu h \quad (56)$$



Consider radial wedge

FIGURE B20. YIELD-LINE ANALYSIS FOR CIRCULAR SLABS

The interaction of the edge compression, P_e , and the deflection, w_o , is expected to be the same as for square slabs

$$M_a = 0.565 w_o P_e$$

From Equation (55)

$$M_a = 5.97 q \mu w_o \quad (57)$$

The total elastic moment at midspan is the sum of the three components given in Equations (54), (56) and (57)

$$M_o = 84.4 q - 5.28 q \mu h + 5.97 q \mu w_o \quad (58)$$

The total plastic moment is derived similarly, using the square slab edge effects, thus

$$M_f = 84.4 q - 3.32 q \mu h + 5.27 q \mu w_o \quad (59)$$

Using the deflection prediction equations, the equilibrium equations, and the computation procedures from Sections C4 and C5 along with the dimensions of the specimen described above, the predicted pressure-deflection diagram has been computed. The diagram is shown in Figure 34 and compared with the square and rectangular specimens on Figure B19 and Table V.

The bearing plate for the circular slab is a complete ring 6 in. X 2 in. X 54 in. O.D. The edge moment due to the torsional resistance of this ring has not been included in the above analysis. This moment term is expected to affect the yield pressure prediction only a few percent on such a thick slab as it did on the 11-inch deep square slabs.

LIST OF REFERENCES

1. de Paiva, H. A. R., Austin, W. J., "Behavior and Design of Deep Structural Members, Part 3, Tests of Reinforced Concrete Deep Beams," Technical Report to Air Force Special Weapons Center, AFSWC-TR-59-72, March 1960.
2. Untrauer, R. E., "Behavior and Design of Deep Structural Members, Part 4, Dynamic Tests of Reinforced Concrete Deep Beams," Technical Report to Air Force Special Weapons Center, AFSWC-TR-59-72, May 1960.
3. Winemiller, J. R., and Austin, W. J., "Behavior and Design of Deep Structural Members, Part 2, Tests of Reinforced Concrete Deep Beams with Web and Compression Reinforcement," Technical Report to Air Force Special Weapons Center, AFSWC-TR-59-72, August 1960.
4. Feldman, A., "Behavior and Design of Deep Structural Members, Part 5, Resistance and Behavior of Reinforced Concrete Beams of Normal Proportions under Rapid Loading," Technical Report to Air Force Special Weapons Center, AFSWC-TR-59-72, March 1960.
5. Keenan, W. A., and Feldman, A., "Behavior and Design of Deep Structural Members, Part 6, The Yield Strength of Intermediate Grade Reinforcing Bars under Rapid Loading," Technical Report to Air Force Special Weapons Center, AFSWC-TR-59-72, November 1959.
6. Untrauer, R. E., "The Investigation of Deep Reinforced Concrete Beams under Static and Dynamic Loading, Vol. I, Strength and Behavior in Flexure," AFSWC-TR-61-47, Vol. I, July 1961.
7. de Paiva, H. A. R., "The Investigation of Deep Reinforced Concrete Beams under Static and Dynamic Loading, Vol. II, Strength and Behavior in Shear," AFSWC-TR-61-47, Vol. II, July 1961.
8. Wood, R. H., "Plastic and Elastic Design of Slabs and Plates," Ronald Press, New York, 1961.
9. Austin, W. J., "Prediction of Flexural Behavior of Deep Reinforced Concrete Slabs under Slowly Applied Loading," Interim Report, Part I, to Air Force Special Weapons Center, December 1962.

10. Gregory, R. K., Austin, W. J., DeHart, R. C., "Prediction of Flexural Behavior of Deep Reinforced Concrete Slabs under Slowly Applied Loading," Interim Report, Part II, to Air Force Special Weapons Center, October 1963.
11. Jensen, V. P., "Ultimate Strength of Reinforced Concrete Beams Related to the Plasticity Ratio of Concrete," University of Illinois Bulletin No. 345, Urbana, Illinois, June 1943.
12. Timoshenko, S., and Woinowsky-Krieger, S., "Theory of Plates and Shells," Second Edition, McGraw-Hill Book Company, 1959.
13. Newmark, N. M., "A Distribution Procedure for the Analysis of Slabs Continuous over Flexible Beams," University of Illinois Bulletin No. 304, Urbana, Illinois, June 1938.
14. Jones, L. L., "Ultimate Load Analysis of Reinforced and Prestressed Concrete Structures," in prep., Wiley (Interscience) Publishers.

DISTRIBUTION

No. cys

HEADQUARTERS USAF

- 1 Hq USAF (AFOCE), Wash, DC 20330
- 1 Hq USAF (AFRNE, Maj Dunn), Wash, DC 20330
- 1 Hq USAF (AFTAC), Wash, DC 20330

MAJOR AIR COMMANDS

- 1 AFSC (SCT), Andrews AFB, Wash, DC 20331
- 1 SAC (DICC), Offutt AFB, Nebr 68113
- 1 AFLC (MCSW), Wright-Patterson AFB, Ohio 45433
- 1 AUL, Maxwell AFB, Ala 36112
- 2 USAFIT, Wright-Patterson AFB, Ohio 45433
- 1 USAFA, Colo 80840

AFSC ORGANIZATIONS

- 1 AFSC Scientific and Technical Liaison Office, Research and Technology Division, AFUPO, Los Angeles, Calif 90045
- 1 AF Materials Laboratory, Wright-Patterson AFB, Ohio 45433
- ASD, Wright-Patterson AFB, Ohio 45433
- 1 (SEPIR)
- 1 (ASAMCV)
- RTD, Bolling AFB, Wash, DC 20332
- 1 (RTN-W, Lt Col Munyon)
- 1 (RTS)
- 1 AEDC (AEYD), Arnold AFS, Tenn 37289
- 1 BSD (BSSF), Norton AFB, Calif 92409
- 2 ESD (ESTI), L. G. Hanscom Fld, Bedford, Mass 01731
- 1 APGC (PGOZF), Eglin AFB, Fla 32542
- 1 RADC (EMLAL-1), Griffiss AFB, NY 13442

KIRTLAND AFB ORGANIZATIONS

- 1 AFSWC (SWEH), Kirtland AFB, NM 87117
- AFWL, Kirtland AFB, NM 87117
- 15 (WLIL)
- 7 (WLRC)

DISTRIBUTION (cont'd)

No. cys

OTHER AIR FORCE AGENCIES

- 1 Director, USAF Project RAND, via: Air Force Liaison Office, The RAND Corporation, ATTN: RAND Library, 1700 Main Street, Santa Monica, Calif 90406
- 1 USAF Engineering Liaison Office, APO 125, New York, NY
- 1 AFOSR (SRGL), Bldg T-D, Wash, DC 20333
- 1 AFCRL, L. G. Hansom Fld, Bedford, Mass 01731

ARMY ACTIVITIES

- 1 Chief of Research and Development, Department of the Army (Special Weapons and Air Defense Division), Wash, DC 20310
- 2 Chief of Engineers (ENGM-EM), Department of the Army, Wash, DC
Director, US Army Waterways Experiment Sta, P. O. Box 631, Vicksburg, Miss 39181
- 2 (WESRL)
- 2 (WESVC)

NAVY ACTIVITIES

- 1 Bureau of Yards and Docks, Department of the Navy, Code 22.102, (Branch Manager, Code 42.330), Wash 25, DC
- 3 Commanding Officer and Director, Naval Civil Engineering Laboratory, Port Hueneme, Calif
- 1 Commander, Naval Ordnance Laboratory, ATTN: Dr. Rudlin, White Oak, Silver Spring, Md 20910
- 1 Officer-in-Charge, Naval Civil Engineering Corps Officers School, US Naval Construction Battalion Center, Port Hueneme, Calif

OTHER DOD ACTIVITIES

- 2 Director, Defense Atomic Support Agency (Document Library Branch), Wash, DC 20301
- 1 Commander, Field Command, Defense Atomic Support Agency (FCAG3, Special Weapons Publication Distribution), Sandia Base, NM 87115
- 1 Office of Director of Defense Research and Engineering, ATTN: John E. Jackson, Office of Atomic Programs, Room 3E 1071, The Pentagon, Wash, DC 20330
- 20 DDC (TIAAS), Cameron Station, Alexandria, Va 22314

AEC ACTIVITIES

- 1 Sandia Corporation (Information Distribution Division), Box 5800, Sandia Base, NM 87115

DISTRIBUTION (cont'd)

No. cys

OTHER

- 1 OTS (CFSTI, Chief, Input Section), Sills Bldg, 5285 Port Royal Road, Springfield, Va 22151
- 1 Langley Research Center (NASA), ATTN: Associate Director, Langley Station, Hampton, Va
- 1 Office of Assistant Secretary of Defense (Civil Defense), Wash, DC 20301
- 1 Massachusetts Institute of Technology, Lincoln Laboratory (Document Library), P. O. Box 73, Lexington, Mass 02173
- 1 Agbabian-Jacobsen & Assoc., ATTN: Dr. Lydik S. Jacobsen, Consultant, 8939 S. Sepulveda Blvd., Los Angeles 45, Calif
- 2 Michigan College of Mining and Technology, ATTN: Dean Frank Kerekes and Dr. George Young, Consultants, Houghton, Mich
- 1 North Carolina State College, School of Engineering, ATTN: Dean Ralph Fadum, Consultant, Raleigh, NC
- 1 Portland Cement Assoc., Research and Development Laboratories, ATTN: Mr. Eivind Hognestad, Consultant, 5420 Old Orchard Road, Skokie, Ill
- 1 St Louis University, Institute of Technology, ATTN: Dr. Carl Kisslinger, Consultant, 3621 Olive Street, St Louis 8, Mo
- 1 University of Illinois, Department of Theoretical and Applied Mechanics ATTN: Prof. A. B. Boresi, Consultant, Urbana, Ill
- 1 University of Michigan, School of Civil Engineering, ATTN: Prof. Frank E. Richart, Jr., Consultant, Ann Arbor, Mich
- 2 AF Shock Tube Facility, ATTN: Dr. Eugene Zwoyer, Box 188, University Station, Albuquerque, NM
- 1 Bureau of Reclamation, ATTN: Mr. O. Olsen, Structural and Concrete Laboratory Branch, Bldg 53, Denver Federal Center, Denver 25, Colo
- 1 General American Transportation Corp., MRD Div., ATTN: Dr. G. L. Neidhardt, 7501 N. Natchez Ave., Niles, Ill
- 1 Illinois Institute of Technology Research Institute, ATTN: Mr. W. F. Riley, 10 West 35th St., Chicago 16, Ill
- 1 Louisiana State University, Engineering Mechanics Dept., ATTN: Dr. Dale Carver, Baton Rouge, La
- 2 Massachusetts Institute of Technology, Dept of Civil and Sanitary Engineering, ATTN: Dr. Robert V. Whitman, Cambridge 39, Mass
- 1 Office of Civil Defense Mobilization, ATTN: Mr. George Sisson, Room 3A-334, The Pentagon, Wash 25, DC
- 1 Paul Weidlinger Assoc., 770 Lexington Ave., New York, NY
- 1 University of Colorado, ATTN: Dr. James Chinn, Boulder, Colo

DISTRIBUTION (cont'd)

No. cys

- 2 University of Illinois, Civil Engineering Dept., ATTN: Dr. N. M. Newmark and Dr. C. P. Siess, 111 Talbot Laboratory, Urbana, Ill
- 2 University of Texas, ATTN: Prof. Phil M. Ferguson, Austin, Tex
- 10 Southwest Research Institute, 8500 Culebra Road, San Antonio, Tex
- 1 Tulane University, Dept. of Civil Engineering, ATTN: Prof. Blessey, New Orleans, La
- 1 Official Record Copy (Lt James A. Eddings, WLRC)

Unclassified

Security Classification

DOCUMENT CONTROL DATA - R&D

(Security classification of title, body of abstract and indexing annotation must be entered when the overall report is classified)

1 ORIGINATING ACTIVITY (Corporate author) Southwest Research Institute San Antonio, Tex		2a REPORT SECURITY CLASSIFICATION Unclassified	
		2b GROUP	
3 REPORT TITLE RESPONSE OF DEEP REINFORCED CONCRETE SLABS			
4 DESCRIPTIVE NOTES (Type of report and inclusive dates) Technical Documentary Report July 62 - April 64			
5 AUTHOR(S) (Last name, first name, initial) Gregory, R. K., DeHart, R. C., Austin, W. J.			
6 REPORT DATE February 1965		7a TOTAL NO. OF PAGES 150	7b NO OF REFS 14
8a CONTRACT OR GRANT NO. AF 29(601)-5385		9a ORIGINATOR'S REPORT NUMBER(S) WL-TDR-64-54	
b PROJECT NO 5710 DASA Subtask No. 13.157		9b OTHER REPORT NO(S) (Any other numbers that may be assigned this report)	
c			
d			
10 AVAILABILITY/LIMITATION NOTICES DDC release to OTS is authorized			
11 SUPPLEMENTARY NOTES		12 SPONSORING MILITARY ACTIVITY AFWL (WLRC) Kirtland AFB, NM	
13 ABSTRACT The response of deep reinforced concrete slabs to uniformly distributed dynamic loads as high as 700 psi was measured and compared with the static behavior of companion slabs. Comparisons between theoretical and experimental results were made. Experience has shown that one of the major difficulties in predicting the static behavior of reinforced concrete slabs results from the varying friction between the slab and bearing plate. The pressure seals and seal devices presented the primary experimental difficulty and made it impossible to yield the strongest slabs.			